Mechanistic investigation of Wnt5a-Ror signaling in mammalian development and Robinow syndrome

By

SARA KONOPELSKI SNAVELY

DISSERTATION

Submitted in partial satisfaction of the requirements for the degree of

DOCTOR OF PHILOSOPHY

in

Biochemistry, Molecular, Cellular, and Developmental Biology

in the

OFFICE OF GRADUATE STUDIES

of the

UNIVERSITY OF CALIFORNIA

DAVIS

Approved:

Henry Ho, Chair

Kermit Carraway

Konstantinos Zarbalis

Committee in Charge

2022

Acknowledgements

A most sincere and heartfelt thank you to my mentor Dr. Henry Ho for opening his lab to me and allowing me to call it home for the last 5 years. I will always be thankful for your willingness to let me creatively develop my interests within the lab into real experiments and projects and for the many times you unknowingly provided encouragement just when I needed it the most. You have truly shaped the scientist that I am today, and I will be forever grateful. Many additional thanks to my committee members Dr. Kermit Carraway and Dr. Kostas Zarbalis. I deeply appreciate your willingness to engage with me and my work over the years and all of your insightful comments. I would also like to thank my advisor Jon Sack for his never-ending optimism, reassurance, and perspective.

Many thanks to both the current and previous members of the Ho lab, who not only provided their mentorship and helping hands, but also welcomed me into the fold from the very beginning. Specifically, I would like to thank Tim Casey-Clyde, Helen Lamb, and Michael Cohen, who, collectively and individually, always brought a smile to my face and lifted my spirits. Additionally, two extra special thank you's to my dear lab mates and friends: First, to Xueer Jiang, thank you for always providing a compassionate heart to listen to me and a sharp mind to poke holes in my hypotheses. I would not have made it this far without you. Second, to Sathya Srinivasan, for her unending encouragement, thoughtful advice and discussions, and willingness to continuously help me improve upon my fledgling microscopy skills. My only regret is that we did not have more time together.

Thank you to my parents, Kathy and Mike, who nurtured my scientific inclinations from the very beginning. Your willingness to participate in science fair projects and logic puzzles strongly shaped my career trajectory and I will be forever grateful for all your love and support. Thank you to my bonus parents, Cindy and Kevin, for the never-ending support and for showing me how to build a life filled with love even when you are busy. To my first (dog) love, Zeus, thank you for always staying by my side late into the night and reminding me to enjoy the simple pleasures in life. Finally, the biggest thank you to my dear husband Alec. You have always encouraged my light to shine, even when it flickered and waned. It takes a certain person to put their dreams on hold while their significant other chases their dreams across the state and then across the country, and to me you are that one in a million. None of this would have been possible without you by my side.

This dissertation is dedicated to Bill and Betty Moon, whose unwavering love and belief in my ability to do anything started it all. I miss you and love you both every day.

Permission to use “Chapter 2: Proteomic analysis identifies the E3 ubiquitin ligase Pdzrn3 as a regulatory target of Wnt5a-Ror signaling” [1] has been granted by Proceedings of the National Academy of Sciences of the United States of America. Permission to include “Whole genome variant association across 100 dogs identifies a frame shift mutation in *DISHEVELLED 2* which contributes to Robinow- like syndrome in Bulldogs and related screw tail dog breeds” [2] in the Appendix has been granted to PLOS Genetics.

References

1. Konopelski Snavely, S.E., et al., *Proteomic analysis identifies the E3 ubiquitin ligase Pdzrn3 as a regulatory target of Wnt5a-Ror signaling.* Proc Natl Acad Sci U S A, 2021. **118**(25).
2. Mansour, T.A., et al., *Whole genome variant association across 100 dogs identifies a frame shift mutation in DISHEVELLED 2 which contributes to Robinow-like syndrome in Bulldogs and related screw tail dog breeds.* PLoS Genet, 2018. **14**(12): p. e1007850.

Abstract

Mammalian embryonic development is a highly stereotyped and coordinated process. Although tremendous diversity exists across species, the fundamental processes that drive spatiotemporal patterning and shaping are regulated by only a few signaling pathways. Wnt signaling is one such pathway that is involved in many aspects and stages of development. The many modalities of Wnt signaling, initiated through different ligand receptor combinations, elicit unique molecular and cellular responses, which historically have been differentiated by their ability to impact either tissue specification or tissue morphogenesis. In this paradigm, canonical Wnt signaling, or Wnt/β-catenin signaling, utilizes the transcriptional co-activator β-catenin to affect gene transcription and cell proliferation, thereby impacting tissue specification. In contrast, non-canonical Wnt signaling relies on β-catenin-independent mechanisms to affect cell migration to drive tissue morphogenesis. While the mechanisms and outputs of canonical Wnt signaling are well-studied in many physiological and pathological contexts, a reciprocal understanding of the molecular and cellular mechanisms governing non-canonical Wnt-driven tissue morphogenesis has remained limited.

This dissertation seeks to augment our understanding of the molecular and cellular mechanisms by which one major non-canonical Wnt pathway – Wnt5a-Ror signaling, defined as the signaling cascade initiated by Wnt5a ligands and Ror receptors – regulates embryonic development and how its misregulation can lead to congenital birth defects. This is achieved through further delineation of the Wnt5a-Ror signaling pathway based on the identification and characterization of a downstream regulatory component, the E3 ubiquitin ligase Pdzrn3, in addition to assessment of the roles of Dishevelled (Dvl) scaffolding proteins as they mediate both Wnt5a-Ror and Wnt/β-catenin signaling pathways in physiological as well as pathological contexts.

In Chapter 1, I briefly overview the history of Wnt signaling as a major developmental signaling network involved in a variety of unique biological processes. I detail the morphogenesis changes associated with misregulation of Wnt5a-Ror signaling in key model organisms, namely the widened and shortened of the body axis, head, tail and limbs. I also discuss the similarity between these Wnt5a-Ror signaling mutant organisms and Robinow syndrome (RS) human patients, which share many overlapping physical features and possess mutations in components of Wnt5a-Ror signaling. Finally, I delve more specifically into RS mutations that occur in DVLs, a family of evolutionarily conserved scaffolding proteins involved in facilitating multiple Wnt signaling pathways and indicate key questions surrounding the function and downstream changes driven by these proteins.

In Chapter 2, I focus on augmenting our mechanistic understanding of Wnt5a-Ror signaling that occurs in normal physiological contexts. In this team effort, I and others use a whole-cell proteomics approach to identify downstream effectors of Wnt5a-Ror signaling, and through this approach discover the E3 ubiquitin ligase Pdzrn3 as a regulatory target. We establish that Pdzrn3 is initially phosphorylated shortly after Wnt5a-Ror signaling is activated, a biochemical event which is required for its subsequent proteasomal degradation. From these findings, we develop a flow cytometry-based reporter to monitor Wnt5a-Ror signaling activity in live cells, one of the first of its kind reporters within the non-canonical Wnt signaling field. Using this reporter assay, we delineate the signaling cascade regulating Pdzrn3 phosphorylation and total protein abundance and determine that the C-terminal LNX3H domain of Pdzrn3 is phosphorylated in response to Wnt5a-Ror signaling. A closely related homolog of Pdzrn3, Lnx4, which possesses its own LNXH3 domain, can similarly undergo Wnt5a-Ror-induced degradation, strongly suggesting that the LNXH3 domain is a Wnt5a-responsive domain. We determine that phospho-regulation of Pdzrn3 is necessary for Wnt5a-Ror-driven cell migration.

We observed that cell migration is reduced with Wnt5a-Ror signaling activity, suggesting this pathway uses Pdzrn3 abundance to modulate this cell biological process.

In Chapter 3, I question the individual and collective contributions of Dvls to Wnt5a-Ror signaling as well as analyze how RS DVL variants affect signaling in this pathway and Wnt/β-catenin signaling. I develop a dual reporter system derived from mouse embryonic maxillary prominences to measure both Wnt5a-Ror and Wnt/β-catenin signaling in live cells and use a gene knockout and replacement approach in these cells to dissect the function of both wild-type and RS DVL variants. Through this approach, I show that Dvls are required for Wnt5a-Ror signal transduction and functionally non-redundant in dual reporter cells. I also demonstrate that the function of the Dvl C-terminus is to auto-regulate the remaining Dvl domains, which are differentially required in Wnt5a-Ror and Wnt/β-catenin signaling. I identified key residues within the Dvl C-terminus that are phosphorylated during Wnt5a-Ror signaling that are differentially required for Wnt5a-Ror signaling activity but not Wnt/β-catenin signaling, providing insight into Dvl pathway specification. Further, evaluation of RS DVL variant activity in multiple Wnt pathways for the first time indicates that they alter Wnt5a-Ror and Wnt/β-catenin signaling through multiple unique mechanisms, collectively demonstrating that misregulation of these pathways through over- or under-activation contributes to RS. Additional and related work concerning the identification and function of RS-like DVL2 variant present in bulldogs and related dog breeds is included in the Appendix.

Collectively, this dissertation establishes fundamental knowledge regarding Wnt5a-Ror signaling mechanisms in multiple contexts and establishes several practical platforms from which even more detailed interrogation of the pathway can be conducted.

Table of Contents

Chapter 1

Wnt5a-Ror signaling in development and Robinow syndrome

A brief overview of Wnt signaling

Wnts are a highly conserved family of glycoproteins that facilitate a variety of cell-cell communications within multicellular organisms in many diverse contexts. Since their independent discoveries, first as a segment polarity gene in *Drosophila* [1] and, subsequently, as a driver of mammary tumors in mice [2], Wnt ligands have garnered several decades of intense study from researchers worldwide. Today, it is recognized that Wnt ligands are a pivotal part of almost all aspects of biology, from the earliest stages of embryonic development to the most severe progression of diseases in addition to many of the physiological and pathological activities in between.

Early studies noted that ectopic expression of some Wnt ligands caused changes in tissue patterning and cell transformations [2-4]. Perhaps most strikingly, overexpression of Wnt1 in *Xenopus* resulted in axis duplication [4]. The subsequent efforts to understand the mechanisms driving such changes, coupled with epistasis experiments in *Drosophila* [5-7], led to delineation of the canonical Wnt signaling pathway. In this signaling cascade, ligands such as Wnt3a signal through Frizzled (Fzd) and low-density lipoprotein receptor-related protein 5 and 6 (Lrp5/6) receptors to inhibit a multiprotein assembly known as the destruction complex, which contains essential components such as Dishevelled (Dvl), Axin, adenomatous polyposis coli (APC), and glycogen synthase kinase (GSK3), and stabilize the transcriptional coactivator β-catenin that controls gene transcription and cell proliferation. This type of Wnt signaling regulates major developmental decisions, including cell proliferation and tissue fate determination, as well as tissue homeostasis, such as stem cell maintenance and tissue regeneration, in adult organisms. As a result, defects in canonical Wnt signaling can result in both devastating congenital defects and diseases, most notably cancer [8, 9].

However, some early reports also observed that some Wnt ligands had no effect on tissue patterning or cell transformations, but rather appeared to influence cell rearrangements and tissue shaping. Wnt5a was the first ligand connected to such changes, and, unlike other Wnts, overexpression of Wnt5a significantly altered *Xenopus* embryo morphology. Whereas previous overexpression of Wnt1, Wnt3a, or Wnt8 in *Xenopus* resulted in axis duplication [4], overexpression of Wnt5a produced *Xenopus* embryos with truncated body axis in addition to head and/or tail defects [10, 11]. The stark contrast between these findings indicated that different Wnt ligands can influence distinct phenotypic outcomes, suggesting the existence of multiple unique signaling pathways driven by Wnts. Notably, other model organisms display similar morphological defects, most notably truncations, in response to change in Wnt5a expression. *Wnt5a* knockout mice exhibit truncated body axes, limbs, and tails, in addition to underdeveloped external genitalia and widened, flattened faces [12] (Figure 1A), features which are largely replicated by Wnt5a overexpression in mice [13] and similar to the morphology of Wnt5a knockdown zebrafish [14]. These phenotypic observations, in combination with additional epistasis experiments conducted in *Drosophila* and loss of function studies in vertebrates, confirmed the existence of β-catenin-independent Wnt signaling [11, 15-20], thus initiating the distinction between canonical Wnt signaling, dependent on β-catenin, and non-canonical Wnt pathways, or β-catenin-independent, pathways.

Since these discoveries, the number of biological processes regulated by non-canonical Wnt pathways has continued to grow [15, 21-26]. Although the number and biochemical regulation of such pathways lacks consensus, collectively non-canonical Wnt pathways appear to culminate in the regulation of cytoskeletal rearrangements [20], thus leading to the cell and tissue morphogenesis changes described above. Much like canonical Wnt signaling, non-canonical Wnt pathways regulate a multitude of processes during embryonic development, and

inappropriate reactivation of non-canonical Wnt pathways contributes significantly to the malignant properties of diverse tumor types [27-34].

Wnt5a-Ror signaling constitutes a major non-canonical Wnt signaling pathway

While Wnt5a has been reported to interact with many different receptors to initiate distinct intracellular signaling cascades [11, 15-20], only deletion of receptor tyrosine kinase like orphan receptor 2 (Ror2) strongly phenocopied *Wnt5a* knockout mice [24, 35-38]. Like previously observed in *Wnt5a* knockouts, genetic deletion of *Ror2* in mice resulted in body axis and limb truncations in addition to flat and widened craniofacial features [24, 35-38]. From these findings started the notion that Ror2 is a major receptor involved in mediating Wnt5a signals [39], hereafter referred to as Wnt5a-Ror signaling.

Efforts to define the signaling cascade underlying Wnt5a-Ror signaling initially identified Dvl2 phosphorylation as a pathway specific change [24]. However, Dvl2 phosphorylation is also a key indicator of signaling activity in several other Wnt pathways [40-44]. This led to expanded efforts to identify additional, pathway specific downstream components of Wnt5a-Ror signaling. Through Ror-dependent whole-cell proteomic screens, Kif26b, an atypical kinesin, was identified as a downstream effector of Wnt5a-Ror signaling [26]. At the molecular level, Wnt5a-Ror signaling activity leads to a reduction in Kif26b protein abundance. Overexpression of Fzd receptors or Dvl1 resulted in degradation of Kif26b [26], indicating that they are other major components of Wnt5a-Ror signaling. In line with the existing evidence that Wnt5a-Ror signaling impacts cell migration and tissue morphogenesis, Kif26b serves as a promigratory factor in multiple organisms and cell types [26, 45-47]. However, Wnt5a-Ror signaling activity reduces cell migration, an affect that is lost with genetic deletion of *Kif26b* [26]. Collectively, these

findings suggest that Wnt5a-Ror signaling tunes Kif26b abundance to modulate cell migration. Thus, the Wnt5a-Ror signaling cascade that is initiated at the cell surface by Wnt5a ligands, Ror2, and Fzd receptors leads to phosphorylation of Dvl2 and degradation Kif26b to modulate cell migration (Figure 1B) [24, 26].

Taken all together, the strong phenotypic similarities observed in both *Wnt5a* and *Ror2* knockout mice, coupled with their co-regulation of downstream effectors Dvl2 and Kif26b, suggested that Wnt5a-Ror signaling constitutes a distinct non-canonical Wnt signaling pathway.

Mutations in components of Wnt5a-Ror signaling cause Robinow syndrome

In parallel to the discovery that Wnt5a ligands can use Ror to initiate non-canonical signaling, ROR2 was implicated as a candidate gene for Robinow syndrome (RS) [36]. RS is a rare congenital disorder that was first described by Dr. Meinhard Robinow in 1969, who noted that patients exhibited dwarfism in addition to unique phenotypes affecting the limbs, hands, genitals, and face [48, 49]. RS can be inherited in both autosomal dominant or autosomal recessive manners. Worldwide, fewer than 50 families have been identified with autosomal dominant RS (ADRS) and fewer than 200 individuals have been diagnosed with autosomal recessive RS (ARRS) [75, 76]. However, these numbers will likely continue to grow as recent technological advances have improved the ease, cost, and frequency of patient genome sequencing and additional candidate genes are established that can routinely be evaluated in tandem with clinical symptoms [48, 49].

Importantly, the distinct morphological features in human RS patients closely mimic the loss of function phenotypes observed in both Wnt5a and Ror2 knockout model organisms [10, 12-14, 35, 38, 39], suggesting an innate connection between RS and Wnt5a-Ror signaling. In

recent years, mutations in additional components of Wnt5a-Ror signaling have similarly been shown to cause Robinow syndrome, including WNT5A, DVL1, DVL2, DVL3, and FZD2 [50-58]. However, in contrast to the homozygous ROR2 loss of function mutations associated with ARRS, the mutations reported in *WNT5A*, *DVL1, DVL2, DVL3*, and *FZD2* are heterozygous and autosomal dominant. Collectively, these findings from human patients indicate that disruption of Wnt5a-Ror signaling in multiple, unique ways can result in the manifestation of RS [51, 53, 54, 58-60], underscoring the importance of this pathway to embryonic development as well as our need to understand it in detail.

Several clinical symptoms are shared by both ADRS and ARRS patients. Majority of reported RS patients exhibit short stature, limb shortening, brachydactyly, genital hypoplasia (in males, primarily) and multiple craniofacial features such as midface hypoplasia and hypertelorism [59, 61]. Unsurprisingly, these physical features arise from the embryonic tissues in which Wnt5a and Rors are highly expressed. In mice, Wnt5a can be detected in the outgrowing regions of the body, with the highest expression observed in the distal portions of the limb and tail buds, facial primordia, and urogenital primordia as well as the mesenchyme of the developing gut [12, 62]. Rors are similarly expressed in these tissues at the same time points in addition to the heart, lungs, mesonephros, as well as cartilage condensations and growth plates at later developmental stages [35, 63-68]. In contrast, Fzd receptors and Dvl scaffolding proteins are more widely expressed during development and adulthood, which likely reflects their involvement in other Wnt signaling pathways besides Wnt5a-Ror signaling [62, 69, 70]. However, Fzd2, the only Fzd receptor thus far associated with RS, is part of a subfamily of Fzd receptors highly expressed in the developing palate, facial prominences, and cardiac outflow tract [71].

While certain key clinical traits are shared, there is tremendous clinical heterogeneity amongst ADRS and ARRS patients [61]. Often, ARRS patients have more distinct appearances

due to severe skeletal defects that can include spinal deformities and rib fusions [49, 61], likely due to the role of Ror2 function in skeletal development [35, 38, 39]. Further, many clinical symptoms have incomplete penetrance, thus leading to variability between two patients who both have ADRS or ARRS as well as between two RS patients with mutations in the same gene. This variability has historically contributed to the difficulties associated with appropriately diagnosing RS versus other similar skeletal disorders, which highlights a need to understand wild-type mechanisms of Wnt5a-Ror signal transduction to appropriately evaluate the signaling deviations driven by RS variants.

Robinow syndrome mutations in DVLs and potential impacts on downstream signaling

Exome sequencing of multiple individuals and families led to the initial discovery of several patients with mutations in *DVL1*, all of which are heterozygous frameshift and splice acceptor mutations located in the penultimate or ultimate exons. Interestingly, all patient mutations result in the generation of the same new -1 open reading frame that affects the C-terminus while leaving preceding N-terminal sequence intact [51, 53]. Thus, the resultant protein product is predicted to be mostly wild-type with a novel C-terminus sequence that is shared by all patients. Subsequent studies identified both heterozygous frameshift mutations and splice acceptor variants *DVL3* as well as the first frameshift mutation in *DVL2* [58, 59, 72]. Like ADRS mutations in *DVL1*, these mutations in *DVL3 and DVL2* similarly occur in the penultimate or ultimate exon and are predicted to generate a novel C-terminus sequence while leaving the preceding sequence unaffected.

Remarkably, an analogous frameshift mutation was identified in *DVL2* gene and is shared among screw-tail dog breeds (colloquially known as Bulldogs, French Bulldogs, and

Boston Terriers and hereafter referred to as Bulldogs). Bulldogs are defined by their shortened and kinked tails ("screw tails") that arise from vertebral malformations such as fused and/or absent vertebrae [56] (for more on my contributions to this work see Appendix). In addition to a variety of skeletal malformations, Bulldogs also exhibit many other morphological similarities to RS patients, such as short limbs and stature as well as several craniofacial features like flat, short, and wide faces, an increased susceptibility to cleft palate [56, 73]. The highly analogous nature of the Bulldog *DVL2* mutation and similar morphological features shared by Bulldogs and human RS patients strongly suggests that Bulldogs have a canine version of RS. Collectively, these studies in human patients and Bulldogs implicate DVL C-termini in ADRS and canine-like RS and strongly suggest a highly important and conserved function for the DVL C-terminus.

Although the mechanisms governing ADRS and canine-like RS are limited, existing data suggest that neither mRNA and/or protein instability contribute to the ADRS phenotype. Transcripts from both *DVL1* and *DVL3* are expressed at levels similar to wild-type transcripts [53, 54], and overexpressed ADRS-DVL1 and Bulldog DVL2 can be detected at levels comparable to their wild-type DVL counterparts in heterologous systems [51, 56]. These findings suggest that a simple loss of function mechanism does not explain the mechanism and phenotypes of ADRS patients and Bulldogs. This concept is further supported by the phenotypes observed in *Dvl* knockout mice, which cover a spectrum of phenotypes ranging from abnormal social behavior in *Dvl1* knockouts [74] to skeletal abnormalities and conotruncal defects in *Dvl2* knockouts [69] to conotruncal and Organ of Corti defects in *Dvl3* knockouts [75]. While these mouse models recapitulate some aspects of the ADRS and canine-like RS phenotype, primarily the skeletal and conotruncal defects observed in *Dvl2* and *Dvl3* knockout mice, the lack of additional similarities suggests that ADRS and canine-like RS arise via a more complex mechanism.

There is also a distinct possibility that ADRS and Bulldog DVL mutations may alter multiple Wnt signaling pathways. Unlike WNT5A and RORs, DVL scaffolding proteins have well established roles in both canonical Wnt/β-catenin and non-canonical Wnt pathways. Evidence suggests that ADRS-DVL1 can increase canonical Wnt signaling in the presence of Wnt3a in a C-terminus dependent manner when overexpressed with wild-type DVL1 in a heterologous system [51]. Similarly, heterologously expressed Bulldog DVL2 exhibits decreased phosphorylation, a key readout of both canonical and non-canonical Wnt5a-Ror signaling, in response to treatment with recombinant Wnt3a or Wnt5a, respectively, suggesting again that multiple Wnt pathways may be disrupted [56]. However, beyond these studies, data indicating potential signaling defects in non-canonical Wnt5a-Ror signaling remains unexamined. Thus, utilization of the molecular readouts of these pathways, in conjunction with more precise genetic manipulations, should be prioritized in future endeavors to clarify the functionality of these DVL variants.

Dissertation Aims

All together, these patient reports further underscore the ever-growing importance of Wnt5a-Ror signaling to appropriate tissue morphogenesis. Additionally, the close phenotypic connections between deviations in Wnt5a-Ror signaling and RS patients strongly suggest that disruption of this key signaling pathways leads to manifestation of the congenital disorder, leading to the overarching hypothesis that misregulation of Wnt5a-Ror signaling causes RS. The increasing number of patient mutations emphasizes a need to deepen our mechanistic understanding of Wnt5a-Ror signaling at the molecular and cellular levels, which can facilitate RS patient mutation modeling to develop therapeutics. In turn, RS patient mutations can be

utilized within existing Wnt5a-Ror signaling assays to further our understanding of physiologically normal mechanisms.

Chapter 2 of this dissertation focuses on continuing to build upon our understanding of Wnt5a-Ror signaling mechanisms that occur under normal, physiological conditions. Here, I and others ask, are multiple downstream effectors are involved in facilitating Wnt5a-Ror signal transduction? How does the pathway biochemically regulate such downstream effectors? In answering these questions, we identify the E3 ubiquitin ligase Pdzrn3 as a regulatory target of Wnt5a-Ror signaling. Through biochemical and epistatic characterization, we begin to recognize the patterns by which Wnt5a-Ror signaling regulates both Pdzrn3 as well as Kif26b to affect similar cell biological processes. Ultimately, this work establishes fundamental knowledge regarding Wnt5a-Ror signaling mechanisms in addition to developing several practical platforms from which even more detailed interrogation of the pathway can be conducted.

Chapter 3 of this dissertation focuses on the role and function of Dvls as a major intersection for Wnt5a-Ror and Wnt/β-catenin signaling pathways. Here, I ask, are Dvls required for Wnt5a-Ror signaling? How do Dvls differentially transmit signals to Wnt5a-Ror or Wnt/β-catenin signaling pathways? Do RS DVL variants only disrupt Wnt5a-Ror signaling or multiple Wnt pathways? In completing this work, I show that Dvls are required for Wnt5a-Ror signaling and that their function is regulated by their C-termini, which possess unique phosphorylation sites differentially required for Wnt5a-Ror but not Wnt/β-catenin signaling. These findings in part explain how RS DVL variants, which have mutated C-termini, impact multiple Wnt signaling pathways as part of their molecular etiology. Overall, the findings presented in this dissertation advance our understanding of Wnt5a-Ror signaling mechanisms in both physiological and pathological contexts.

Figures

Figure 1. Mutations in Wnt5a-Ror signaling cause Robinow syndrome A) *Wnt5a* knockout mouse embryos at 11.5 days of gestation exhibit body axis, limb, and tail truncations in addition to underdeveloped external genitalia and craniofacial malformations compared to wild-type littermates. These physical features are largely phenocopied in Robinow syndrome patients. Scale bars are 1 millimeter. **B)** During Wnt5a-Ror signaling, Wnt5a ligand interactions with Frizzled and Rors result in the downstream phosphorylation of Dvl1-3. Subsequently, the downstream effectors Kif26b and Pdzrn3 are degraded, leading to cytoskeleton rearrangements that influence cell and tissue morphogenesis. Red asterisks denote pathway components that are mutated in Robinow syndrome.

A.

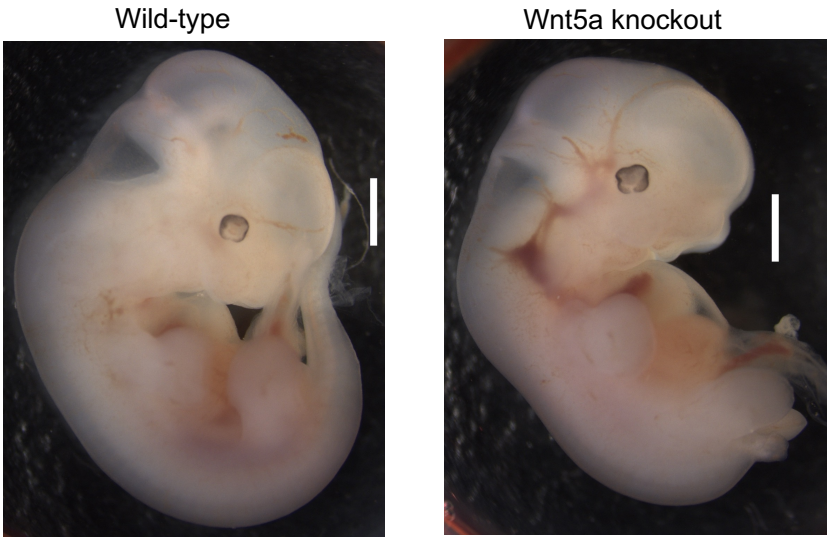
Wild-type
Wnt5a knockout

B.

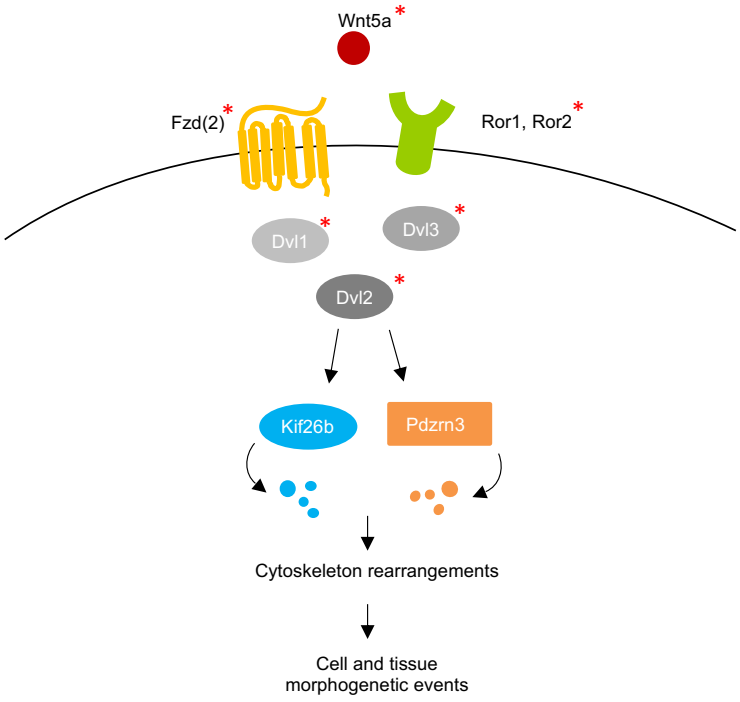
Wnt5a *
Fzd(2) *
Ror1, Ror2 *
Dvl1 *
Dvl3 *
Dvl2 *
Kif26b
Pdzrn3
Cytoskeleton rearrangements
Cell and tissue morphogenetic events

References

1. Nusslein-Volhard, C. and E. Wieschaus, *Mutations affecting segment number and polarity in Drosophila.* Nature, 1980. **287**(5785): p. 795-801.
2. Nusse, R. and H.E. Varmus, *Many tumors induced by the mouse mammary tumor virus contain a provirus integrated in the same region of the host genome.* Cell, 1982. **31**(1): p. 99-109.
3. Wong, G.T., B.J. Gavin, and A.P. McMahon, *Differential transformation of mammary epithelial cells by Wnt genes.* Mol Cell Biol, 1994. **14**(9): p. 6278-86.
4. McMahon, A.P. and R.T. Moon, *Ectopic expression of the proto-oncogene int-1 in Xenopus embryos leads to duplication of the embryonic axis.* Cell, 1989. **58**(6): p. 1075-84.
5. Noordermeer, J., et al., *dishevelled and armadillo act in the wingless signalling pathway in Drosophila.* Nature, 1994. **367**(6458): p. 80-3.
6. Peifer, M., et al., *wingless signal and Zeste-white 3 kinase trigger opposing changes in the intracellular distribution of Armadillo.* Development, 1994. **120**(2): p. 369-80.
7. Siegfried, E., T.B. Chou, and N. Perrimon, *wingless signaling acts through zeste-white 3, the Drosophila homolog of glycogen synthase kinase-3, to regulate engrailed and establish cell fate.* Cell, 1992. **71**(7): p. 1167-79.
8. Clevers, H. and R. Nusse, *Wnt/beta-catenin signaling and disease.* Cell, 2012. **149**(6): p. 1192-205.
9. Nusse, R. and H. Varmus, *Three decades of Wnts: a personal perspective on how a scientific field developed.* EMBO J, 2012. **31**(12): p. 2670-84.
10. Moon, R.T., et al., *Xwnt-5A: a maternal Wnt that affects morphogenetic movements after overexpression in embryos of Xenopus laevis.* Development, 1993. **119**(1): p. 97-111.

11. Du, S.J., et al., *Identification of distinct classes and functional domains of Wnts through expression of wild-type and chimeric proteins in Xenopus embryos.* Mol Cell Biol, 1995. **15**(5): p. 2625-34.

12. Yamaguchi, T.P., et al., *A Wnt5a pathway underlies outgrowth of multiple structures in the vertebrate embryo.* Development, 1999. **126**(6): p. 1211-23.

13. van Amerongen, R., et al., *Wnt5a can both activate and repress Wnt/beta-catenin signaling during mouse embryonic development.* Dev Biol, 2012. **369**(1): p. 101-14.

14. Schambony, A. and D. Wedlich, *Wnt-5A/Ror2 regulate expression of XPAPC through an alternative noncanonical signaling pathway.* Dev Cell, 2007. **12**(5): p. 779-92.

15. Boutros, M., et al., *Dishevelled activates JNK and discriminates between JNK pathways in planar polarity and wingless signaling.* Cell, 1998. **94**(1): p. 109-18.

16. Boutros, M. and M. Mlodzik, *Dishevelled: at the crossroads of divergent intracellular signaling pathways.* Mech Dev, 1999. **83**(1-2): p. 27-37.

17. Miller, J.R., et al., *Mechanism and function of signal transduction by the Wnt/beta-catenin and Wnt/Ca2+ pathways.* Oncogene, 1999. **18**(55): p. 7860-72.

18. Kuhl, M., et al., *The Wnt/Ca2+ pathway: a new vertebrate Wnt signaling pathway takes shape.* Trends Genet, 2000. **16**(7): p. 279-83.

19. Kuhl, M., *Non-canonical Wnt signaling in Xenopus: regulation of axis formation and gastrulation.* Semin Cell Dev Biol, 2002. **13**(3): p. 243-9.

20. Veeman, M.T., J.D. Axelrod, and R.T. Moon, *A second canon. Functions and mechanisms of beta-catenin-independent Wnt signaling.* Dev Cell, 2003. **5**(3): p. 367-77.

21. Slusarski, D.C., V.G. Corces, and R.T. Moon, *Interaction of Wnt and a Frizzled homologue triggers G-protein-linked phosphatidylinositol signalling.* Nature, 1997. **390**(6658): p. 410-3.

22. Slusarski, D.C., et al., *Modulation of embryonic intracellular Ca2+ signaling by Wnt-5A.* Dev Biol, 1997. **182**(1): p. 114-20.

23. Axelrod, J.D., et al., *Differential recruitment of Dishevelled provides signaling specificity in the planar cell polarity and Wingless signaling pathways.* Genes Dev, 1998. **12**(16): p. 2610-22.

24. Ho, H.Y., et al., *Wnt5a-Ror-Dishevelled signaling constitutes a core developmental pathway that controls tissue morphogenesis.* Proc Natl Acad Sci U S A, 2012. **109**(11): p. 4044-51.

25. Butler, M.T. and J.B. Wallingford, *Planar cell polarity in development and disease.* Nat Rev Mol Cell Biol, 2017. **18**(6): p. 375-388.

26. Susman, M.W., et al., *Kinesin superfamily protein Kif26b links Wnt5a-Ror signaling to the control of cell and tissue behaviors in vertebrates.* Elife, 2017. **6**.

27. Weeraratna, A.T., et al., *Wnt5a signaling directly affects cell motility and invasion of metastatic melanoma.* Cancer Cell, 2002. **1**(3): p. 279-88.

28. Pukrop, T., et al., *Wnt 5a signaling is critical for macrophage-induced invasion of breast cancer cell lines.* Proc Natl Acad Sci U S A, 2006. **103**(14): p. 5454-9.

29. Anastas, J.N., et al., *A protein complex of SCRIB, NOS1AP and VANGL1 regulates cell polarity and migration, and is associated with breast cancer progression.* Oncogene, 2012. **31**(32): p. 3696-708.

30. Nishioka, M., et al., *Possible involvement of Wnt11 in colorectal cancer progression.* Mol Carcinog, 2013. **52**(3): p. 207-17.

31. Asad, M., et al., *FZD7 drives in vitro aggressiveness in Stem-A subtype of ovarian cancer via regulation of non-canonical Wnt/PCP pathway.* Cell Death Dis, 2014. **5**(7): p. e1346.

32. Daulat, A.M., et al., *PRICKLE1 Contributes to Cancer Cell Dissemination through Its Interaction with mTORC2.* Dev Cell, 2016. **37**(4): p. 311-325.

33. Wald, J.H., et al., *Suppression of planar cell polarity signaling and migration in glioblastoma by Nrdp1-mediated Dvl polyubiquitination.* Oncogene, 2017. **36**(36): p. 5158-5167.

34. Dart, D.A., et al., *Wnt-11 Expression Promotes Invasiveness and Correlates with Survival in Human Pancreatic Ductal Adeno Carcinoma.* Genes (Basel), 2019. **10**(11).

35. DeChiara, T.M., et al., *Ror2, encoding a receptor-like tyrosine kinase, is required for cartilage and growth plate development.* Nat Genet, 2000. **24**(3): p. 271-4.

36. Afzal, A.R., et al., *Recessive Robinow syndrome, allelic to dominant brachydactyly type B, is caused by mutation of ROR2.* Nat Genet, 2000. **25**(4): p. 419-22.

37. Takeuchi, S., et al., *Mouse Ror2 receptor tyrosine kinase is required for the heart development and limb formation.* Genes Cells, 2000. **5**(1): p. 71-8.

38. Nomi, M., et al., *Loss of mRor1 enhances the heart and skeletal abnormalities in mRor2-deficient mice: redundant and pleiotropic functions of mRor1 and mRor2 receptor tyrosine kinases.* Mol Cell Biol, 2001. **21**(24): p. 8329-35.

39. Oishi, I., et al., *The receptor tyrosine kinase Ror2 is involved in non-canonical Wnt5a/JNK signalling pathway.* Genes Cells, 2003. **8**(7): p. 645-54.

40. Rothbacher, U., et al., *Dishevelled phosphorylation, subcellular localization and multimerization regulate its role in early embryogenesis.* EMBO J, 2000. **19**(5): p. 1010-22.

41. Yanagawa, S., et al., *The dishevelled protein is modified by wingless signaling in Drosophila.* Genes Dev, 1995. **9**(9): p. 1087-97.

42. Gonzalez-Sancho, J.M., et al., *Functional consequences of Wnt-induced dishevelled 2 phosphorylation in canonical and noncanonical Wnt signaling.* J Biol Chem, 2013. **288**(13): p. 9428-37.

43. Gonzalez-Sancho, J.M., et al., *Wnt proteins induce dishevelled phosphorylation via an LRP5/6- independent mechanism, irrespective of their ability to stabilize beta-catenin.* Mol Cell Biol, 2004. **24**(11): p. 4757-68.

44. Fukukawa, C., et al., *Activation of the non-canonical Dvl-Rac1-JNK pathway by Frizzled homologue 10 in human synovial sarcoma.* Oncogene, 2009. **28**(8): p. 1110-20.

45. Guillabert-Gourgues, A., et al., *Kif26b controls endothelial cell polarity through the Dishevelled/Daam1-dependent planar cell polarity-signaling pathway.* Mol Biol Cell, 2016. **27**(6): p. 941-53.

46. Forrester, W.C., et al., *Identification of Caenorhabditis elegans genes required for neuronal differentiation and migration.* Genetics, 1998. **148**(1): p. 151-65.

47. Wightman, B., et al., *The C. elegans gene vab-8 guides posteriorly directed axon outgrowth and cell migration.* Development, 1996. **122**(2): p. 671-82.

48. Roifman, M., et al., *Autosomal Dominant Robinow Syndrome*, in *GeneReviews((R))*, M.P. Adam, et al., Editors. 1993: Seattle (WA).

49. Patton, M.A. and A.R. Afzal, *Robinow syndrome.* J Med Genet, 2002. **39**(5): p. 305-10.

50. Person, A.D., et al., *WNT5A mutations in patients with autosomal dominant Robinow syndrome.* Dev Dyn, 2010. **239**(1): p. 327-37.

51. Bunn, K.J., et al., *Mutations in DVL1 cause an osteosclerotic form of Robinow syndrome.* Am J Hum Genet, 2015. **96**(4): p. 623-30.

52. Roifman, M., et al., *De novo WNT5A-associated autosomal dominant Robinow syndrome suggests specificity of genotype and phenotype.* Clin Genet, 2015. **87**(1): p. 34-41.

53. White, J., et al., *DVL1 frameshift mutations clustering in the penultimate exon cause autosomal-dominant Robinow syndrome.* Am J Hum Genet, 2015. **96**(4): p. 612-22.

54. White, J.J., et al., *DVL3 Alleles Resulting in a -1 Frameshift of the Last Exon Mediate Autosomal-Dominant Robinow Syndrome.* Am J Hum Genet, 2016. **98**(3): p. 553-561.

55. Danyel, M., et al., *Autosomal dominant Robinow syndrome associated with a novel DVL3 splice mutation.* Am J Med Genet A, 2018. **176**(4): p. 992-996.

56. Mansour, T.A., et al., *Whole genome variant association across 100 dogs identifies a frame shift mutation in DISHEVELLED 2 which contributes to Robinow-like syndrome in Bulldogs and related screw tail dog breeds.* PLoS Genet, 2018. **14**(12): p. e1007850.

57. Nagasaki, K., et al., *Nonsense mutations in FZD2 cause autosomal-dominant omodysplasia: Robinow syndrome-like phenotypes.* Am J Med Genet A, 2018. **176**(3): p. 739-742.

58. White, J.J., et al., *WNT Signaling Perturbations Underlie the Genetic Heterogeneity of Robinow Syndrome.* Am J Hum Genet, 2018. **102**(1): p. 27-43.

59. Zhang, C., et al., *Novel pathogenic variants and quantitative phenotypic analyses of Robinow syndrome: WNT signaling perturbation and phenotypic variability.* HGG Adv, 2022. **3**(1): p. 100074.

60. Zhang, C., et al., *Novel pathogenic genomic variants leading to autosomal dominant and recessive Robinow syndrome.* Am J Med Genet A, 2021. **185**(12): p. 3593-3600.

61. Mazzeu, J.F., et al., *Clinical characterization of autosomal dominant and recessive variants of Robinow syndrome.* Am J Med Genet A, 2007. **143**(4): p. 320-5.

62. Summerhurst, K., et al., *3D representation of Wnt and Frizzled gene expression patterns in the mouse embryo at embryonic day 11.5 (Ts19).* Gene Expr Patterns, 2008. **8**(5): p. 331-48.

63. Oishi, I., et al., *Spatio-temporally regulated expression of receptor tyrosine kinases, mRor1, mRor2, during mouse development: implications in development and function of the nervous system.* Genes Cells, 1999. **4**(1): p. 41-56.

64. Matsuda, T., et al., *Expression of the receptor tyrosine kinase genes, Ror1 and Ror2, during mouse development.* Mech Dev, 2001. **105**(1-2): p. 153-6.

65. Hikasa, H., et al., *The Xenopus receptor tyrosine kinase Xror2 modulates morphogenetic movements of the axial mesoderm and neuroectoderm via Wnt signaling.* Development, 2002. **129**(22): p. 5227-39.

66. Schwabe, G.C., et al., *Ror2 knockout mouse as a model for the developmental pathology of autosomal recessive Robinow syndrome.* Dev Dyn, 2004. **229**(2): p. 400-10.

67. Stricker, S., et al., *Cloning and expression pattern of chicken Ror2 and functional characterization of truncating mutations in Brachydactyly type B and Robinow syndrome.* Dev Dyn, 2006. **235**(12): p. 3456-65.

68. Schille, C., et al., *Ror2 signaling is required for local upregulation of GDF6 and activation of BMP signaling at the neural plate border.* Development, 2016. **143**(17): p. 3182-94.

69. Hamblet, N.S., et al., *Dishevelled 2 is essential for cardiac outflow tract development, somite segmentation and neural tube closure.* Development, 2002. **129**(24): p. 5827-38.

70. Wynshaw-Boris, A., *Dishevelled: in vivo roles of a multifunctional gene family during development.* Curr Top Dev Biol, 2012. **101**: p. 213-35.

71. Yu, H., et al., *Frizzled 1 and frizzled 2 genes function in palate, ventricular septum and neural tube closure: general implications for tissue fusion processes.* Development, 2010. **137**(21): p. 3707-17.

72. Zhang, C., et al., *Novel pathogenic genomic variants leading to autosomal dominant and recessive Robinow syndrome.* Am J Med Genet A, 2020.

73. Niskanen, J.E., et al., *Canine DVL2 variant contributes to brachycephalic phenotype and caudal vertebral anomalies.* Hum Genet, 2021. **140**(11): p. 1535-1545.

74. Lijam, N., et al., *Social interaction and sensorimotor gating abnormalities in mice lacking Dvl1.* Cell, 1997. **90**(5): p. 895-905.

75. Etheridge, S.L., et al., *Murine dishevelled 3 functions in redundant pathways with dishevelled 1 and 2 in normal cardiac outflow tract, cochlea, and neural tube development.* PLoS Genet, 2008. **4**(11): p. e1000259.

Chapter 2

Proteomic analysis identifies the E3 ubiquitin ligase Pdzrn3 as a regulatory target of Wnt5a-Ror signaling

Abstract

Wnt5a-Ror signaling is a conserved pathway that regulates morphogenetic processes during vertebrate development [1], but its downstream signaling events remain poorly understood. Through a large-scale proteomic screen in mouse embryonic fibroblasts, we identified the E3 ubiquitin ligase Pdzrn3 as a regulatory target of the Wnt5a-Ror pathway. Upon pathway activation, Pdzrn3 is degraded in a β-catenin-independent, ubiquitin-proteasome system-dependent manner. We developed a flow cytometry-based reporter to monitor Pdzrn3 abundance and delineated a signaling cascade involving Frizzled, Dishevelled, CK1, and GSK3 that regulates Pdzrn3 stability. Epistatically, Pdzrn3 is regulated independently of Kif26b, another Wnt5a-Ror effector [2]. Wnt5a-dependent degradation of Pdzrn3 requires phosphorylation of three conserved amino acids within its C-terminal LNX3H domain [3], which acts as a bona fide Wnt5a-responsive element. Importantly, this phospho-dependent degradation is essential for Wnt5a-Ror modulation of cell migration. Collectively, this work establishes a new Wnt5a-Ror cell morphogenetic cascade involving Pdzrn3 phosphorylation and degradation.

Significance

Wnt5a-Ror signaling is a master regulator of tissue shape, and dysfunction of the pathway contributes to congenital birth defects and cancer metastasis. The molecular underpinnings of this pathway, however, remain unclear. To identify subcellular protein changes driven by Wnt5a-Ror signaling, we conducted a large-scale proteomic screen and identified the E3 ubiquitin ligase Pdzrn3 as a downstream target. Wnt5a-Ror signaling initially induces Pdzrn3 phosphorylation, which subsequently triggers the ubiquitin/proteasome-dependent degradation of Pdzrn3. Importantly, Wnt5a-Ror signaling uses this phospho-degradation process to regulate cell migration. From these findings, we further developed a flow cytometry-based reporter to monitor Pdzrn3 abundance and delineated the signaling cascade regulating Pdzrn3 stability. Collectively, our study establishes Pdzrn3 phosphorylation and degradation as a key component of Wnt5a-Ror signaling.

Introduction

Embryonic development in vertebrates is a highly stereotyped and coordinated process that depends on a handful of core signaling pathways. One major mode of signaling involves Wnt ligands, a diverse and highly conserved family of glycoproteins that signal in many spatiotemporal contexts, including tissue specification and tissue morphogenesis in addition to tissue homeostasis in adult organisms [4-6]. Thus, Wnts play unique and critical roles in both developing and adult organisms.

Traditionally, Wnt pathways have been classified as either canonical or non-canonical. Canonical Wnt signaling utilizes β-catenin as a transcriptional co-activator to regulate cell fate and proliferation and its mechanism of action and biological functions are relatively well understood. In contrast, non-canonical Wnt signaling, which regulates tissue morphogenetic processes in a β-catenin-independent manner, remains poorly characterized [4-9]. Numerous studies in a variety of model organisms have demonstrated that alterations to the expression of Wnt5a, the prototypic non-canonical Wnt ligand, can cause drastic morphogenesis defects such as body axis truncations, shortened limbs and tails, and craniofacial malformations [1, 10, 11]. These phenotypic abnormalities closely mirror those of Ror1 and Ror2 double knockout mice, further underscoring the growing evidence that Ror receptors mediate Wnt5a signals to orchestrate tissue morphogenetic events [12, 13].

Importantly, the phenotypic characteristics observed in *WNT5A* and *ROR1; ROR2* double mutants have also been observed in human Robinow syndrome patients, and several recent publications have reported that many Robinow syndrome patients possess mutations in various components of the Wnt5a-Ror signaling pathway, including *WNT5A*, *ROR2*, *FRIZZLED2* (*FZD2*), *DISHEVELLED1* (*DVL1*), and *DISHEVELLED3* (*DVL3*) [14-20]. Further,

bulldogs and other closely related dog breeds possess a mutation in *DISHEVELLED2* (*DVL2*) that is highly analogous to the human Robinow syndrome mutations in *DVL1* and *DVL3*, and these breeds exhibit skeletal and craniofacial features that are reminiscent of human Robinow syndrome [21]. Collectively, these recent findings strongly support the idea that Wnt5a-Ror signaling is conserved and critical to tissue morphogenesis in a variety of vertebrates. However, despite the significance of Wnt5a-Ror signaling in normal development and disease contexts, the mechanisms by which Wnt5a signals are transmitted and processed within the cell remain unclear. Progress within the field is further hampered by a lack of consensus regarding the number of non-canonical pathways, the biochemical nature of their regulation, and variability in the methods used to measure signaling [7].

To deepen our understanding of Wnt5a-Ror signaling, we have taken systematic approaches to identify downstream cellular events that occur in response to pathway activation. Previously, we genetically ablated Ror1 and Ror2 receptors in primary mouse embryonic fibroblast (MEF) cultures and used a proteomic approach to uncover downstream signaling events that are misregulated. From this analysis, we identified the atypical kinesin Kif26b as a downstream component of Wnt5a-Ror signaling that is degraded upon Wnt5a-Ror pathway activation [2].

In this follow-up study, we hypothesized that the identification of additional downstream regulatory targets would augment our mechanistic understanding of Wnt5a-Ror signaling. Thus, we conducted a second large-scale proteomic screen to identify cellular proteins whose abundance and phosphorylation state are altered by *acute* stimulation of Wnt5a-Ror signaling. Through this approach, we identified the E3 ubiquitin ligase Pdzrn3 as a downstream target. Pdzrn3 has been implicated in non-canonical Wnt signaling previously based on its interactions with Dvl3 and shown to function as a promigratory factor in several morphogenetic contexts, including synaptic growth and maturation, vascular morphogenesis, and neuronal positioning

[22-24]. However, how non-canonical Wnt signaling regulates Pdzrn3 at a biochemical level still remains unknown. We discovered that Pdzrn3 is degraded by Wnt5a-Ror signaling via a mechanism independent of β-catenin but dependent on the ubiquitin-proteasome system (UPS). This regulation is mediated by a signaling cascade involving Frizzled (Fzd), Dishevelled (Dvl), Casein kinase 1 (CK1), and Glycogen synthase kinase 3 (GSK3), which is remarkably similar to the cascade that regulates Kif26b. Despite these similarities, we find that Wnt5a-induced degradation of Pdzrn3 is not dependent on Kif26b and vice versa. Further, Wnt5a-dependent degradation of Pdzrn3 requires phosphorylation of three specific amino acid residues on its C-terminal LNX3H domain. Critically, the phosphorylation and degradation of Pdzrn3 serves as a mechanism through which Wnt5a-Ror signaling can regulate cell migration. Lastly, we demonstrated that the LNX3H domain is required for Wnt5a-dependent degradation of not only Pdzrn3 but also its structural homolog Lnx4, suggesting that the LNX3H domain may generally function as a Wnt5a-responsive domain. Together, these findings establish the mechanisms through which the Wnt5a-Ror pathway regulates Pdzrn3 abundance to facilitate signal transduction, thus providing a platform from which a deeper mechanistic and cell morphogenetic understanding of non-canonical Wnt signaling can be attained.

Materials and methods

Cell lines

Primary MEFs were isolated directly from mouse embryos as described [13] and used within 3 passages. NIH/3T3 Flp-In (R76107, Thermo Fisher Scientific) cells were purchased and were not re-authenticated; cells tested negative for mycoplasma contamination using the Universal Mycoplasma Detection Kit (30-1012K, ATCC). All cell lines were cultured at 37C and 5% CO2 in Dulbecco's Modified Eagles Medium (MT15017CV, Corning) supplemented with 1x glutamine (25-005-CI, Corning), 1x penicillin-streptomycin (30-002-CI, Corning) and 10% fetal bovine serum (16000069, Thermo Fisher Scientific).

TMT/MS3 proteomic screen

Primary *Wnt5a*$^{-/-}$ MEFs (derived and pooled from three different E12.5 *Wnt5a*$^{-/-}$ embryos) were seeded in six 10-cm plates at 50% confluency 3 days before rWnt5a stimulation (day 0), such that cells would be fully confluent for 2 days. On the day of stimulation (day 3), cells in each 10-cm plate were treated either with rWnt5a (100ng/mL final concentration) for 1h or 6hr, or with the control buffer (1x PBS, 0.1% bovine serum albumin, 0.5% w/v CHAPS) for 6hr. The entire stimulation experiment was conducted in two independent replicates. At the end of the Wnt5a stimulation time course, cells were washed once with ice-cold PBS and plates were scraped into 1 mL of ice-cold lysis buffer (8 M urea, 75 mM NaCl, 50 mM Tris pH 8.2, 1 mM NaF, 1 mM β-glycerophosphate, 1 mM Na_3VO_4, 10 mM $Na_4P_2O_7$, 1 mM PMSF, and Complete protease inhibitor (-EDTA, Roche)). Cells were homogenized by pipetting up and down using a P-1000

and then sonicated in a Bioruptor (17 x 30s ON/OFF cycles). Cell lysates were then centrifuged at 40,000 RPM for 20 min at 4C. The clarified high-speed supernatants were collected, snap frozen in liquid nitrogen and stored at -80C until the TMT/MS3 analysis was performed. Protein concentrations were determined using BCA reagents (Pierce) and normalized.

To perform the TMT/MS3 screen, tryptic peptides were prepared from whole cell lysates and the peptide mixtures from the different experimental conditions were labeled with the six TMT reagents, such that reporter ions at m/z of 126, 127, 128, 129, 130 and 131 would be generated in the tandem spectrometry. Phosphopeptides were enriched by TiO_2 chromatography. Liquid chromatography, MS3 tandem mass spectrometry and data analysis were carried out as previously described [25-27].

Cloning of mouse Pdzrn3, Lnx1, Lnx2, Lnx4, and Lnx5 cDNA

For cloning of mouse Pdzrn3 cDNA, a first strand cDNA pool was generated from MEF total RNA Maxima H Minus reverse transcriptase and oligo dT primers according to manufacturer's instructions (EP0751, ThermoFisher Scientific). This cDNA library was then used as template for PCR amplification of the *Pdzrn3* open reading frame with the following primers, forward: gatcGGCCGGCCtACCatgggtttcgagttggatcgc; reverse: gatcGGCGCGCCTTATACAGTAGTCACCGACAGGAA. The PCR product was subcloned into a modified pCS2+ vector using the FseI and AscI restriction sites. The entire *Pdzrn3* open reading frame was confirmed by Sanger sequencing.

For cloning the Lnx1, Lnx2, Lnx4, and Lnx5 cDNAs, the same workflow was used, except that E14.5 mouse brain RNA was used to generate the first strand cDNA pool. The following primers were used to PCR amplify and subclone the respective cDNAs: mLnx1

forward, gatcGGCCGGccTACCatgaaccaaccggaccttgcagat; mLnx1 reverse, gatcGGCGCGCCTTATAAAAAAGTACCAGGCCAAGAAG; mLnx2 forward, gatcGGCCGGccTACCatgggaacaaccagtgacgagatgg; mLnx2 reverse, gatcGGCGCGCCCTATACGAGGCTGCCTGGCCAGCAG; mLnx4 forward, gatcggccggccTaccATGGGCTTCGCTTTGGAGCGTCTC; mLnx4 reverse, gatcGGCGCGCCtcaTACGGTGGTCACCGACAGAAAGGC; mLnx5 forward, gatcGGCCGgCCTACCatgggatgtaatatgtgtgtggtc; mLnx5 reverse, gatcGGCGCGCCTCAGACAGTGGTGACAGAGAGCAG. All constructs were confirmed by Sanger sequencing.

Antibodies

Antibodies against Ror1, Ror2, and Kif26b were described previously [2, 13]. The following antibodies were purchased: rabbit anti-Dvl2 (#3216, Cell Signaling) and mouse anti-α-tubulin (clone DM1A, #ab7291, Abcam).

Initial analyses of Pdzrn3 were conducted using a commercial antibody (SC-99507, Santa Cruz Biotechnology); however, the antibody was discontinued and all subsequent analyses (including all data presented in this paper) were conducted using anti-Pdzrn3 antibodies produced in-house. To generate anti-Pdzrn3 antisera, rabbits were immunizing with a mixture of two different antigens: 1) a synthetic peptide with the sequence LLTHGTKSPDGTRVYNSFLSVTC, conjugated to keyhole limpet hemocyanin (77600, ThermoFisher Scientific), and 2) a maltose binding protein N-terminally fused to a Pdzrn3 protein fragment extending from amino acids 902 to 1063, recombinantly expressed in and purified from E. coli. Antibodies were affinity purified from antisera over a column with a full-

length recombinant Pdzrn3 protein covalently immobilized to Sepharose beads (AminoLink Plus, 20501, ThermoFisher Scientific). Full length Pdzrn3 was expressed in insect cells using the Bac-to-Bac baculovirus expression system (10359016, ThermoFisher Scientific); the protein was insoluble and was purified under denatured conditions using 5.5M guanidinium hydrochloride, coupled to AminoLink Plus Resin, and renatured by gradually removing guanidinium hydrochloride.

Western blotting

Protein lysates for SDS-PAGE and western blotting were prepared in 1x - 2x Laemmli sample buffer or LDS sample buffer (Life Technologies). Protein lysates used for Kif26b western blotting were not heated, as the Kif26b signal weakens substantially after heating, likely due to heat-induced protein aggregation [2]. All other protein lysates were heated at 90C for 5 min before SDS-PAGE and western blotting.

Quantitative western blotting was performed using the Odyssey infrared imaging system (Li-Cor Biosciences) according to the manufacturer's instructions. The median background method was used with a border width of two pixels on all sides around the perimeter of the area being quantified. Non-saturated protein bands were quantified by using Odyssey software with the gamma level set at 1.

Generation of stable NIH/3T3 cell lines

To construct the GFP-Pdzrn3 expression plasmid, the eGFP open reading frame was first subcloned into pENTR-2B (Life Technologies), and the full-length mouse Pdzrn3 open reading frame was subcloned in frame to the C-terminus of GFP. The resulting construct was verified by sequencing and then recombined with the pEF5-FRT-V5 vector (Life Technologies) using LR Clonase (Life Technologies) to create pEF5-GFP-Pdzrn3-FRT. The pEF5-GFP-Pdzrn3-FRT plasmid was used to generate stable isogenic cell lines using the Flp-In system and Flp-In NIH/3T3 cell line (Life Technologies). DNA transfection was performed in 10-cm plates with GenJet In Vitro Transfection Reagent (SL100488; SignaGen Laboratories). Cells that stably integrate the Flp-In constructs were selected using 200μg/ml hygromycin B and expanded. Cell lines expressing phosphoinhibitory or phosphomimetic Pdzrn3, Lnx1, Lnx2, Lnx4, Lnx5, Pdzrn3ΔLNX3H, and Lnx4ΔLNX3H were similarly created by cloning the open reading frame to the C-terminus of GFP in frame and conducting the workflow described above.

Lentivirus-mediated protein overexpression

Recombinant lentiviruses were generated using the pLEX_307 (for all Fzd and DVL constructs) vectors, which uses the EF1 promoter to drive transgene expression. pLEX_307 was a gift from David Root (Addgene plasmid # 41392). The human DVL1 and DVL3 open reading frames were cloned by PCR from a HeLa cell cDNA pool using the following primers; hDVL1 forward, gatcGAATTCCACCatgggcgagaccaagattatctac; hDVL1 reverse, gatcGGCGCGCCTCACATGATGTCCACGAAGAACTC; hDVL3 forward, TTCAGGCCGGCCTACCATGGGCGAGACCAAGATCATCTAC; hDVL3 reverse, GAGGCGCGCCTCACATCACATCCACAAAGAACTC. Similarly, the human DVL2 open reading frame was cloned by PCR from a separate HeLa cDNA pool. The following primers were used:

hDvl2 forward, gcggcggcgGcCgGccaatggcgggtagcagcactggggg; hDVL2 reverse, gtcgacgGgCGcgcctacataacatccacaaagaactcg. The mouse Fzd1 and Fzd7 open reading frames were PCR amplified from Addgene plasmids #42253 and 42259 (gifts from Jeremy Nathans), respectively, using the following primers: mFzd1 forward, gatcggccggcctaccatggctgaggaggcggcgcctag; mFzd1 reverse, gatcggcgcgccTCAGACGGTAGTCTCCCCCTGTTTG; mFzd7 forward, gatcggccggcctaccatgcggggccccggcacggcggcg; mFzd7 reverse, gatcggcgcgccTCATACCGCAGTTTCCCCCTTGC. The mFzd2 open reading frame was cloned via PCR from mouse brain via the following primers: mFzd2 forward, gatcggccggcctaccatgcgggcccgcagcgccctg; mFzd2 reverse, gatcggcgcgccTCACACAGTGGTCTCGCCATGC. The open reading frames of all lentiviral constructs were verified by sequencing. Lentiviruses were packaged and produced in HEK293T cells by co-transfection of the lentiviral vectors with the following packaging plasmids: pRSV-REV, pMD-2-G and pMD-Lg1-pRRE (gifts from Thomas Vierbuchen). 0.75ml or 0.25 ml of the viral supernatants was used to infect GFP-Pdzrn3 reporter cells seeded at 20% confluency in 24-well plates. Puromycin selection (0.002 mg/ml) was carried out for three days. Cells from the viral titer that killed a large proportion of cells (60-90%) were expanded and used for flow cytometry; this ensured that the multiplicity of infection (MOI) is ~1 for all cell lines used in the experiments. This same workflow was utilized to establish GFP-Pdzrn3 and GFP-Kif26b reporters in Kif26a/b dKO cells and Pdzrn3/4 dKO cells, respectively; in lieu of puromycin selection, GFP-positive cells were sorted (MoFlo Astrios Cell Sorter, Beckman Coulter, 488nm laser) and expanded prior to degradation analysis.

Generation of double knockout cell lines

Kif26b knockout cells were previously described (the mutant clone with +1 and -13 frameshifts, generated using sgRNA 1; [2]). This *Kif26b* mutant clone was subject to a second round of mutagenesis to knock out *Kif26a* via CRISPR/Cas9-mediated genome editing according to [28]. Briefly, a modified version of LentiCRISPR V2 (Addgene #52961), in which the puromycin selection cassette was modified with a blasticidin selection cassette, was used to generate lentiviruses expressing small guide RNAs (sgRNAs) with the following sequence: GCTCGTGGAGCTAAAACGAC. In wild-type NIH/3T3 cells, Pdzrn3 was similarly targeted using the following sequence: AGCTGCCCCGCGCGTTGTCG. Following lentivirus infection, cells were passaged for 5 days to allow time for mutagenesis to occur. Cells were subsequently selected using blasticidin (0.002mg/mL) in the case of *Kif26a* mutagenesis, or puromycin (0.002mg/mL) in the case of *Pdzrn3* mutagenesis. Individual cell clones were picked from cell populations targeted with each of these sgRNAs, expanded and then validated by deep sequencing the relevant genomic regions amplified by PCR.

To generate *Pdzrn3/Lnx4* double knockout cells, *Pdzrn3* knockout NIH/3T3 cells were electroporated with CRISPR/Cas9 ribonucleoprotein complexes targeting *Lnx4* using the following gRNA sequence: GCCAACAUCGGCAUGACUCGUUUUAGAGCUAUGCU. 24 hours after electroporation, cells were subjected to fluorescence activated cell sorting (MoFlo Astrios Cell Sorter, Beckman Coulter, 561nm laser) to plate individual cells in 96-well plates; cells were allowed to recover for two weeks prior to expansion and validation of mutations via deep sequencing the relevant genomic regions amplified by PCR.

Recombinant proteins and inhibitors

The following recombinant proteins and drugs were purchased: human/mouse Wnt5a (654-WN-010, R&D Systems); mouse Wnt3a (1324-WN-002, R&D Systems); Wnt-C59 (C7641-2s; Cellagen Technology); epoxomicin (A2606, ApexBio); PYR-41 (B1492, ApexBio); MLN4924 (I50201M, R&D systems); mouse Dkk-1 (5897-DK-010, R&D Systems); IWR-1-endo (B2306, ApexBio); D4476 (A3342, ApexBio); and CHIR99021 (A3011, ApexBio).

Reverse transcription and qPCR

Total RNA was isolated from *Wnt5a* KO MEFs stimulated with rWnt5a for 0, 1, or 6 hours using the RNeasy Plus Mini Kit (Qiagen, #74134), and cDNA was synthesized using QuantiNova Reverse Transcription Kit (Qiagen, #205411), both according to the manufacturer's instructions. The cDNA was the source of input for qPCR, using QuantiNova SYBR Green PCR Kit (Qiagen, #208054). The following qPCR primer pairs were used: mPdzrn3 forward, CTGCGCTACCAGAAGAAGTTC; mPdzrn3 reverse, TCCATCTTGATTGTCCACACAG; mGapdh forward, AGGTCGGTGTGAACGGATTTG; mGapdh reverse, TGTAGACCATGTAGTTGAGGTCA.

Flow cytometry

NIH/3T3 cells were plated at a density of 0.09-0.095M/well in 48-well plates either directly in complete media containing Wnt-C59 (10nM) or in complete media and later changed to complete media containing Wnt-C59 24 hours after plating; all rWnt5a and rWnt3a stimulations and inhibitor pretreatments and treatments were conducted in the presence of Wnt-C59. 48

hours after plating, cells were stimulated with rWnt5a (200ng/mL) or rWnt3a (100ng/mL) for 6 hours. For inhibitor treatments, cells were pretreated with the appropriate inhibitor for 1 hour prior to rWnt5a treatment for 6 hours in the presence of the same inhibitor. Cells were then harvested, resuspended in PBS + 0.5% FBS and analyzed using a flow cytometer (Becton Dickinson FACScan, 488nm laser). Raw data were acquired with CellQuest (Becton Dickinson) and processed in FlowJoX (Treestar, Inc). Processing entailed gating out dead cells, calculation of median fluorescence, percent change of medians, and overlay of histograms. Dose-response curves based on percent change were fitted in Prism (GraphPad Software).

Live cell imaging and 2D cell migration

Pdzrn3/Lnx4 knockout cells, Pdzrn3 WT cells, and Pdzrn3 phosphoinhibitory cells (all NIH/3T3 cells) were cultured in complete media or in Wnt-C59 containing media for 72 hours (for experiments involving rWnt5a stimulation). Cells were subsequently plated at a density of approximately 0.01M cells per 24 well plate for live cell imaging. rWnt5a treatment was initiated immediately prior to imaging. Multipoint time lapse images were collected every 10 minutes for 20 hours on an Andor Dragonfly spinning disc confocal system in a humidity controlled chamber (37C). Cell migration was tracked using the ImageJ manual tracking plugin, and cells that divided, moved out of frame, or died were excluded from further analysis. Total distance traversed was calculated using the ImageJ Chemotaxis tool plugin. Statistical analysis was done using Prism 8 (GraphPad Software).

Results

Large-scale proteomic screen identifies the E3 ubiquitin ligase Pdzrn3 as a downstream regulatory target of Wnt5a-Ror signaling

To profile both early and late molecular events driven by Wnt5a-Ror signaling, we conducted a large-scale proteomic screen in which primary E12.5 *Wnt5a* KO MEFs [2, 10, 13] were acutely stimulated with purified recombinant Wnt5a (rWnt5a) for 0, 1 or 6 hours, and then used quantitative tandem mass tag (TMT) mass spectrometry to globally assess changes in the abundance and phosphorylation state of cellular proteins over time (Figure 1A; see Dataset S1 for full list) [25]. Two independent replicates of *Wnt5a* KO MEF cultures were analyzed for rigor and reproducibility. Potential proteins of interest were defined as tryptic peptides or phospho-tryptic peptides that exhibited (1) a negative or positive change of > 1.5-fold in abundance and (2) a change with a p-value < 0.05 across the two replicates.

Based on these criteria, our top candidate was Pdzrn3, an E3 ubiquitin ligase which exhibited significant changes in both steady-state protein abundance and phosphorylation state after rWnt5a stimulation. Although 1 hour of rWnt5a stimulation did not yield any detectable changes, after 6 hours of rWnt5a stimulation we observed that Pdzrn3 abundance was significantly downregulated by 1.72-fold (p= 0.013, Figure 1B, 1C and 1F Table S1). Additionally, we identified multiple phospho-tryptic peptides derived from two different regions of Pdzrn3 that exhibited significant changes after rWnt5a stimulation (Figure 1D and 1E). A phospho-tryptic peptide containing S843 and S845 (dotted line, Figure 1G) and another one containing T955, T956 and S962 (dashed line, Figure 1G) both showed an initial increase at 1 hour, followed by a decrease at 6 hours. Likewise, a third phospho-tryptic peptide containing

S775 (dot dashed line, Figure 1G), though not a “hit” based on its significance value (p=0.076), also exhibited a similar pattern of change. Lastly, a phospho-tryptic peptide containing S845 (solid line, Figure 1G) decreased gradually after 1 hour and more extensively after 6 hours. Importantly, all phospho-tryptic peptides decreased by 6 hours to a similar extent as that of the non-phosphorylated tryptic peptide (Figure 1F). This overall pattern thus raised the hypothesis that Wnt5a signaling first induces the phosphorylation of Pdzrn3 at 1 hour, followed by downregulation of Pdzrn3 protein abundance at 6 hours, and these two biochemical events are kinetically and mechanistically coupled.

In addition to Pdzrn3, the proteomic screen also identified other known components of the Wnt5a-Ror signaling pathway (Table S1). At both the 1 hour and 6 hour timepoints, a phospho-tryptic peptide from Kif26b was scored as a “hit” (1.70- and 2.03-fold decrease, respectively). At the 6 hour timepoint, a phospho-tryptic peptide from CK1 isoform gamma-3 was also scored as a “hit” (1.52-fold increase). Moreover, a phospho-tryptic peptide from Dvl2 exhibited a 1.49-fold increase in abundance after 6 hours of rWnt5a stimulation. The identification of these previously described Wnt5a signaling targets further validates the selectivity and sensitivity of the proteomic screening approach. Other hits of interest include Irf2bpl, another E3 ubiquitin ligase which has been shown to reduce canonical Wnt signaling in gastric cancer [29] as well as several proteins with connections to the cytoskeleton, such as Cttnbp2nl [30], Jmy [31-33], Cit [34], Svil [35, 36], Ppfibp1 [37], Marcks [38, 39], Cald1 [40-42], and Map2 [43, 44] or tissue morphogenesis, including Fam193a and Nhs1 [45, 46].

To independently confirm that Pdzrn3 abundance is indeed regulated by Wnt5a signals, we generated rabbit polyclonal antibodies against Pdzrn3 and used western blotting to analyze the steady-state cellular levels of Pdzrn3 after rWnt5a stimulation. Consistent with our proteomic screening results, we observed that the abundance of Pdzrn3 significantly decreased after 6 hours of rWnt5a stimulation (Figure 2A and 2B). This change parallels other previously

described responses of Wnt5a-Ror signaling, including increased phosphorylation of Ror1, Ror2 and Dvl2, and decreased Kif26b abundance (Figure 2A and 2B) [2, 13].

To test whether Ror receptors are required for Wnt5a signaling to Pdzrn3, we utilized conditional Ror receptor family knockout MEFs derived from E12.5 *Ror1*$^{fl/fl}$*; Ror2*$^{fl/fl}$*; CAG-CreER* embryos. These MEFs undergo robust autocrine/paracrine Wnt5a-Ror signaling without exogenous Wnt5a [13]. We treated cells with 4-hydroxytamoxifen (4OHT) to induce CreER-mediated deletion of the *Ror1*$^{fl/fl}$ and *Ror2*$^{fl/fl}$ alleles. We observed that loss of Ror receptor expression significantly increased Pdzrn3 levels, which correlated with decreased Dvl2 phosphorylation and increased in Kif26b abundance (Figure 2C and 2D). Thus, these results indicate that Ror receptors are required to facilitate Wnt5a-driven regulation of Pdzrn3 abundance, which is a genuine endogenous Wnt5a-Ror signaling event.

To test whether Wnt5a regulation of Pdzrn3 protein abundance also occurs transcriptionally, we treated *Wnt5a* knockout MEFs with rWnt5a for 1 or 6 hours and analyzed the levels of *Pdzrn3* mRNA by reverse transcription-quantitative polymerase chain reaction (RT-qPCR). Unlike Pdzrn3 protein, *Pdzrn3* transcripts did not change significantly after 1 or 6 hours of rWnt5a stimulation (Figure 2E). Thus, Wnt5a-Ror signaling regulates Pdzrn3 protein abundance through a post-transcriptional mechanism. Overall, these experiments establish that regulation of Pdzrn3 protein abundance is a physiological response of Wnt5a-Ror signaling.

A non-canonical Wnt signaling cascade involving Fzd, Dvl, CK1, GSK3 and the ubiquitin-proteasome system regulates Pdzrn3 degradation

To dissect the molecular mechanisms mediating Wnt5a regulation of Pdzrn3, we designed a flow cytometry-based reporter in which we stably expressed GFP-Pdzrn3 in NIH/3T3

cells (referred to as WRP reporter cells for Wnt5a-Ror-Pdzrn3). Consistent with our observations in primary *Wnt5a* knockout MEFs, treating WRP reporter cells with rWnt5a for 6 hours, under conditions in which endogenous Wnt signaling is inhibited with the small molecule PORCN inhibitor Wnt-C59, resulted in a significant downregulation of GFP-Pdzrn3 reporter signal, thereby demonstrating the fidelity of this reporter assay (Figure 3A). Moreover, we established that a saturable dose-dependent relationship exists between rWnt5a concentrations and GFP-Pdzrn3 downregulation, with a calculated EC_{50} of 77.1 ng/mL, which is similar to other Wnt induced responses (Figure 3B) [13, 47-51].

We next used WRP reporter cells to investigate the biochemical nature of Pdzrn3 downregulation. We pharmacologically tested the role of the ubiquitin-proteasome system (UPS) in Pdzrn3 downregulation as the UPS is a major regulatory pathway involved in many signaling systems and our previous study demonstrated that it is required for Wnt5a-dependent degradation of Kif26b [2]. We treated WRP cells with a panel of small-molecule inhibitors that block different components of the UPS: epoxomicin, which targets the proteasome [52]; PYR-41, which targets the ubiquitin-activating enzyme E1 [53]; and MLN4924, which targets Cullin E3 ligases [54]. Each of these drugs significantly inhibited Wnt5a-dependent Pdzrn3 downregulation (Figure 3C), indicating that the UPS and the Cullin family of E3 ligases are required for Wnt5a-dependent degradation of Pdzrn3.

To test whether Wnt5a-Ror-dependent Pdzrn3 degradation occurs via non-canonical Wnt signaling mechanisms independent of the Wnt/β-catenin pathway, we treated WRP reporter cells with Dkk-1 and IWR-1-endo, which block canonical Wnt/β-catenin signaling at the receptor and destruction complex level, respectively [55-57]. We observed that neither inhibitor blocked Wnt5a-induced degradation of GFP-Pdzrn3, indicating that this regulation occurs independently of the canonical Wnt pathway (Figure 3D). Similarly, we observed that the prototypic canonical Wnt ligand, rWnt3a, can also drive degradation of Pdzrn3, but this regulation likely occurs

through a non-canonical mechanism as it is also insensitive to Dkk1-1 and IWR-1 treatment (Figure S1). This finding is similar to what we previously reported for Kif26b and suggests that Wnt3a can signal non-canonically in some contexts or, alternatively, that rWnt3a can exhibit promiscuous activity within our experimental setting [2]. Further, we noted that both inhibitors, in the absence of either rWnt5a or rWnt3a, slightly increased the basal fluorescence of the GPF-Pdzrn3 reporter; the mechanism behind this regulation is currently unclear. Collectively, these results demonstrate that Wnt5a-Ror-Pdzrn3 signaling is a bona fide non-canonical Wnt pathway.

We next investigated if other established Wnt signaling mediators are also involved in Pdzrn3 degradation. We focused on the Fzd1, Fzd2, and Fzd7 subfamily of Fzd receptors and all three members of the family of Dvl scaffolding proteins based on their emerging connection to Robinow syndrome [14-20]. We overexpressed mouse Fzd1, Fzd2, or Fzd7 and human DVL1, DVL2 or DVL3 in WRP reporter cells via lentivirus-mediated transduction and observed that overexpression of each Fzd and DVL protein mimicked the effect of rWnt5a by decreasing the WRP reporter signal significantly, whereas overexpression of the Myc epitope tag as a negative control did not decrease WRP reporter fluorescence (Figure 3E and 3F). These findings suggest that Fzd and DVL family proteins function downstream of Wnt5a to regulate Pdzrn3 degradation.

Beyond Fzd and DVL proteins, several kinases are known to be involved in both canonical and non-canonical Wnt signaling; specifically, GSK3 and CK1 have been reported to phosphorylate Ror receptors (Yamamoto et al., 2007; Grumolato et al., 2010), and Dvl2 and Dvl3 [47, 58], respectively. To address whether these phosphorylation events are required for Wnt5a-dependent regulation of Pdzrn3, we treated WRP reporter cells with small-molecule inhibitors targeting CK1 (D4476) or GSK3 (CHIR99021). Both treatments significantly reduced

Wnt5a-induced GFP-Pdzrn3 degradation (Figure 3G), thus demonstrating a functional role of both CK1 and GSK3 in Wnt5a-Ror-Pdzrn3 signal transduction.

We previously reported that the atypical kinesin Kif26b is another downstream regulatory target of Wnt5a-Ror signaling [2, 59]. Because Pdzrn3 and Kif26b are both regulated by the Wnt5a-Ror-Dvl axis, we sought to define the epistatic relationship between Pdzrn3 and Kif26b (i.e., whether these two proteins functions in a linear cascade or in parallel branches). To distinguish between these possibilities, we used CRISPR/Cas9 gene editing to generate cells lacking Kif26b and its homolog Kif26a (Kif26a/b dKO cells; Figure S2), which we previously showed is also a target of Wnt5a-Ror signaling [59], and tested whether the GFP-Pdzrn3 reporter is still degraded with rWnt5a stimulation. We observed that genetic deletion of *Kif26a* and *Kif26b* did not hinder rWnt5a-induce GFP-Pdzrn3 degradation; however, there was a slight but significant increase in GFP-Pdzrn3 degradation in the Kif26a/b dKO cells that was reversed with re-expression of Kif26b (Figure 3H). In the converse experiment, we again used CRISPR/Cas9 to generate cells lacking *Pdzrn3* and its homolog *Lnx4* (Pdzrn3/4 dKO cells; Figure S2), which is structurally similar to Pdzrn3 (see Figure 5A). We observed that rWnt5a-induced GFP-Kif26b degradation still largely occurred (Figure 3I). However, loss of *Pdzrn3* and *Lnx4* did slightly reduce GFP-Kif26b degradation, which was alleviated upon re-expression of Pdzrn3. Taken together, these data indicate that Wnt5a regulation of Pdzrn3 does not require Kif26b and vice versa, suggesting that these two targets are epistatically parallel to each other. However, there may be some degree of cross-talk through a currently unknown mechanism.

Pdzrn3 phosphorylation is required for its degradation and serves as a molecular switch to modulate Wnt5a-driven cell migration

We next sought to define the structural elements within Pdzrn3 required for its degradation and explore the possible role of phosphorylation in this regulation. Pdzrn3 is a cytosolic protein that contains an N-terminal RING domain that confers its putative E3 ligase activity, two internal PDZ domains that mediate protein-protein interactions, a C-terminal LNX3 homology (LNX3H) domain with no described function, and a C-terminus PDZ domain binding motif (Figure 4A) [3, 23]. The six phosphorylation sites identified in our phosphoproteomic analysis cluster into two groups: Group 1 phosphorylation sites (S775, S843, and S845) reside within the linker region between the second PDZ domain and the LNX3H domain, and Group 2 phosphorylation sites (T955, T956, and S962) are located within the LNX3H domain itself. Interestingly, while phosphorylation of Group 1 sites showed only a slight increase at 1 hour and then decreased after 6 hours (compare Figure 1F with dot dashed, dotted, and solid lines in 1G), phosphorylation of Group 2 sites increased significantly after 1 hour of rWnt5a stimulation, prior to Pdzrn3 degradation, and then decreased after 6 hours of rWnt5a stimulation (compare Figure 1F with dashed line in 1G), which raised the hypothesis that phosphorylation of these sites, particularly those in Group 2, may be required for Wnt5a-regulation of Pdzrn3 degradation.

To test this hypothesis, we systematically generated phosphoinhibitory mutants (T or S to A substitutions) of all three sites in either Group 1 or Group 2 and examined rWnt5a-induced Pdzrn3 degradation. We observed that while mutation of Group 1 sites had no effect on rWnt5a-induced Pdzrn3 degradation, mutation of Group 2 sites strongly abolished GFP-Pdzrn3 degradation (Figure 4B). To further dissect which specific sites within Group 2 are required for Pdzrn3 degradation, we individually mutated each of the three sites and observed that any of the three single mutations significantly reduced rWnt5a-induced GFP-Pdzrn3 degradation (Figure 4C). To further test whether phosphorylation of these three residues is sufficient to mimic Wnt5a-induced Pdzrn3 degradation, we generated a triple phosphomimetic mutant (T or

S to E) and observed that these mutations, in the absence of exogenous rWnt5a stimulation, constitutively decreased the Pdzrn3 reporter signal to a level comparable to that of wild-type Pdzrn3 upon rWnt5a stimulation, and no further degradation was induced by rWnt5 stimulation (Figure 4D). These experiments establish that Wnt5a-dependent phosphorylation of the three Group 2 sites in the LNX3H domain is both required and sufficient to drive Pdzrn3 degradation.

We next investigated the cell biological consequences of Pdzrn3 phosphorylation and degradation. Since we previously demonstrated that Wnt5a-Ror signaling can modulate cell migration through regulation of Kif26b abundance [2], we wondered if Wnt5a-Ror regulation of effector abundance might be a general paradigm through which Pdzrn3 is similarly controlled. This possibility seemed particularly salient given that others have demonstrated that Pdzrn3 can function as a promigratory factor in cell morphogenetic events [23, 24]. Thus, we hypothesized that Pdzrn3 abundance might ultimately serve to regulate cell migration.

To evaluate our hypothesis, we used real-time single cell tracking to first assess the role of Pdzrn3 itself on cell migration. We took advantage of the Pdzrn3/4 dKO cells, which provided a platform in which we could directly compare the function and regulation of wild-type Pdzrn3 (Pdzrn3 WT cells) to Group 2 phosphoinhibitory site mutant Pdzrn3 (Pdzrn3 phosphoinhibitory cells) without potential influence from the structural homolog Lnx4. First, we observed that cells expressing WT Pdzrn3 cells migrated significantly greater distances than Pdzrn3/4 dKO cells (Figure 4E and 4F), thereby confirming that Pdzrn3 functions as a promigratory factor [23, 24]. Interestingly, we noticed that Pdzrn3 phosphoinhibitory cells migrated significantly further than both Pdzrn3/4 dKO cells and Pdzrn3 WT cells, suggesting that inhibiting Pdzrn3 phosphorylation could potentially enhance cell migration.

We next assayed for the influence of the Wnt5a-Ror-Pdzrn3 axis on cell migration. We observed that while rWnt5a stimulation had no effect on the distance traveled by Pdzrn3/4 dKO cells, it strongly reduced the distance travelled by WT Pdzrn3 cells (Figure 4G and 4H).

Importantly, this Wnt5a effect on cell migration was completely abolished in Pdzrn3 phosphoinhibitory cells. Together, these results establish that phosphorylation-dependent degradation of Pdzrn3 is required for Wnt5a to modulate cell migration.

The C-terminal LNX3H domain functions as a Wnt5a-responsive domain to regulate protein abundance of Pdzrn3 and related homologs

Pdzrn3 belongs to the Ligand of Numb-X (Lnx) family of E3 ligases (Figure 5A). Like Pdzrn3, each Lnx family member possesses an N-terminal RING domain (except Lnx5) and one to four internal PDZ binding domains. Furthermore, Lnx4 and Lnx5 each additionally possess a C-terminal LNX3H domain and a C-terminus PDZ domain binding motif [3, 23]. Notably, the LNX3H domains of Lnx4 and Lnx5 also contain the Group 2 phosphorylation sites found in Pdzrn3 (Figure 5B). Based on our finding that these sites regulate Wnt5a-induced Pdzrn3 degradation, we hypothesized that Lnx4 and possibly Lnx5 may also be regulated by Wnt5a signals and that the LNX3H domain may function as a Wnt5a-responsive domain. To test this hypothesis, we generated reporter cell lines stably expressing GFP-Lnx1, -Lnx2, -Lnx4, or -Lnx5 fusion proteins and assessed their ability to undergo degradation in response to rWnt5a stimulation. As predicted, when stimulated with rWnt5a, GFP-Lnx1 and GFP-Lnx2 did not degrade, whereas GFP-Lnx4 exhibited a modest but significant degradation response (Figure 5C). Curiously, GFP-Lnx5 did not degrade after rWnt5a stimulation (Figure 5C). We therefore conclude that, like Pdzrn3, Lnx4 is also a target of Wnt5a signaling. Moreover, the Wnt5a responsiveness of Lnx family members correlates with the presence of both LNX3H and RING domains, as the primary difference between Lnx5 and Pdzrn3/Lnx4 is the N-terminal RING domain.

To further test the idea that the LNX3H domain might act as a Wnt5a-responsive domain, we generated truncation mutants of GFP-Pdzrn3 and GFP-Lnx4 lacking this domain. We observed that rWnt5a-induced degradation was completely abolished in these mutant cells (Figure 5D and 5E). In addition, the steady-state fluorescence of unstimulated reporter cells was also substantially reduced (Figure 5D and 5E). These observations suggest that the LNX3H domain of Pdzrn3 and Lnx4 acts not only as a Wnt5a-responsive domain but may do so by regulating overall protein stability, possibly by inhibiting the N-terminal RING domain to prevent auto-ubiquitination and degradation. While the mechanism by which the LNX3H domain responds to Wnt5a signals remains unknown and is beyond the scope of this study, our finding defines the LNX3H domain as a bona fide Wnt5a-responsive domain that regulates Pdzrn3 and Lnx4 stability.

Discussion

In this study, we conducted a whole proteome-scale mass spectrometry screen in primary *Wnt5a* knockout MEFs to identify early and late downstream events driven by Wnt5a-Ror signaling and identified the E3 ubiquitin ligase Pdzrn3 as a regulatory target. Activation of Wnt5a-Ror signaling results in the regulation of Pdzrn3 abundance in a β-catenin-independent manner mediated by a signaling cascade involving Fzd receptors, Dvl scaffolding proteins, GSK3, and CK1 that culminates in UPS-dependent degradation of Pdzrn3. We observed that Kif26b is not required for Wnt5a-mediated Pdzrn3 degradation nor is Pdzrn3 required for Kif26b degradation, although there is some potential cross-talk between the two effectors (Figure 5F). Importantly, we determined that the Wnt5a-Ror-Pdzrn3 signaling axis serves to modulate cell migration. Wnt5a-induced Pdzrn3 phosphorylation at three residues on its C-terminal LNXH3 domain is required for its subsequent degradation, which is also required for Wnt5a-Ror signaling to reduce cell migration in NIH/3T3 cells. Thus, the biochemical changes observed in our Wnt5a-Ror signaling cascade connect to a distinct cell biological behavior. Finally, we noted that truncation of the LNX3H domain results in constitutive destabilization of Pdzrn3 even in the absence of Wnt5a, suggesting that the LNX3H domain may function as both a Wnt5a-responsive domain and an intrinsic regulator of Pdzrn3 stability. From these findings, we propose that the LNX3H domain of Pdzrn3 may function to prevent Pdzrn3 auto-ubiquitination and self-degradation mediated by its RING domain. Prior to Wnt5a stimulation, Pdzrn3 may adopt a “closed” conformation as its C-terminal PDZ domain binding motif interacts with one of its internal PDZ domains to block its E3 ligase activity. Upon Wnt5a stimulation, Pdzrn3 is C-terminally phosphorylated on its LNX3H domain by an unidentified kinase to switch the “closed” conformation into an “open” conformation, allowing Pdzrn3 to catalyze the ubiquitination of its substrates and itself. Notably, this “opened/closed” conformation paradigm has been previously

described in other components of Wnt signaling, including Axin and Dvl [60-62]. Conceivably, the equilibrium between the “closed” and “open” Pdzrn3 could be modulated through either intramolecular interactions within a single Pdzrn3 molecule or through intermolecular interactions between Pdzrn3 dimers or multimers. Future detailed biochemical experiments are required to directly evaluate these possibilities as well as assess whether Pdzrn3 is phosphorylated by a kinase known to be involved in non-canonical Wnt signaling (e.g., CK1 or GSK3) or another one, as well as how the kinase itself is regulated by Wnt5a-Ror signaling.

It is well established that several core components of canonical Wnt signaling (e.g., β-catenin, adenomatous polyposis coli (APC), and Axin) are regulated by proteasomal degradation [57, 63, 64]. The present work, together with other recent studies, establishes that multiple effectors of non-canonical Wnt pathways, including Pdzrn3, Kif26a, Kif26b and Syndecan4, are also subject to regulation by the ubiquitin-proteasome pathway [2, 59, 65]. Collectively, these findings suggest that regulated proteolysis to tune the abundance of downstream effectors and thus, signaling outcomes, may be a conserved paradigm common to both canonical and non-canonical Wnt signaling pathways. This concept will continue to evolve as additional Wnt signaling components are characterized.

While our study addresses the biochemical regulation of Pdzrn3 by Wnt5a-Ror signaling, previous work supports the physiological importance of Pdzrn3 in non-canonical Wnt signaling. One particularly notable study focuses on the role of Pdzrn3 in vascular morphogenesis during embryonic development [23]. Here, Sewduth et al. identified a binding interaction between Pdzrn3 and Dvl3 via a yeast 2-hybrid screen and subsequent co-immunoprecipitation, going on to demonstrate that loss of Pdzrn3 *in vivo* results in increased vasculature disorganization in both the embryonic yolk sac and developing mouse brain. Furthermore, deletion of Pdzrn3 reduces persistent directional migration in HUVECs *in vitro*. Importantly, our findings further build upon this model by demonstrating that Wnt5a-Ror signaling modulates cell migration

through Pdzrn3 by triggering its phosphorylation and subsequent degradation. Our study, in conjunction with existing Pdzrn3 literature, indicates that changes in Pdzrn3 abundance results in non-canonical Wnt signaling defects that can be observed at the molecular, cell, and organismal levels, supporting a physiologically relevant role for Pdzrn3 in Wnt5a-dependent morphogenetic regulation.

Although the substrates ubiquitinated by Pdzrn3 (or Pdzrn3-containing E3 ligase complexes) during active Wnt5a-Ror signaling remain unclear, previous work examining the role of Pdzrn3 at the neuromuscular junction may provide a clue. Lu et al. reported that PDZRN3 regulates MuSK (Muscle-Specific Kinase) receptor expression levels at the surface of myotubes adjacent to the neuromuscular junction through ubiquitination, leading to their endocytosis from the cell surface and downregulation of signaling [22]. Given the high degree of homolog between MuSK and ROR1/ROR2 receptors [66-68], it is possible that Pdzrn3 may similarly regulate Ror receptor trafficking to limit their surface availability; by inducing the degradation of Pdzrn3, Wnt5a may in turn increase Ror receptor levels on the cell surface. Alternatively, Pdzrn3 might ubiquitin-label Ror1 and Ror2 for trafficking purposes to enhance signaling. Identifying the physiologically relevant substrates of Pdzrn3 will be crucial to test this hypothesis in future studies.

The similar means by which Pdzrn3 and Kif26b are regulated indicate that the Wnt5a-Ror pathway has evolved multiple effectors to exert appropriate biological outcomes. Pdzrn3 and Kif26b are regulated by highly similar signaling cascades that utilize known Wnt signaling components, including Ror receptors, Dvl scaffolding proteins, and GSK3, culminating in UPS-dependent degradation of both effectors. Further, both Pdzrn3 and Kif26b perform related functions at the cell behavioral level. Here, we describe the mechanism by which Wnt5a-Ror signaling utilizes Pdzrn3 phosphorylation and degradation to modulate NIH/3T3 cell migration. This paradigm is remarkably similar to the one we reported previously, wherein Wnt5a-mediated

Kif26b degradation also results in decreases in cell migration as assayed via wound closure in scratch assays [2]. Our genetic epistasis experiments indicate that Pdzrn3 and Kif26b reside neither upstream nor downstream of each other but do influence each other's Wnt5a-driven degradation, further suggesting that these two components work in parallel to properly execute signaling functions.

However, it is curious that neither *PDZRN3* nor *KIF26B* mutant mice exhibit the systemic tissue truncation phenotypes of *WNT5A* and *ROR1; ROR2* double mutants. *KIF26B* mutant mice display kidney agenesis/hypoplasia and primordial germ cell migration phenotypes [2, 69] while *PDZRN3* mutants display the vascular defects described above. These distinct tissue specific phenotypes of *KIF26B* and *PDZRN3* imply that multiple downstream signaling effectors likely exist to carry out the many biological functions of the pathway. Alternatively, there many be compensatory effects driven by closely related homologs (e.g., Lnx4 and Kif26a). These different phenotypic outcomes necessitate the evaluation of a *PDZRN3; KIF26B* double mutant mice in addition to further identification of potential Wnt5a-Ror signaling targets.

The lack of quantitative and reliable readouts for Wnt5a-Ror signaling has been a major limitation in the field. We leveraged our discovery of Pdzrn3 and its regulation by Wnt5a-Ror signaling to develop a new flow cytometry-based reporter that enables sensitive and quantitative detection of pathway activity in live cells. Beyond dissecting the mechanisms that mediate Pdzrn3 degradation, this reporter assay could also be utilized to interrogate other biochemical steps in the pathway upstream of Pdzrn3, understand various disease-associated mutations, and serve as an important platform for high throughput screening of small molecules that target Wnt5a-Ror-driven developmental disorders and cancers.

Figures

Figure 1. Identification of the E3 ubiquitin ligase Pdzrn3 as a downstream regulatory target of Wnt5a-Ror signaling. A) Workflow of whole cell proteomics screen. Primary MEF cultures were generated from *Wnt5a* knockout E12.5 mouse embryos and stimulated with rWnt5a (0.1μg/mL) for 0, 1, or 6 hours. After rWnt5a stimulation, whole cell lysates were collected and processed for LC/MS3 tryptic/phospho-tryptic peptide identification and quantification. The rWnt5a stimulation and proteomic analysis were conducted in two independent technical replicates. **B and C**) Volcano plots showing changes in the abundance of detected tryptic peptides in response to rWnt5a stimulation (0.1μg/mL) after 1 hour (B) or 6 hours (C). The abundance of a tryptic peptide from Pdzrn3 (orange dots) changed strongly after 6 hours of rWnt5a stimulation. **D and E)** Volcano plots showing changes in the abundance of detected phospho-tryptic peptides after 1 hour (D) or 6 hours (E) of rWnt5a stimulation (0.1μg/mL). Five phosphosites from Pdzrn3 (S843, S845, T955, T956, and S962) grouped in two clusters within the protein were detected and exhibited distinct patterns of change after rWnt5a stimulation (orange dots). **F and G)** Line plots showing Wnt5a-induced changes in the abundance of individual tryptic (F) or phospho-tryptic peptides (G) from Pdzrn3 after 1 hour or 6 hours of rWnt5a stimulation. A sixth phosphor-tryptic peptide site (S775) in did not pass the initial filter (p-value = 0.076), but also showed clear changes with rWnt5a stimulation. Error bars represent ± SEM calculated from two technical replicates.

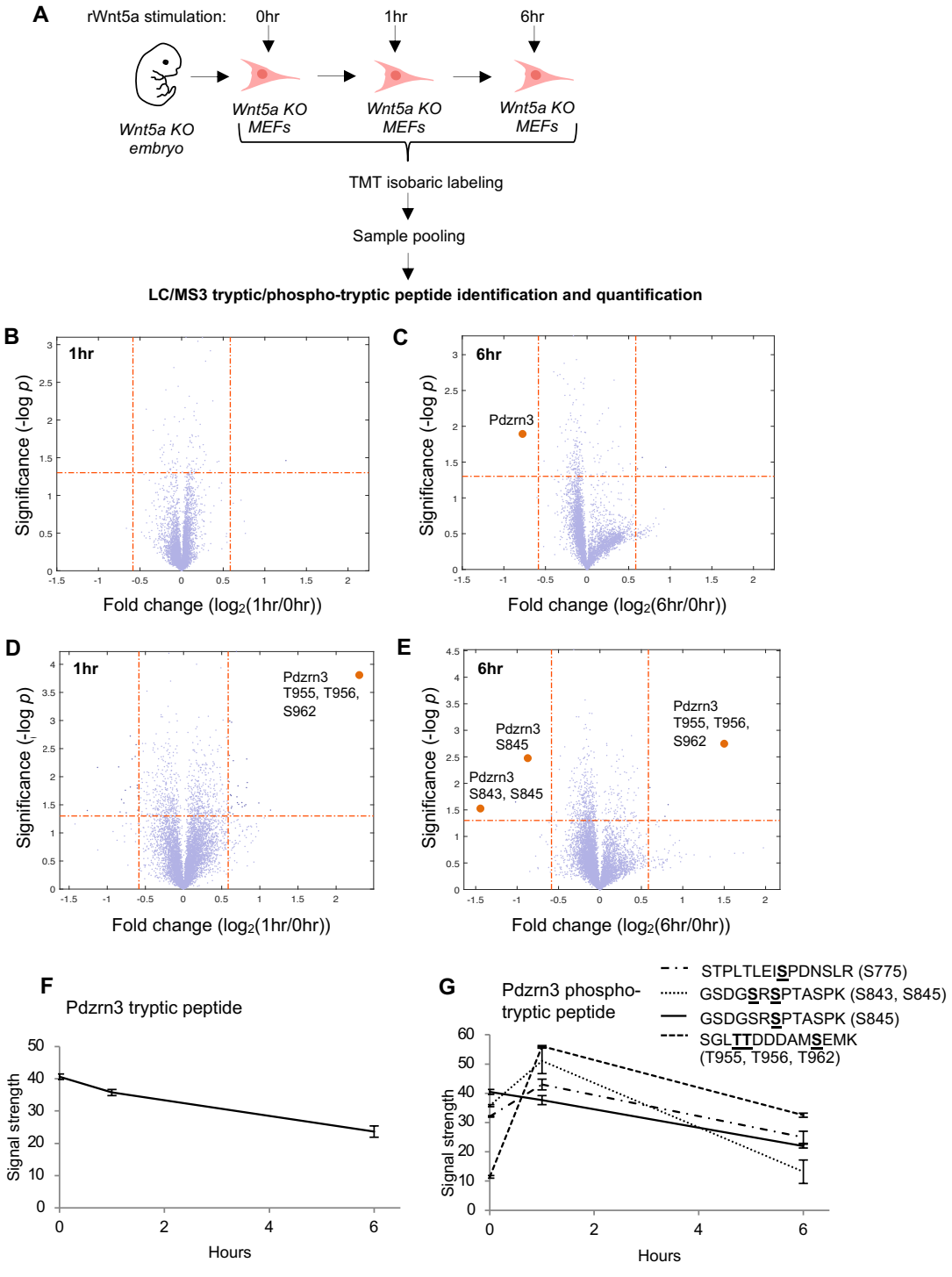
A
rWnt5a stimulation:
0hr
1hr
6hr
Wnt5a KO embryo
Wnt5a KO MEFs
Wnt5a KO MEFs
Wnt5a KO MEFs
TMT isobaric labeling
Sample pooling
LC/MS3 tryptic/phospho-tryptic peptide identification and quantification
B
1hr
Significance (-log p)
Fold change (log2(1hr/0hr))
C
6hr
Pdzrn3
Significance (-log p)
Fold change (log2(6hr/0hr))
D
1hr
Pdzrn3
T955, T956,
S962
Significance (-log p)
Fold change (log2(1hr/0hr))
E
6hr
Pdzrn3
S845
Pdzrn3
S843, S845
Pdzrn3
T955, T956,
S962
Significance (-log p)
Fold change (log2(6hr/0hr))
F
Pdzrn3 tryptic peptide
Signal strength
Hours
G
Pdzrn3 phospho-
tryptic peptide
STPLTLEISPDNSLR (S775)
GSDGSRSPTASPK (S843, S845)
GSDGSRSPTASPK (S845)
SGLTTDDDAMSEMK
(T955, T956, T962)
Signal strength
Hours

Figure 2. Validation of Pdzrn3 as a downstream regulatory target of Wnt5a-Ror signaling. **A)** Western blot showing downregulation of Pdzrn3 steady-state levels in response to rWnt5a stimulation. Primary *Wnt5a* knockout MEF cultures were stimulated with rWnt5a (0.2μg/mL) for 0, 1, or 6 hours, and membranes were blotted with antibodies against Kif26b, Pdzrn3, Ror1, Ror2, Dvl2 and Tubulin. **B)** Quantification of (A). **C)** Western blots showing the requirement of endogenous Ror receptors for Pdzrn3 regulation. Protein lysates were analyzed by western blotting using antibodies against Kif26b, Pdzrn3, Ror1, Ror2, Dvl2 and Tubulin. **D)** Quantification of (C). **E)** Plot showing the effect of Wnt5a stimulation on *Pdzrn3* transcript levels. Primary *Wnt5a* knockout MEFs were stimulated with rWnt5a (0.2μg/mL) for 0, 1, or 6 hours, and the relative abundance of *Pdzrn3* mRNA were determine by RT-qPCR. Error bars represent ± SEM. P-values: *=p<0.05, **=p<0.01, ***=p<0.001.

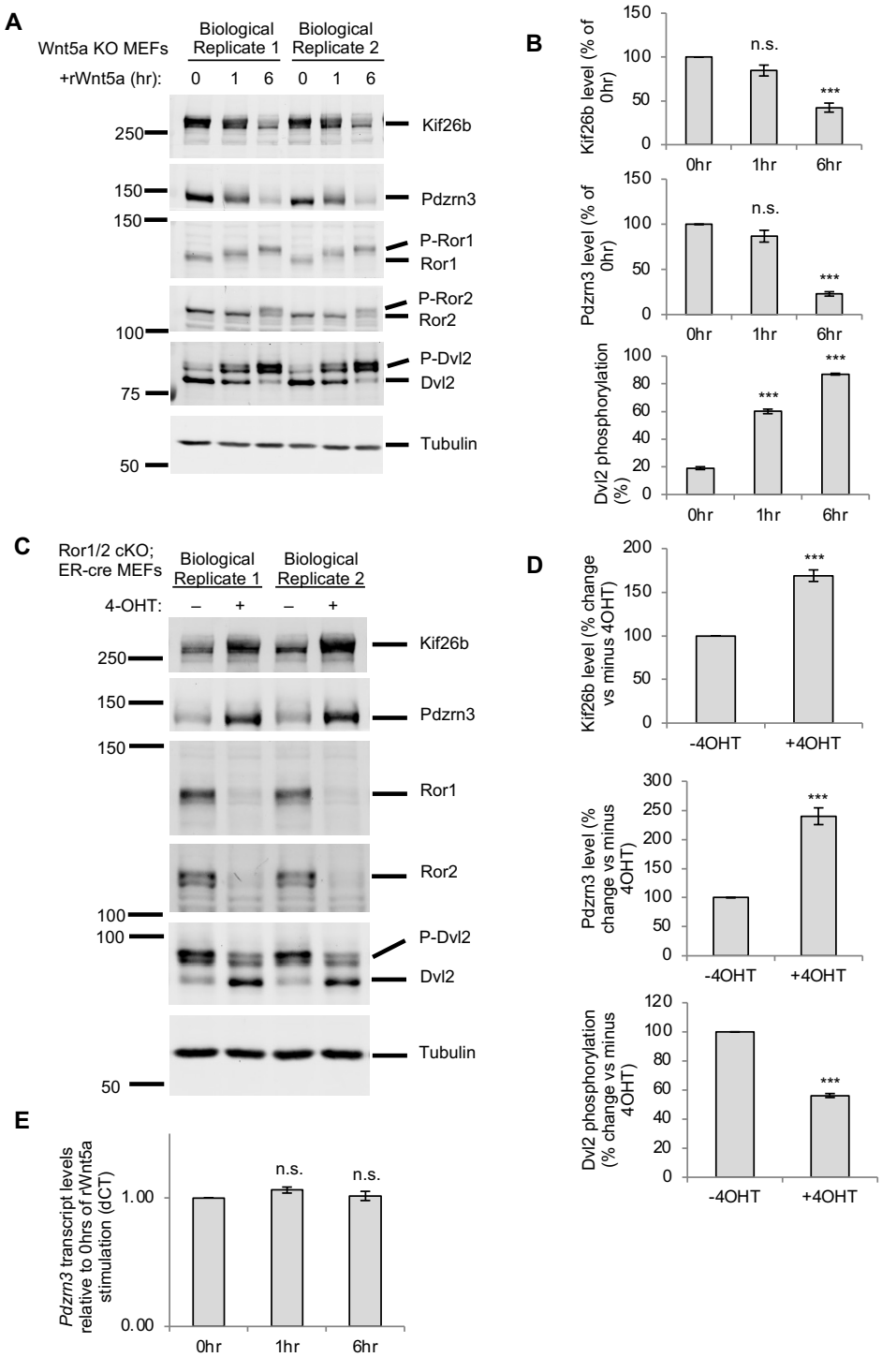
A
Wnt5a KO MEFs
Biological Replicate 1
Biological Replicate 2
+rWnt5a (hr):
0 1 6 0 1 6
250
150
150
100
75
50
Kif26b
Pdzrn3
P-Ror1
Ror1
P-Ror2
Ror2
P-Dvl2
Dvl2
Tubulin
B
Kif26b level (% of 0hr)
Pdzrn3 level (% of 0hr)
Dvl2 phosphorylation (%)
n.s.
***
0hr 1hr 6hr
C
Ror1/2 cKO; ER-cre MEFs
Biological Replicate 1
Biological Replicate 2
4-OHT: – + – +
250
150
150
100
100
50
Kif26b
Pdzrn3
Ror1
Ror2
P-Dvl2
Dvl2
Tubulin
D
Kif26b level (% change vs minus 4OHT)
Pdzrn3 level (% change vs minus 4OHT)
Dvl2 phosphorylation (% change vs minus 4OHT)
-4OHT +4OHT
E
Pdzrn3 transcript levels relative to 0hrs of rWnt5a stimulation (dCT)
1.00
0.00
n.s.
0hr 1hr 6hr

Figure 3. A signaling cascade links non-canonical Wnt5a-Ror signaling to Pdzrn3 degradation. A) Representative histogram showing the effect of rWnt5a treatment on NIH/3T3 GFP-Pdzrn3 (WRP) reporter cells. WRP cells were treated with rWnt5a (0.2μg/mL) for 6 hours, and GFP-Pdzrn3 fluorescence was measured by flow cytometry. **B)** Dose-response curve showing GFP-Pdzrn3 downregulation as a function of rWnt5a concentration in the WRP reporter assay. **C)** Quantification of the effects of proteasome inhibitor (epoxomicin, 10μM), ubiquitin-activating enzyme E1 inhibitor (PYR41, 10μM) and Cullin inhibitor (MLN4924, 10μM) on rWnt5a-induced Pdzrn3 downregulation in WRP reporter cells. **D)** Quantification of the effects of canonical Wnt inhibitors, Dkk-1 (2μg/μL) and IWR-1-endo (10μM) on rWnt5a-induced Pdzrn3 degradation in the WRP reporter cells. **E)** Quantification of the effects of Fzd1, Fzd2 and Fzd7 overexpression on the median fluorescence of WRP reporter cells. **F)** Quantification of the effects of DVL1, DVL2 and DVL3 overexpression on the median fluorescence of WRP reporter cells. **G)** Quantification of the effects of CK1 (D4476, 100μM) and GSK (CHIR99021, 100μM) inhibitors on rWnt5a-induced Pdzrn3 degradation in the WRP reporter cells. **H)** Quantification of the effect of genetically ablating *Kif26a* and *Kif26b* on rWnt5a-induced GFP-Pdzrn3 reporter degradation. **I)** Quantification of the effect of genetically ablating *Pdzrn3* and *Lnx4* on rWnt5a-induced GFP-Kif26b reporter (WRK) degradation. Error bars represent ± SEM. P-values: *=p<0.05, **=p<0.01, ***=p<0.001.

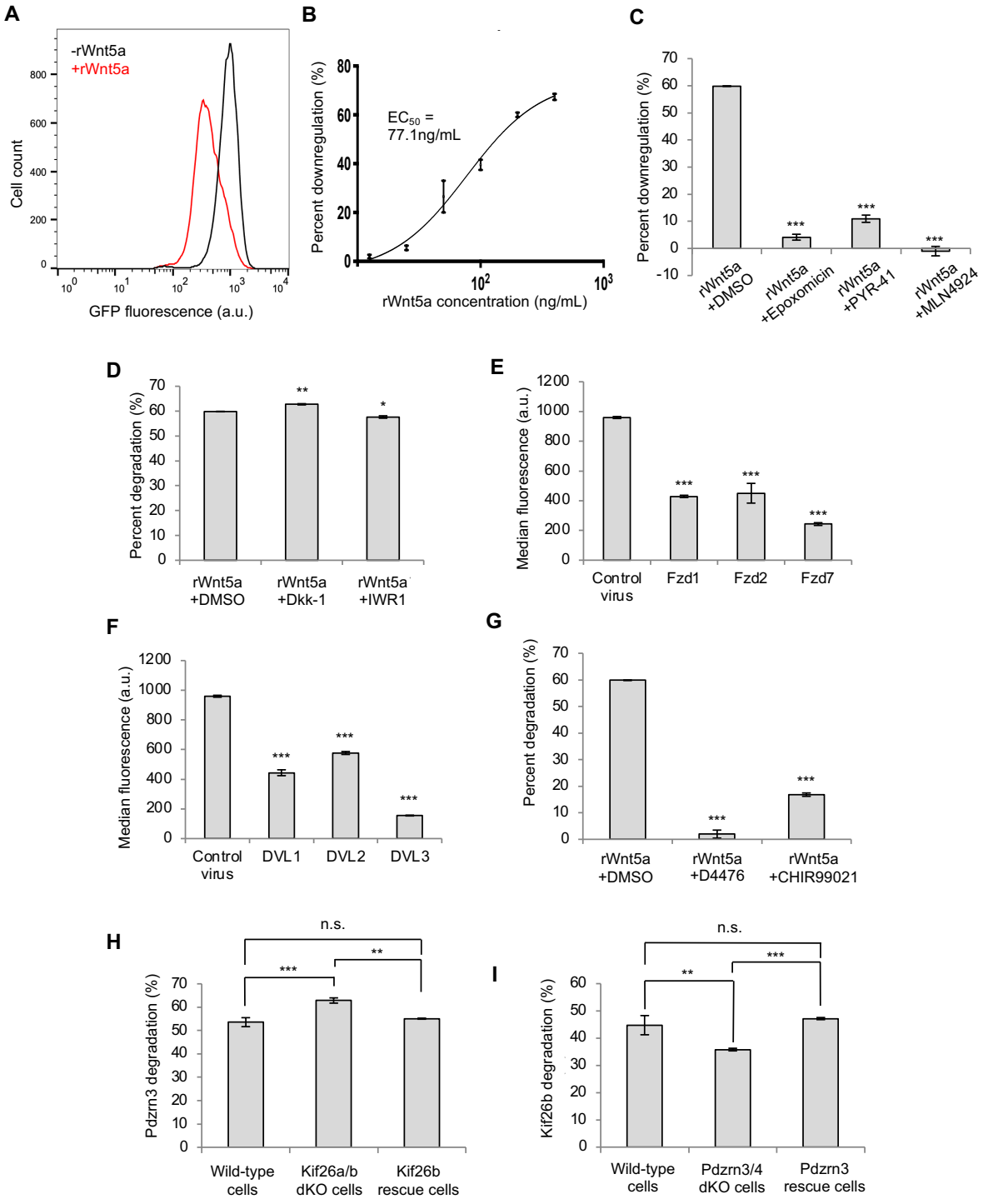
A
-rWnt5a
+rWnt5a
Cell count
GFP fluorescence (a.u.)
B
EC50 = 77.1ng/mL
Percent downregulation (%)
rWnt5a concentration (ng/mL)
C
Percent downregulation (%)
rWnt5a +DMSO
rWnt5a +Epoxomicin
rWnt5a +PYR-41
rWnt5a +MLN4924
D
Percent degradation (%)
rWnt5a +DMSO
rWnt5a +Dkk-1
rWnt5a +IWR1
E
Median fluorescence (a.u.)
Control virus
Fzd1
Fzd2
Fzd7
F
Median fluorescence (a.u.)
Control virus
DVL1
DVL2
DVL3
G
Percent degradation (%)
rWnt5a +DMSO
rWnt5a +D4476
rWnt5a +CHIR99021
H
n.s.
Pdzrn3 degradation (%)
Wild-type cells
Kif26a/b dKO cells
Kif26b rescue cells
I
n.s.
Kif26b degradation (%)
Wild-type cells
Pdzrn3/4 dKO cells
Pdzrn3 rescue cells

Figure 4. Wnt5a-mediated Pdzrn3 phosphorylation is required for its degradation and modulation of cell migration. A) Schematic of domains and identified phosphorylation sites of Pdzrn3. **B)** Quantification of the effects of mutating Group 1 and Group 2 sites on Wnt5a-induced Pdzrn3 degradation. **C)** Quantification of the effects of mutating individual Group 2 sites on Wnt5a-induced Pdzrn3 degradation. **D)** Quantification of the effects of Group 2 phosphomimetic mutations on Pdzrn3 reporter signals. **E)** Single cell tracking plots of Pdzrn3 and Lnx4 double knockout cells (Pdzrn3/4 dKO cells), Pdzrn3/4 dKO cells re-expressing wild-type Pdzrn3 (Pdzrn3 WT cells), or Pdzrn3/4 dKO cells re-expressing Pdzrn3 with phosphoinhibitory mutations at Group 2 sites (Pdzrn3 phosphoinhibitory cells) without any Wnt-C59 or rWnt5a treatments. Axes extend to 600 microns. **F)** Quantification of (E). **G)** Single cell tracking plots of Pdzrn3/4 dKO cells, Pdzrn3 WT cells, and Pdzrn3 phosphoinhibitory cells treated with or without rWnt5a in the presence of Wnt-C59. Axes extend to 600 microns. **H)** Quantification of (G). Error bars represent ± SEM . P-values: *=$p<0.05$, **=$p<0.01$, ***=$p<0.001$.

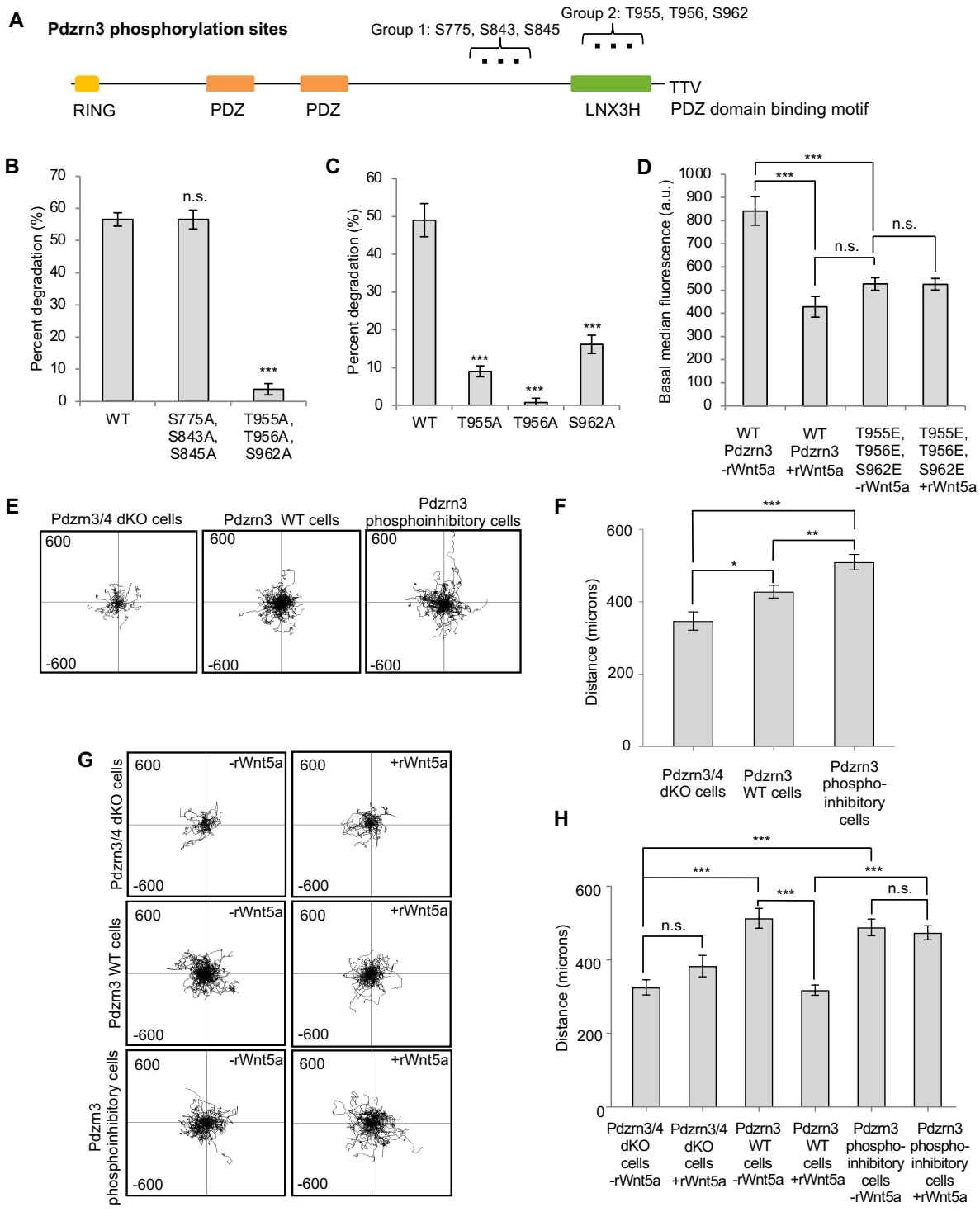
A
Pdzrn3 phosphorylation sites
Group 1: S775, S843, S845
Group 2: T955, T956, S962
RING
PDZ
PDZ
LNX3H
TTV
PDZ domain binding motif
B
Percent degradation (%)
n.s.
***
WT
S775A, S843A, S845A
T955A, T956A, S962A
C
Percent degradation (%)
***
WT
T955A
T956A
S962A
D
Basal median fluorescence (a.u.)
***
n.s.
WT Pdzrn3 -rWnt5a
WT Pdzrn3 +rWnt5a
T955E, T956E, S962E -rWnt5a
T955E, T956E, S962E +rWnt5a
E
Pdzrn3/4 dKO cells
Pdzrn3 WT cells
Pdzrn3 phosphoinhibitory cells
600
-600
F
Distance (microns)
*
**
Pdzrn3/4 dKO cells
Pdzrn3 WT cells
Pdzrn3 phospho-inhibitory cells
G
-rWnt5a
+rWnt5a
H
Distance (microns)
n.s.
Pdzrn3/4 dKO cells -rWnt5a
Pdzrn3/4 dKO cells +rWnt5a
Pdzrn3 WT cells -rWnt5a
Pdzrn3 WT cells +rWnt5a
Pdzrn3 phospho-inhibitory cells -rWnt5a
Pdzrn3 phospho-inhibitory cells +rWnt5a

Figure 5. The C-terminal LNX3H domain acts as a general Wnt5a-responsive domain for Pdzrn3 and its homologs. A) Schematic of Lnx family members and their conserved domains. Pdzrn3 is structurally most homologous to Lnx4. **B)** Alignment of a portion of the LNX3H domain shared by Pdzrn3, Lnx4, and Lnx5. The Pdzrn3 Group 2 phosphorylation sites identified through our MS screen are conserved (red stars and boxes). **C)** Quantification of the effects of Wnt5a on the steady-state abundance of GFP-Lnx family member reporter cell lines. For clarity and ease of comparison across family members, the median reporter signal for the +Wnt5a condition was normalized to the –Wnt5a condition within the individual Lnx reporter. **D)** Quantification of the effect of LNX3H truncation mutation on Pdzrn3 steady-state abundance. **E)** Quantification of the effect of LNX3H truncation mutation on Lnx4 steady-state abundance. **F)** Model of Wnt5a-Ror-Dvl-Pdzrn3 signaling. Error bars represent ± SEM . P-values: *=$p<0.05$, **=$p<0.01$, ***=$p<0.001$.

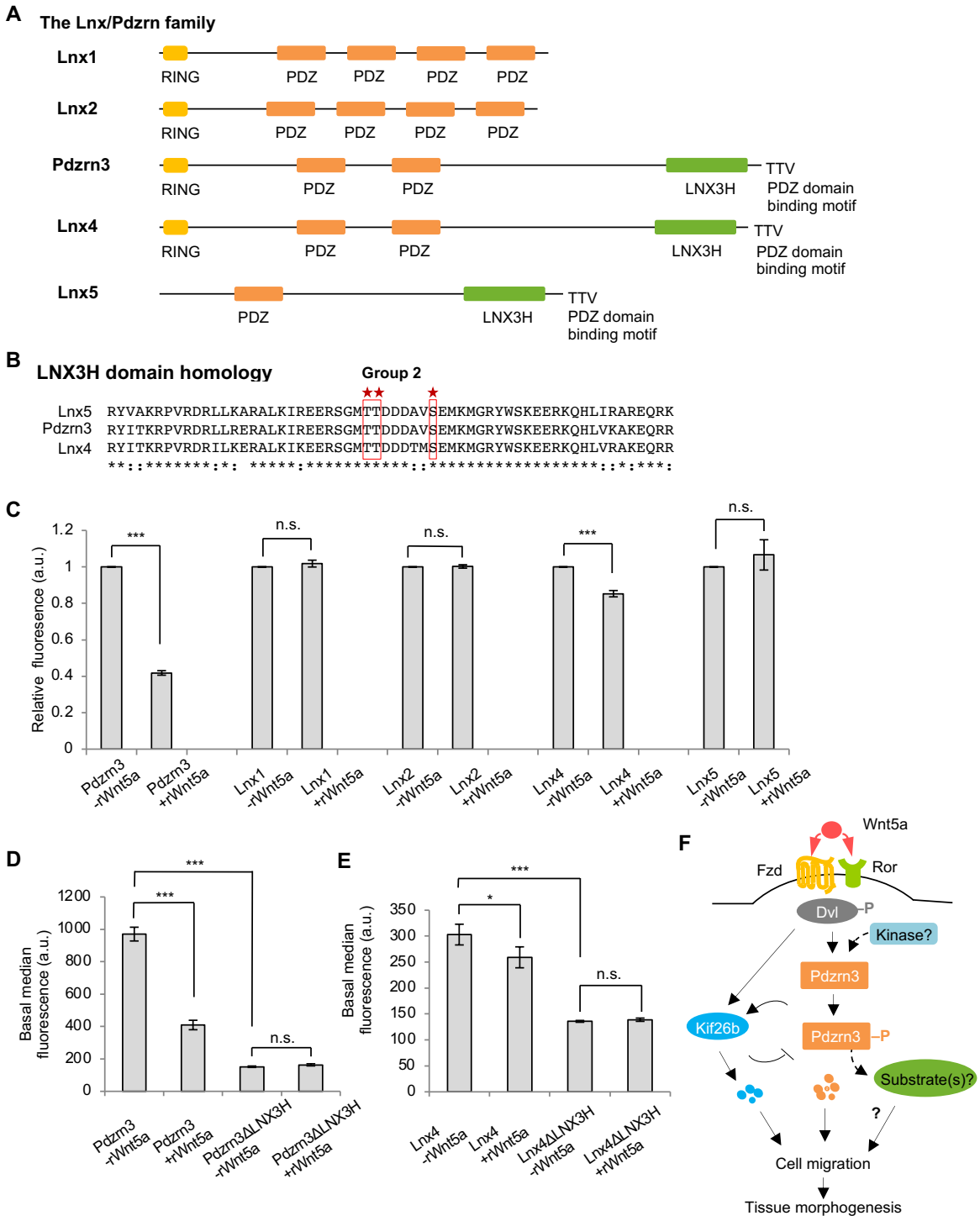
A
The Lnx/Pdzrn family
Lnx1
RING
PDZ
PDZ
PDZ
PDZ
Lnx2
RING
PDZ
PDZ
PDZ
PDZ
Pdzrn3
RING
PDZ
PDZ
LNX3H
TTV
PDZ domain binding motif
Lnx4
RING
PDZ
PDZ
LNX3H
TTV
PDZ domain binding motif
Lnx5
PDZ
LNX3H
TTV
PDZ domain binding motif
B
LNX3H domain homology
Group 2
Lnx5 RYVAKRPVRDRLLKARALKIREERSGMTTDDDAVSEMKMGRYWSKEERKQHLIRAREQRK
Pdzrn3 RYITKRPVRDRLLRERALKIREERSGMTTDDDAVSEMKMGRYWSKEERKQHLVKAKEQRR
Lnx4 RYITKRPVRDRILKERALKIKEERSGMTTDDDTMSEMKMGRYWSKEERKQHLVRAKEQRR
C
Relative fluoresence (a.u.)
1.2
1
0.8
0.6
0.4
0.2
0
***
n.s.
n.s.
***
n.s.
Pdzrn3 -rWnt5a
Pdzrn3 +rWnt5a
Lnx1 -rWnt5a
Lnx1 +rWnt5a
Lnx2 -rWnt5a
Lnx2 +rWnt5a
Lnx4 -rWnt5a
Lnx4 +rWnt5a
Lnx5 -rWnt5a
Lnx5 +rWnt5a
D
Basal median fluorescence (a.u.)
1200
1000
800
600
400
200
0
***
***
n.s.
Pdzrn3 -rWnt5a
Pdzrn3 +rWnt5a
Pdzrn3ΔLNX3H -rWnt5a
Pdzrn3ΔLNX3H +rWnt5a
E
Basal median fluorescence (a.u.)
350
300
250
200
150
100
50
0
***
*
n.s.
Lnx4 -rWnt5a
Lnx4 +rWnt5a
Lnx4ΔLNX3H -rWnt5a
Lnx4ΔLNX3H +rWnt5a
F
Wnt5a
Fzd
Ror
Dvl
P
Kinase?
Pdzrn3
Kif26b
Pdzrn3
P
Substrate(s)?
?
Cell migration
Tissue morphogenesis

Figure S1. rWnt3a induces Pdzrn3 degradation via a mechanism independent of canonical Wnt signaling. A) Effects of canonical Wnt inhibitors, Dkk-1 (2μg/μL) and IWR-1-endo (10μM) on rWnt3a-induced Pdzrn3 degradation in the WRP reporter cells. Error bars represent ± SEM calculated from three technical replicates. t-test (unpaired) was performed to determine statistical significance for the following comparisons: inhibitors vs. the vehicle control DMSO. P-values: *** = p<0.001.

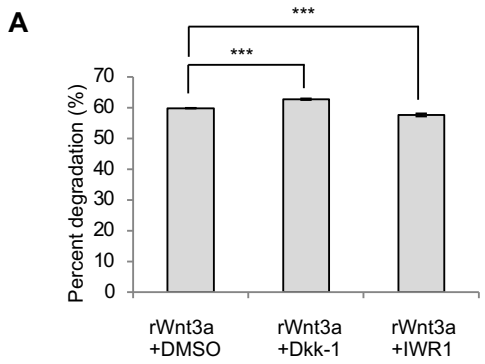

Figure S2. CRISPR/Cas9 mediated genetic deletions of *Kif26a*, *Pdzrn3*, and *Lnx4*. Reference sequences for *Kif26a* (A), *Pdzrn3* (B), and *Lnx4* (C) aligned to mutant alleles generated via targeting with short guide RNAs (sgRNAs) (underlined in reference, green refers to PAM sequence) unique to each gene. Multiple deep sequencing results indicate that *Lnx4* is triploid, which is consistent with previous karyotyping of NIH/3T3 cells [70].

A

```
Kif26a reference     CTGCCACACGAAGCTCGTGGAGCTAAAACGACAGGCGTGGAAGTTGGTCAGCG
Mutant allele 1      ctgccacacgaagctcg--------------------tggaagttggtcagcg (-20)
Mutant allele 2      ctgccacacgaa------------------gtggcgtggaagttggtcagcg (-19)
```

B

```
Pdzrn3 reference     GGGCAGCTGCCCCGCGCGTTGTCGCGGTCGCCTATCGGCCAAGGAGCTCAAC
Mutant allele 1      gggcagctgccccgcgc--------ggtcgcctgtcggccaaggagctcaac (-8)

Pdzrn3 reference     GGGCAGCTGCCCCGCGCGTTGTC---------GCGGTCGCCTATCGGCCAAGGA
Mutant allele 2      GGGCAGCTGCCCCGcgcactaccCAGGTCGCctggtcgcctgtcggccaaggA (+8)
```

C

```
Lnx4 reference       GGCGGACTCCCCTCAGCCGGCCAACATACGGCATGACTCCGGAAGTACAGCTCACGAATGCCAGCACACA
Mutant allele 1      ggcggactcccctcagccgtatgt------------------tggccggctcacgaatgccagcacaca (-19)
Mutant allele 2      ggcggactcccctcag----------------------------------------------ccggccaaca (-44)
Mutant allele 3      ggcggactcccctcag----------------------ccggaagtacagctcacgaatgccagcacaca (-22)
```

Table S1. Hits from Wnt5a knockout MEF TMT/MS3 screen.

Protein abundance changes after 1 hour of rWnt5a stimulation

Upregulated

Gene symbol	Protein description	Fold change	p (<0.05)	>1.5-fold change
Egr1	Early growth response protein	2.38439693	0.0344972	

No genes upregulated with a >1.4-fold change

Downregulated

Gene symbol	Protein description	Fold change	p (<0.05)	>1.5-fold change

No genes downregulated with a >1.5-fold change
No genes downregulated with a >1.4-fold change

Protein abundance changes after 6 hours of rWnt5a stimulation

Upregulated

Gene symbol	Protein description	Fold change	p (<0.05)	>1.5-fold change
Wnt5a	Isoform 2 of Protein Wnt-5a	1.926572071	0.0372307	
Tomm20	Mitochondrial import receptor subunit	1.584886724	0.0272765	
Mgst3	Microsomal glutathione S-transferase 3	1.523255756	0.039168	
ORF3	UPF0480 protein	1.432621015	0.0335934	**>1.4-fold change**

Downregulated

Gene symbol	Protein description	Fold change	p (<0.05)	>1.5-fold change
Pdzrn3	Isoform 2 of E3 ubiquitin-protein ligase PDZRN3	-1.721349071	0.0127063	
Pex19	Peroxisomal biogenesis factor 19	-1.430724427	0.030568	**>1.4-fold change**

Phosphopeptides after 1 hour of rWnt5a stimulation

Upregulated

Gene symbol	Protein description	Fold change	p (<0.05)	>1.5-fold change
Pdzrn3	Isoform 2 of E3 ubiquitin-protein ligase PDZRN3	4.896348357	0.0001449	
Cttnbp2nl	CTTNBP2 N-terminal-like protein	2.203736423	0.0393089	

Fam193a	Protein FAM193A	1.981844414	0.029347
Cttnbp2nl	CTTNBP2 N-terminal-like protein	1.788686436	0.0497643
Smad5	Mothers against decapentaplegic homolog 5	1.784890332	0.0126982
Ppm1g	Protein phosphatase 1G	1.775551219	0.0048398
Myo9b	Uncharacterized protein	1.771688246	0.0156362
Trim28	Transcription intermediary factor 1-beta	1.760720212	0.0314117
Ythdf2	Uncharacterized protein	1.742086231	0.0329148
Pitpnb	Phosphatidylinositol transfer protein beta isoform	1.704670166	0.034315
Runx2	Isoform 2 of Runt-related transcription factor 2	1.698910434	0.02888
Golga4	Golgin subfamily A member 4	1.649886032	0.0309652
Wiz	Isoform S of Protein Wiz	1.640105026	0.0145591
Jmy	Isoform 3 of Junction-mediating and -regulatory protei	1.631593172	0.0289719
Ccs	Copper chaperone for superoxide dismutase	1.62410293	0.0227867
Znf516	Zinc finger protein 516	1.617240291	5.93E-05
Cit	Isoform 3 of Citron Rho-interacting kinase	1.572172861	0.0051839
Pfkfb3	6-phosphofructo-2-kinase/fructose-2,6-biphosphatase	1.567213032	0.0461306
Cbl	E3 ubiquitin-protein ligase CBL	1.550467653	0.0338964
Nhsl1	Isoform 3 of NHS-like protein 1	1.547785737	0.0010735
-	Uncharacterized protein FLJ45252 homolog	1.543401032	0.0362246
Svil	Uncharacterized protein	1.541439146	0.0216903

Sos1	Son of sevenless homolog 1	1.53135359	0.0208929	
Plcg1	1-phosphatidylinositol-4,5-bisphosphate phosphodiesterase gamma-1	1.523480149	0.0436799	
Pfkfb3	6-phosphofructo-2-kinase/fructose-2,6-biphosphatase	1.52089246	0.0010185	
Ppfibp1	Isoform 3 of Liprin-beta-1	1.51729378	0.0041726	
Ptpn11	Isoform 2 of Tyrosine-protein phosphatase non-receptor type 11	1.511873546	0.0122703	
Nhsl1	Isoform 3 of NHS-like protein 1	1.508148194	0.0425997	
Myc	Myc proto-oncogene protein	1.491238902	0.0109896	**>1.4-fold change**
Lmo7	Uncharacterized protein	1.48729622	0.0270909	
Cald1	Uncharacterized protein	1.487011776	0.0365313	
Dvl2	Segment polarity protein dishevelled homolog DVL-2	1.480867174	0.0020118	
Nf1	Isoform 1 of Neurofibromin	1.480753688	0.030678	
Fer	Isoform 2 of Tyrosine-protein kinase Fer	1.480398556	0.0165349	
Nup98	Uncharacterized protein	1.461330834	0.0420834	
Rpl29	60S ribosomal protein L29	1.443290474	0.0460321	
Abl1	Isoform IV of Tyrosine-protein kinase ABL1	1.441619928	0.0276514	
Maged1	Melanoma-associated antigen D1	1.439971967	0.0394429	
Ccnl1	Cyclin-L1	1.432298248	0.00098	
Ndrg1	Protein NDRG1	1.42850036	0.0200542	
Golga4	Isoform 2 of Golgin subfamily A member 4	1.427006333	0.0476538	
Clasp1	Uncharacterized protein	1.425851006	0.0138966	

Eps15l1	Isoform 2 of Epidermal growth factor receptor substrate 15-like 1	1.419254806	0.0138281	
Rin3	Ras and Rab interactor 3	1.412800262	0.0337847	
Arhgap28	Isoform 2 of Rho GTPase-activating protein 28	1.408606784	0.0030105	
E2f7	Transcription factor E2F7	1.407879959	0.016597	
Fam21	WASH complex subunit FAM21	1.40421895	0.0001156	

Downregulated

Gene symbol	Protein description	Fold change	p (<0.05)	>1.5-fold change
Marcks	Myristoylated alanine-rich C-kinase substrate	-2.397385873	0.0399184	
Nolc1	Uncharacterized protein	-2.184400738	0.006836	
Ahnak	Uncharacterized protein	-1.802661345	0.0066954	
Ahnak	Uncharacterized protein	-1.779703849	0.0423348	
Cald1	Uncharacterized protein	-1.757038896	0.0253685	
Marcks	Myristoylated alanine-rich C-kinase substrate	-1.720977029	0.0293862	
Kif26b	Kinesin-like protein KIF26B	-1.696671456	0.0174274	
Anln	Actin-binding protein anillin	-1.683390739	0.0438076	
Mcm4	DNA replication licensing factor MCM4	-1.622414541	0.0018911	
-	Uncharacterized protein C1orf198 homolog	-1.621420817	0.0152447	
Irf2bpl	Interferon regulatory factor 2-binding protein-like	-1.596016772	0.0048498	
Nufip2	Nuclear fragile X mental retardation-interacting protein 2	-1.551199699	0.004365	
Map2	Microtubule-associated protein 2	-1.538812914	0.0026877	

Zc3hc1	Isoform 2 of Nuclear-interacting partner of ALK	-1.523258252	0.0141898	
Nufip2	Nuclear fragile X mental retardation-interacting protein 2	-1.522469062	0.0159711	
Ssfa2	Sperm-specific antigen 2 homolog	-1.51550061	0.0395126	
Cald1	Uncharacterized protein	-1.511821188	0.0219948	
Sdpr	Serum deprivation-response protein	-1.493030833	0.0350097	**>1.4-fold change**
Ncapd2	Isoform 2 of Condensin complex subunit 1	-1.486112341	0.0289368	
Ezh2	Isoform ENX-1B of Histone-lysine N-methyltransferase EZH2	-1.473826192	0.0237322	
Cep170	Centrosomal protein of 170 kD	-1.469973667	0.0161887	
Zc3hc1	Isoform 2 of Nuclear-interacting partner of ALK	-1.461750162	0.0467709	
Osbpl11	Oxysterol-binding protein-related protein 11	-1.461438049	0.0109181	
Cep170	Centrosomal protein of 170 kD	-1.45845822	0.0419282	
Ankrd11	Uncharacterized protein	-1.454792091	0.0126582	
Aak1	Isoform 2 of AP2-associated protein kinase 1	-1.45099807	0.0025651	
Plec	Isoform PLEC-1A of Plectin	-1.441775673	0.0035308	
Rab11fip5	MKIAA0857 protein (Fragment)	-1.432795113	0.0258916	
Larp1	La-related protein 1	-1.430574545	0.0083536	
Map1b	Microtubule-associated protein 1	-1.430378805	0.0182238	
Lasp1	LIM and SH3 domain protein 1	-1.412415759	0.0025684	
Sorbs1	Uncharacterized protein	-1.410531488	0.0302538	
R3hdm1	R3hdm1 protein	-1.402954494	0.0369368	

Nolc1	Uncharacterized protein	-1.400048941	0.0266456	

Phosphopeptides after 6 hours of rWnt5a stimulation

Upregulated

Gene symbol	Protein description	Fold change	p (<0.05)	>1.5-fold change
Pdzrn3	Isoform 2 of E3 ubiquitin-protein ligase PDZRN3	2.838676045	0.0016949	
Bnip3l	BCL2/adenovirus E1B 19 kDa protein-interacting protein 3-like	1.769999423	0.0251346	
Fndc3a	Fibronectin type III domain-containing protein	1.723675391	0.0418099	
Csnk1g3	Casein kinase I isoform gamma-3	1.519774279	0.0119983	
Dvl2	Segment polarity protein dishevelled homolog DVL-2	1.488214495	0.0033044	**>1.4-fold change**
Mia3	Isoform 3 of Melanoma inhibitory activity protein 3	1.481093471	0.0492331	

Downregulated

Gene symbol	Protein description	Fold change	p (<0.05)	>1.5-fold change
Pdzrn3	Isoform 2 of E3 ubiquitin-protein ligase PDZRN3	-2.717441623	0.0300813	
Kif26b	Kinesin-like protein KIF26B	-2.025993912	0.0224467	
Pdzrn3	Isoform 2 of E3 ubiquitin-protein ligase PDZRN3	-1.844370147	0.003328	
-	UPF0690 protein C1orf52 homolog	-1.500122588	0.0414135	
Pebp1	Phosphatidylethanolamine-binding protein 1	-1.43679002	0.0346749	**>1.4-fold change**
Ahnak2	Uncharacterized protein	-1.404234685	0.0054494	

Table S1. Hits from Wnt5a knockout MEF TMT/MS3 screen

References

1. Moon, R.T., et al., *Xwnt-5A: a maternal Wnt that affects morphogenetic movements after overexpression in embryos of Xenopus laevis.* Development, 1993. **119**(1): p. 97-111.
2. Susman, M.W., et al., *Kinesin superfamily protein Kif26b links Wnt5a-Ror signaling to the control of cell and tissue behaviors in vertebrates.* Elife, 2017. **6**.
3. Flynn, M., O. Saha, and P. Young, *Molecular evolution of the LNX gene family.* BMC Evol Biol, 2011. **11**: p. 235.
4. Clevers, H. and R. Nusse, *Wnt/beta-catenin signaling and disease.* Cell, 2012. **149**(6): p. 1192-205.
5. Nusse, R. and H. Varmus, *Three decades of Wnts: a personal perspective on how a scientific field developed.* EMBO J, 2012. **31**(12): p. 2670-84.
6. Steinhart, Z. and S. Angers, *Wnt signaling in development and tissue homeostasis.* Development, 2018. **145**(11).
7. Veeman, M.T., J.D. Axelrod, and R.T. Moon, *A second canon. Functions and mechanisms of beta-catenin-independent Wnt signaling.* Dev Cell, 2003. **5**(3): p. 367-77.
8. Mikels, A.J. and R. Nusse, *Purified Wnt5a protein activates or inhibits beta-catenin-TCF signaling depending on receptor context.* PLoS Biol, 2006. **4**(4): p. e115.
9. Oishi, I., et al., *The receptor tyrosine kinase Ror2 is involved in non-canonical Wnt5a/JNK signalling pathway.* Genes Cells, 2003. **8**(7): p. 645-54.
10. Yamaguchi, T.P., et al., *A Wnt5a pathway underlies outgrowth of multiple structures in the vertebrate embryo.* Development, 1999. **126**(6): p. 1211-23.
11. Hikasa, H., et al., *The Xenopus receptor tyrosine kinase Xror2 modulates morphogenetic movements of the axial mesoderm and neuroectoderm via Wnt signaling.* Development, 2002. **129**(22): p. 5227-39.

12. Nomi, M., et al., *Loss of mRor1 enhances the heart and skeletal abnormalities in mRor2-deficient mice: redundant and pleiotropic functions of mRor1 and mRor2 receptor tyrosine kinases.* Mol Cell Biol, 2001. **21**(24): p. 8329-35.
13. Ho, H.Y., et al., *Wnt5a-Ror-Dishevelled signaling constitutes a core developmental pathway that controls tissue morphogenesis.* Proc Natl Acad Sci U S A, 2012. **109**(11): p. 4044-51.
14. Afzal, A.R., et al., *Recessive Robinow syndrome, allelic to dominant brachydactyly type B, is caused by mutation of ROR2.* Nat Genet, 2000. **25**(4): p. 419-22.
15. Afzal, A.R. and S. Jeffery, *One gene, two phenotypes: ROR2 mutations in autosomal recessive Robinow syndrome and autosomal dominant brachydactyly type B.* Hum Mutat, 2003. **22**(1): p. 1-11.
16. Person, A.D., et al., *WNT5A mutations in patients with autosomal dominant Robinow syndrome.* Dev Dyn, 2010. **239**(1): p. 327-37.
17. Bunn, K.J., et al., *Mutations in DVL1 cause an osteosclerotic form of Robinow syndrome.* Am J Hum Genet, 2015. **96**(4): p. 623-30.
18. White, J., et al., *DVL1 frameshift mutations clustering in the penultimate exon cause autosomal-dominant Robinow syndrome.* Am J Hum Genet, 2015. **96**(4): p. 612-22.
19. White, J.J., et al., *DVL3 Alleles Resulting in a -1 Frameshift of the Last Exon Mediate Autosomal-Dominant Robinow Syndrome.* Am J Hum Genet, 2016. **98**(3): p. 553-561.
20. White, J.J., et al., *WNT Signaling Perturbations Underlie the Genetic Heterogeneity of Robinow Syndrome.* Am J Hum Genet, 2018. **102**(1): p. 27-43.
21. Mansour, T.A., et al., *Whole genome variant association across 100 dogs identifies a frame shift mutation in DISHEVELLED 2 which contributes to Robinow-like syndrome in Bulldogs and related screw tail dog breeds.* PLoS Genet, 2018. **14**(12): p. e1007850.
22. Lu, Z., et al., *Regulation of synaptic growth and maturation by a synapse-associated E3 ubiquitin ligase at the neuromuscular junction.* J Cell Biol, 2007. **177**(6): p. 1077-89.

23. Sewduth, R.N., et al., *The ubiquitin ligase PDZRN3 is required for vascular morphogenesis through Wnt/planar cell polarity signalling.* Nat Commun, 2014. **5**: p. 4832.

24. Baizabal, J.M., et al., *The Epigenetic State of PRDM16-Regulated Enhancers in Radial Glia Controls Cortical Neuron Position.* Neuron, 2018. **99**(1): p. 239-241.

25. Ting, L., et al., *MS3 eliminates ratio distortion in isobaric multiplexed quantitative proteomics.* Nat Methods, 2011. **8**(11): p. 937-40.

26. McAlister, G.C., et al., *MultiNotch MS3 enables accurate, sensitive, and multiplexed detection of differential expression across cancer cell line proteomes.* Anal Chem, 2014. **86**(14): p. 7150-8.

27. Paulo, J.A., et al., *Effects of MEK inhibitors GSK1120212 and PD0325901 in vivo using 10-plex quantitative proteomics and phosphoproteomics.* Proteomics, 2015. **15**(2-3): p. 462-73.

28. Ran, F.A., et al., *Double nicking by RNA-guided CRISPR Cas9 for enhanced genome editing specificity.* Cell, 2013. **154**(6): p. 1380-9.

29. Higashimori, A., et al., *Forkhead Box F2 Suppresses Gastric Cancer through a Novel FOXF2-IRF2BPL-beta-Catenin Signaling Axis.* Cancer Res, 2018. **78**(7): p. 1643-1656.

30. O'Connell, M.E., et al., *The Drosophila protein, Nausicaa, regulates lamellipodial actin dynamics in a Cortactin-dependent manner.* Biol Open, 2019. **8**(6).

31. Zuchero, J.B., et al., *p53-cofactor JMY is a multifunctional actin nucleation factor.* Nat Cell Biol, 2009. **11**(4): p. 451-9.

32. Wrighton, K.H., *JMY: actin up in cell motility.* Nat Rev Mol Cell Biol, 2009. **10**(5): p. 304.

33. Azevedo, M.M., et al., *Jmy regulates oligodendrocyte differentiation via modulation of actin cytoskeleton dynamics.* Glia, 2018. **66**(9): p. 1826-1844.

34. Tan, I., et al., *Chelerythrine perturbs lamellar actomyosin filaments by selective inhibition of myotonic dystrophy kinase-related Cdc42-binding kinase.* FEBS Lett, 2011. **585**(9): p. 1260-8.

35. Chen, X., et al., *Supervillin promotes epithelial-mesenchymal transition and metastasis of hepatocellular carcinoma in hypoxia via activation of the RhoA/ROCK-ERK/p38 pathway.* J Exp Clin Cancer Res, 2018. **37**(1): p. 128.

36. Crowley, J.L., et al., *Supervillin reorganizes the actin cytoskeleton and increases invadopodial efficiency.* Mol Biol Cell, 2009. **20**(3): p. 948-62.

37. Serra-Pages, C., et al., *Liprins, a family of LAR transmembrane protein-tyrosine phosphatase-interacting proteins.* J Biol Chem, 1998. **273**(25): p. 15611-20.

38. Bjorkblom, B., et al., *c-Jun N-terminal kinase phosphorylation of MARCKSL1 determines actin stability and migration in neurons and in cancer cells.* Mol Cell Biol, 2012. **32**(17): p. 3513-26.

39. Aderem, A., *Signal transduction and the actin cytoskeleton: the roles of MARCKS and profilin.* Trends Biochem Sci, 1992. **17**(10): p. 438-43.

40. Mayanagi, T. and K. Sobue, *Diversification of caldesmon-linked actin cytoskeleton in cell motility.* Cell Adh Migr, 2011. **5**(2): p. 150-9.

41. Lin, J.J., et al., *Chapter 1: roles of caldesmon in cell motility and actin cytoskeleton remodeling.* Int Rev Cell Mol Biol, 2009. **274**: p. 1-68.

42. Tseng, H.C., et al., *Cytoskeleton network and cellular migration modulated by nuclear-localized receptor tyrosine kinase ROR1.* Anticancer Res, 2011. **31**(12): p. 4239-49.

43. Mohan, R. and A. John, *Microtubule-associated proteins as direct crosslinkers of actin filaments and microtubules.* IUBMB Life, 2015. **67**(6): p. 395-403.

44. Sanchez, C., J. Diaz-Nido, and J. Avila, *Phosphorylation of microtubule-associated protein 2 (MAP2) and its relevance for the regulation of the neuronal cytoskeleton function.* Prog Neurobiol, 2000. **61**(2): p. 133-68.

45. Hannes, F., et al., *A microdeletion proximal of the critical deletion region is associated with mild Wolf-Hirschhorn syndrome.* Am J Med Genet A, 2012. **158A**(5): p. 996-1004.

46. Huang, K.M., et al., *Xcat, a novel mouse model for Nance-Horan syndrome inhibits expression of the cytoplasmic-targeted Nhs1 isoform.* Hum Mol Genet, 2006. **15**(2): p. 319-27.

47. Bryja, V., et al., *Wnt-5a induces Dishevelled phosphorylation and dopaminergic differentiation via a CK1-dependent mechanism.* J Cell Sci, 2007. **120**(Pt 4): p. 586-95.

48. Witze, E.S., et al., *Wnt5a control of cell polarity and directional movement by polarized redistribution of adhesion receptors.* Science, 2008. **320**(5874): p. 365-9.

49. Witze, E.S., et al., *Wnt5a directs polarized calcium gradients by recruiting cortical endoplasmic reticulum to the cell trailing edge.* Dev Cell, 2013. **26**(6): p. 645-57.

50. Park, H.W., et al., *Alternative Wnt Signaling Activates YAP/TAZ.* Cell, 2015. **162**(4): p. 780-94.

51. Connacher, M.K., J.W. Tay, and N.G. Ahn, *Rear-polarized Wnt5a-receptor-actin-myosin-polarity (WRAMP) structures promote the speed and persistence of directional cell migration.* Mol Biol Cell, 2017. **28**(14): p. 1924-1936.

52. Meng, L., et al., *Epoxomicin, a potent and selective proteasome inhibitor, exhibits in vivo antiinflammatory activity.* Proc Natl Acad Sci U S A, 1999. **96**(18): p. 10403-8.

53. Yang, Y., et al., *Inhibitors of ubiquitin-activating enzyme (E1), a new class of potential cancer therapeutics.* Cancer Res, 2007. **67**(19): p. 9472-81.

54. Tong, S., et al., *MLN4924 (Pevonedistat), a protein neddylation inhibitor, suppresses proliferation and migration of human clear cell renal cell carcinoma.* Sci Rep, 2017. **7**(1): p. 5599.

55. Bafico, A., et al., *Novel mechanism of Wnt signalling inhibition mediated by Dickkopf-1 interaction with LRP6/Arrow.* Nat Cell Biol, 2001. **3**(7): p. 683-6.

56. Lee, E., et al., *The roles of APC and Axin derived from experimental and theoretical analysis of the Wnt pathway.* PLoS Biol, 2003. **1**(1): p. E10.

57. Huang, S.M., et al., *Tankyrase inhibition stabilizes axin and antagonizes Wnt signalling.* Nature, 2009. **461**(7264): p. 614-20.

58. Bryja, V., G. Schulte, and E. Arenas, *Wnt-3a utilizes a novel low dose and rapid pathway that does not require casein kinase 1-mediated phosphorylation of Dvl to activate beta-catenin.* Cell Signal, 2007. **19**(3): p. 610-6.

59. Karuna, E.P., M.W. Susman, and H.H. Ho, *Quantitative Live-cell Reporter Assay for Noncanonical Wnt Activity.* Bio-protocol 2018. **8**(6): p. e2762.

60. Kim, S.E., et al., *Wnt stabilization of beta-catenin reveals principles for morphogen receptor-scaffold assemblies.* Science, 2013. **340**(6134): p. 867-70.

61. Lee, H.J., D.L. Shi, and J.J. Zheng, *Conformational change of Dishevelled plays a key regulatory role in the Wnt signaling pathways.* Elife, 2015. **4**: p. e08142.

62. Qi, J., et al., *Autoinhibition of Dishevelled protein regulated by its extreme C terminus plays a distinct role in Wnt/beta-catenin and Wnt/planar cell polarity (PCP) signaling pathways.* J Biol Chem, 2017. **292**(14): p. 5898-5908.

63. Papkoff, J., et al., *Wnt-1 regulates free pools of catenins and stabilizes APC-catenin complexes.* Mol Cell Biol, 1996. **16**(5): p. 2128-34.

64. Choi, J., et al., *Adenomatous polyposis coli is down-regulated by the ubiquitin-proteasome pathway in a process facilitated by Axin.* J Biol Chem, 2004. **279**(47): p. 49188-98.

65. Carvallo, L., et al., *Non-canonical Wnt signaling induces ubiquitination and degradation of Syndecan4.* J Biol Chem, 2010. **285**(38): p. 29546-55.

66. Glass, D.J., et al., *The receptor tyrosine kinase MuSK is required for neuromuscular junction formation and is a functional receptor for agrin.* Cold Spring Harb Symp Quant Biol, 1996. **61**: p. 435-44.

67. Masiakowski, P. and R.D. Carroll, *A novel family of cell surface receptors with tyrosine kinase-like domain.* J Biol Chem, 1992. **267**(36): p. 26181-90.

68. Valenzuela, D.M., et al., *Receptor tyrosine kinase specific for the skeletal muscle lineage: expression in embryonic muscle, at the neuromuscular junction, and after injury.* Neuron, 1995. **15**(3): p. 573-84.

69. Uchiyama, Y., et al., *Kif26b, a kinesin family gene, regulates adhesion of the embryonic kidney mesenchyme.* Proc Natl Acad Sci U S A, 2010. **107**(20): p. 9240-5.

70. Leibiger, C., et al., *First molecular cytogenetic high resolution characterization of the NIH 3T3 cell line by murine multicolor banding.* J Histochem Cytochem, 2013. **61**(4): p. 306-12.

Chapter 3

Dual reporter system facilitates structure-function analysis of Dishevelled as a mediator of Wnt5a-Ror and Wnt/β-catenin signaling

Abstract

Non-canonical Wnt5a-Ror and canonical Wnt/β-catenin signaling pathways regulate many diverse biological processes. Dishevelled (Dvl) scaffolding proteins have long been used as an indicator of signaling activity in both pathways, and mutations in DVLs can cause congenital disorders such as Robinow syndrome. However, how Dvls contribute to Wnt5a-Ror signal transduction, as well as how they facilitate signal transduction of multiple distinct Wnt pathways overall, remains unclear. To investigate this question, we developed a dual reporter system capable of monitoring Wnt5a-Ror and Wnt/β-catenin signaling in cells derived from embryonic mouse craniofacial tissues, which undergo both types of signaling. By conducting a genetic loss-of-function approach in dual reporter cells, we determined that individual Dvls are differentially required and utilized in Wnt5a-Ror versus Wnt/β-catenin signaling. Using a rescue strategy coupled with this loss-of-function approach, we identified the Dvl domains required for Wnt5a-Ror and Wnt/β-catenin signal transduction. Importantly, we identified key phosphorylation sites within the Dvl C-terminus that are specific to Wnt5a-Ror signaling but not Wnt/β-catenin signaling, which constitute a key molecular switch involved in differential regulation of the pathways. Finally, we noted that Robinow and Robinow-like syndrome mutations in DVL1-3 that alter the DVL C-terminus sequence impact Wnt5a-Ror and Wnt/β-catenin signaling via multiple distinct mechanisms. Collectively, this work defines the roles of Dvls as they regulate two major Wnt signaling pathways and uncovers unique mechanisms underlying Dvl variants.

Introduction

Wnt ligands are a family of secreted glycoproteins that govern a multitude of biological processes throughout the many stages of life. During vertebrate embryonic development, Wnts are involved in processes such as tissue specification and tissue morphogenesis that are required to establish a body plan and develop tissues. In adult organisms, Wnts regulate a variety of tissue homeostatic processes, such as stem cell maintenance and tissue renewal and regeneration. As a result, misregulation of Wnt signaling pathways can result in congenital birth defects as well as contribute to several diseases, most notably cancer [1-3].

Wnt signaling pathways are broadly classified into two categories. In canonical Wnt signaling, also referred to as Wnt/β-catenin signaling, pathway activation via ligands such as Wnt3a leads to inhibition of the destruction complex, a multiprotein assembly containing components such as Dishevelled (Dvl), Axin, APC, and GSK3, and stabilization of the transcriptional coactivator β-catenin. The stabilization and increased abundance of β-catenin enables its interactions with the transcription factors Tcf/Lef that translocate into the nucleus to regulate cell proliferation and gene expression [4, 5], processes that impact tissue patterning during development. In contrast, non-canonical Wnt signaling utilizes β-catenin-independent mechanisms to affect tissue morphogenesis. While there are several recognized non-canonical Wnt pathways, one major branch is the Wnt5a-Ror pathway, which is known to affect tissue elongation of the body axis, limbs, tail, and craniofacial features [6-9]. In Wnt5a-Ror signaling, the prototypical ligand Wnt5a initiates a signaling cascade using Ror and Frizzled (Fzd) receptors that leads to the phosphorylation of Dishevelled (Dvl) scaffolding proteins and proteasomal degradation of the downstream effectors Kif26b and Pdzrn3 [6, 8, 9], which impacts cell migration and tissue morphogenesis. While they mediate different cell biological

outcomes, proper spatiotemporal regulation of both Wnt5a-Ror and Wnt/β-catenin signaling is critical to ensure appropriate development.

Both Wnt5a-Ror and Wnt/β-catenin signaling pathways have connections to Dvls, a family of scaffolding proteins known to mediate a variety of protein-protein interactions to facilitate signal transduction for multiple Wnt pathways, making them the ultimate branchpoint within the larger Wnt signaling network. Mammals possess three homologs, Dvl1-3 (also known as Dsh in *Drosophila*), which are evolutionarily conserved from sponges to humans and display significant sequence homology to each other and across species. While recognized as major signaling hubs, several long-standing questions still surround Dvl structure and function. For instance, although it is widely accepted that Dvl homologs regulate multiple Wnt signaling pathways [10-13], whether Dvl homologs are required for Wnt5a-Ror signaling remains experimentally untested. Another major question is whether Dvl1, Dvl2, and Dvl3 are redundant or possess specialized, individual roles in certain contexts. In general, Dvl proteins are considered to be redundant with a few notable exceptions [14], but single, double, and triple Dvl knockout mouse models suggest potentially more individualized roles in certain tissues [15-18]. Additionally, phosphorylation of Dvl2 is a well-established post-translational modification associated with both non-canonical and canonical Wnt signaling pathways, but its functional requirement in either signaling pathway is not well understood [6, 14, 19-22]; even less is known about the functional consequences of Dvl1 and Dvl3 phosphorylation in non-canonical and canonical Wnt signaling pathways. Answers to such questions would provide fundamental knowledge concerning Dvl function as well as greatly facilitate the interpretation of mechanistic changes driven by congenital disorder causing Dvl variants.

Several congenital disorder causing DVL variants have been identified in humans, such as Robinow syndrome (RS). RS is a rare congenital disorder characterized by systemic tissue elongation defects such as dwarfism, limb shortening, and several distinct craniofacial features.

To date, RS causing mutations have been identified in human *DVL1, DVL2,* and *DVL3* [23-27] as well as an analogous mutation in the bulldog *DVL2* gene [28], which we previously reported likely contributes in part to the Robinow-like features of this dog breed. In addition to the mutation in *DVLs*, causative mutations also have been identified in *WNT5A, ROR2,* and *FRIZZLED2*, which are all key components of Wnt5a-Ror signaling. The discovery that several critical components of Wnt5a-Ror signaling can harbor mutations that cause RS in humans strongly suggests that disruption of this key signaling pathway ultimately leads to manifestation of the disorder. However, molecular studies examining the underlying pathologies of RS mutations remain limited, and, currently, no studies have been conducted examining the effects of RS DVLs on multiple Wnt signaling pathways.

In this study, we examined these long-standing questions surrounding Dvl function in Wnt5a-Ror signaling and Wnt/β-catenin signaling. To monitor both pathways in a highly physiologically relevant and quantitative manner, we developed a dual reporter system in which different colored fluorescent reporters measure signaling activity in both pathways in cells derived from mouse facial prominences, a tissue type that undergoes robust Wnt5a-Ror and Wnt/β-catenin signaling. Using CRISPR/Cas9 to genetically ablate all three Dvl family members in this system, we established for the first time that Dvls are required for Wnt5a-Ror signaling. Further, we determined that individual Dvls are differentially required and used in Wnt5a-Ror versus Wnt/β-catenin signaling. By conducting rescue experiments within this Dvl triple KO reporter background, we determined that Dvl domains are differentially used in Wnt5a-Ror and Wnt/β-catenin signal transduction. We also identified key Wnt5a-Ror-induced phosphorylation residues in the Dvl C-terminus that constitute a molecular switch involved in directing signals downstream to the Wnt5a-Ror pathway. Interrogation of Robinow and Robinow-like syndrome (RS) mutations in DVL1-3 that disrupt the DVL C-terminus indicates that RS DVL variants

disrupt both Wnt5a-Ror and Wnt/β-catenin signaling via three distinct mechanisms. Collectively, our work defines the individual and collective roles of Dvls in two major Wnt signaling pathways.

Materials and methods

Maxillary prominence (MaxP) cells

Maxillary prominence (MaxP) cells were derived from E11.5 *Ror1$^{f/f}$; Ror2$^{f/f}$; ER-Cre* embryos. The maxillary prominences were microdissected from both sides of the developing face from multiple embryos (n=8) and pooled together. Prominences were dissociated into single cells prior to plating. Three days later, MaxP cells were immortalized by electroporating CRISPR/Cas9 constructs targeting *Tp53* using the Neon Transfection System (Thermo Fisher) as described previously [29] (Addgene #88846 and 88847). MaxP cell lines were cultured at 37C and 5% CO2 in Dulbecco's Modified Eagles Medium (MT15017CV, Corning) supplemented with 1x glutamine (25-005-CI, Corning), 1x penicillin-streptomycin (30-002-CI, Corning) and 10% fetal bovine serum (16000069, Thermo Fisher Scientific).

Generation of dual reporter system

To generate the dual reporter system, the fluorescence-based Wnt/β-catenin signaling reporter 7TGP plasmid (Addgene #24305) was modified such that the GFP sequence was removed and replaced by the miRFP760 sequence (derived from Addgene #79987) to make the "7TR" plasmid. The modified construct was verified by Sanger sequencing and introduced into MaxP cells via lentivirus transduction. A similar workflow was used to introduce the GFP-Kif26b-C plasmid, which expresses the C-terminal degron of Kif26b N-terminally fused to GFP [30], into MaxP cells expressing the 7TR reporter. After the introduction of the GFP-Kif26b-C reporter, the

resultant cell populations were treated with Wnt-C59 for 4 days. Cells with the lowest positive GFP signal were sorted (MoFlo Astrios Cell Sorter, Beckman Coulter, 488nm laser) and cloned into individual wells in 96-well plates containing a 50-50 mixture of mouse embryonic fibroblast (MEF) conditioned medium and complete medium. Individual clones were analyzed through flow cytometry (Becton Dickinson FACScan, 488nm laser) and selected for further analysis based on a robust Wnt5a-induced GFP-Kif26b-C degradation response.

Dvl knockout cell lines

MaxP dual reporter cells were electroporated with CRISPR/Cas9 ribonucleoprotein (RNP) complexes targeting mouse *Dvl1, Dvl2, and Dvl3* using the following gRNA sequences: mDvl1, AAUCAUCUACCACAUGGACG; mDvl2, CCGAAUCUGUCGUAUCACUG; mDvl3, CCACCUUCGAUGGAACGCAC (Integrated DNA Technologies). 4 days after electroporation of RNP complexes, MaxP cells were subjected to fluorescence activated cell sorting (MoFlo Astrios Cell Sorter, Beckman Coulter, 561nm laser). Cells containing RNP complexes were identified based on the presence of ATTO550 signal, which is conjugated to the tracrRNA of each RNP complex. ATTO550 positive cells were cloned as single cells in 96-well plates containing a mixture of fresh complete media and conditioned media supplemented with additional fetal bovine serum (16000069, Thermo Fisher Scientific), non-essential amino acids (1x final concentration; Gibco, 11140050), sodium pyruvate (1mM final concentration; Gibco, 11360070), and 2-mercaptoethanol (0.1mM final concentration; BioRad, #1610710). All knockout mutations were screened and validated through a combination of western blotting and deep sequencing. Dvl TKO dual reporter cells were generated by electroporating RNP

complexes targeting *Dvl2* and *Dvl3* into validated Dvl1 KO cells. These cells were then subjected to cell sorting and cloning in 96-well plates as described above.

Dvl constructs

For cloning of mouse Dvl1-3, a cDNA pool was generated from mouse embryonic fibroblasts (MEFs) using total RNA Maxima H Minus reverse transcriptase and oligo dT primers according to manufacturer's instructions (EP0751, ThermoFisher Scientific). This cDNA library was then used as template for PCR amplification of the *Dvl1, Dvl2, and Dvl3* open reading frames with the following primers, *Dvl1* forward: gatcggccggccTaccATGGCGGAGACCAAAATCATCTAC; *Dvl1* reverse: gatcGGCGCGCCTCACATGATGTCCACAAAGAACTC; *Dvl2* forward: GATCGGCCGGCCTACCATGGCGGGCAGCAGCGCGGG; *Dvl2* reverse: GATCGGCGCGCCCTACATAACATCCACAAAAAACTC; *Dvl3* forward: gatcggccggccTaccATGGGCGAGACCAAGATCATCTAC; *Dvl3* reverse: gatcGGCGCGCCTCACATCACATCCACAAAGAACTC. A similar workflow occurred for the human DVL1 and 3 constructs using cDNA derived from HeLa cells and the following primers, *DVL1* forward: gatcGAATTCCACCatgggcgagaccaagattatctac, *DVL1* reverse: gatcGGCGCGCCTCACATGATGTCCACGAAGAACTC, *DVL3* forward: TTCAGGCCGGCCTACCATGGGCGAGACCAAGATCATCTAC,

DVL3 reverse: GAGGCGCGCCTCACATCACATCCACAAAGAACTC. All PCR products were subcloned into a modified pENTR-2B (Life Technologies) vector in frame with an N-terminal myc tag using FseI and AscI restriction sites. Resultant constructs were verified by Sanger sequencing and recombined with a modified pLEX307 vector (Addgene #41392, a gift from David Root) containing an intron-less EF1 promoter [62], using LR Clonase (Thermo Fisher).

Plasmids containing mouse Dvl3 truncations, mouse Dvl3^{K435M}, mouse Dvl1-3 phosphomutants, and human DVL1 and DVL3 RS mutants were similarly created by following the workflow described above. Generation of the wild-type and bulldog DVL2 constructs were described previously [28].

Lentivirus-mediated Dvl rescue in Dvl KO cells

Lentiviruses were packaged and produced in HEK293T cells by co-transfection of the lentiviral vectors with the packaging plasmids pRSV-REV, pMD-2-G and pMD-Lg1-pRRE (gifts from Thomas Vierbuchen). 0.075mL of the viral supernatants was used to infect Dvl TKO MaxP dual reporter cells seeded at 20% confluency in 24-well plates. Puromycin selection (0.003 mg/ml) was carried out for five days. Cells from the viral titer that killed ~90% of cells were expanded and used for flow cytometry; this ensured that the multiplicity of infection (MOI) is ~1 for all cell lines used in the experiments.

Antibodies

Antibodies against Ror1, Ror2, Kif26b, and Pdzrn3 were described previously [6, 8, 9]. The following antibodies were purchased: rabbit anti Dvl2 (#3216, Cell Signaling), mouse anti Dvl3 (Santa Cruz Biotechnology, sc-8027), mouse anti C-myc (clone 9E10, Thermo Fisher Scientific, catalog #9801) and mouse anti-α-tubulin (Abcam, ab7291 clone DM1A). Dvl1 antibodies were generated in-house. Rabbits were immunizing with a synthetic peptide with the sequence RNRDEAARTNGHPRGDRRRDLGLPP conjugated to keyhole limpet hemocyanin (77600,

ThermoFisher Scientific). Antibodies were affinity purified from antisera over a column with the antigen Dvl1 peptide covalently immobilized to Sepharose beads (AminoLink Plus, 20501, ThermoFisher Scientific).

Western blotting

Protein lysates for SDS-PAGE and western blotting were prepared in 2x Laemmli sample buffer or RIPA. Protein lysates used for Kif26b western blotting were not heated as previously described [9]. All other protein lysates were heated at 95C for 5 min before SDS-PAGE and western blotting. Quantitative western blotting was performed using the Azure Sapphire Biomolecular Imager (Azure Biosystems) according to the manufacturer's instructions.

Recombinant proteins and inhibitors

The following recombinant proteins and drugs were purchased and used at the corresponding concentrations: human/mouse Wnt5a (200ng/mL, 654-WN-010, R&D Systems); Wnt3a (100ng/mL, 1324-WN-002, R&D Systems); Wnt-C59 (10nM, C7641-2s; Cellagen Technology).

Reverse transcription and qPCR

Total RNA was isolated from MaxP dual reporter cells using the RNeasy Plus Mini Kit (Qiagen, #74134), and cDNA was synthesized using Maxima H Minus reverse transcriptase and oligo dT

primers (EP0751, ThermoFisher Scientific), both according to the manufacturer's instructions. The cDNA generated from the reverse transcription reaction was used in the QuantiNova SYBR Green PCR Kit (Qiagen, #208054). The following qPCR primer pairs were used: mAxin2 forward: GATGTCTGGCAGTGGATGTTAG, mAxin2 reverse: GACTCCAATGGGTAGCTCTTTC.

Flow cytometry

MaxP dual reporter cells (and all subsequent knockout and rescue derivative lines) were plated at a density of 0.08-0.9M/well in 48-well plates directly in complete media containing Wnt-C59 (10nM). 48 hours after plating, cells were stimulated overnight with rWnt5a or rWnt3a in the presence of Wnt-C59. The following day cells were harvested, resuspended in PBS + 0.5% FBS, and analyzed via flow cytometry (Beckman Coulter CytoFLEX, 488nm and 638nm lasers). Raw data were acquired with CytExpert (Beckman Coulter) and processed in FlowJoX (Treestar, Inc). Processing entailed gating out dead cells, calculation of median fluorescence, percent change (Wnt5a-Ror signaling) or fold change (Wnt/β-catenin signaling) of median values and overlay of histograms. All dose-response curves were fitted in Prism (GraphPad Software).

Results

MaxP dual reporter cells facilitate analysis of Dvl function in Wnt5a-Ror and Wnt/β-catenin signaling

To investigate the Dvl family's function as mediators of multiple Wnt signaling pathways, we sought to develop a physiologically relevant and quantitative assay system derived from cells that undergo robust Wnt5a-Ror and Wnt/β-catenin signaling. Ideally, in this system we could simultaneously measure both Wnt pathways in live cells, which would be amenable to long-term downstream genetic manipulation. Based on these criteria, we derived primary cell lines from E11.5 mouse maxillary prominences (MaxP), which, at this particular developmental timepoint, express both non-canonical and canonical Wnt signaling components [31] such as Wnt5a and Wnt3a as well as several Frizzled receptors [32]. MaxP from multiple embryos were microdissected, pooled, and dissociated into single cells (Figure 1A). Subsequently, MaxP cells were immortalized through CRISPR/Cas9 mediated deletion of the *TP53* gene, an approach we have used before to immortalize primary mouse embryonic fibroblasts [29, 62].

Initially we assessed whether immortalized MaxP cells could indeed undergo robust Wnt5a-Ror and Wnt/β-catenin signaling. To determine this, we treated cells with Wnt-C59 to block endogenous Wnts and, in the presence of Wnt-C59, stimulated them with recombinant Wnt5a (rWnt5a) to activate the Wnt5a-Ror signaling pathway. Through western blotting, we observed that MaxP cells indeed undergo robust Wnt5a-Ror signaling as evidenced by a decrease in Kif26b and Pdzrn3 protein abundance over time as well as increases in Ror2 and Dvl2 phosphorylation (Figure 1B), all indicators of Wnt5a-Ror signaling activity that we previously reported [6, 8, 9]. To assay for Wnt/β-catenin signaling, we similarly added

recombinant Wnt3a (rWnt3a) to Wnt-C59 treated MaxP cells and observed increases in *Axin2* mRNA levels, a transcriptional target of Wnt/β-catenin signaling, based on real-time quantitative PCR (RT-qPCR) (Figure 1C) [33-35]. Thus, from these experiments we concluded that MaxP cells respond to both Wnt5a-Ror signaling and Wnt/β-catenin signaling and therefore are suitable for the functional investigation of Dvls in these pathways.

We next implemented a more high-throughput means to quantitatively measure both Wnt5a-Ror and Wnt/β-catenin signaling activity in live MaxP cells. We developed a dual reporter strategy in which two different fluorescence-based reporters were stably expressed in MaxP cells: 1) a GFP-based reporter, in which GFP is fused to a C-terminal fragment of Kif26b (GFP-Kif26b-C, Figure 1D), a downstream effector of Wnt5a-Ror signaling that is degraded upon pathway activation [9, 30] and 2) a miRFP670-based reporter, in which miRFP670 expression is upregulated by activation of Wnt/β-catenin signaling (7TR, Figure 1D) [36]. We stably introduced these reporters into MaxP cells and derived single clones through which we could analyze changes in both Wnt signaling activities in live cells via multi-color flow cytometry. Through treatment of these cells with rWnt5a or rWnt3a, in the presence of Wnt-C59, we were able to quantify both GPF-Kif26b-C degradation and the induction of 7TR expression (Figure 1Ei and 1Eiii, respectively). Dose-response analysis indicated that each fluorescent-reporter exhibited EC_{50} values comparable to other Wnt-induced responses, including those we have previously reported (Figure 1Eii and 1Eiv) [6, 8, 9, 37-41]. Additionally, we noted that rWnt3a could activate both fluorescent reporters whereas rWnt5a only activated the GFP-Kif26b-C reporter, findings that we have observed previously in other cell types [8, 9]. Thus, MaxP dual reporter cells are an ideal substrate in which to interrogate Dvl activity in multiple Wnt signaling pathways.

Individual Dvl homologs are differentially required and utilized in Wnt5a-Ror and Wnt/β-catenin signaling

Using the MaxP dual reporter system, we could now begin to ask questions about Dvl activity at the branchpoint of Wnt5a-Ror and Wnt/β-catenin signaling. As the first step in this analysis, we tested which Dvl family members are expressed in MaxP cells. Using anti-Dvl1 rabbit polyclonal antibodies that we generated in house, as well as commercially available antibodies against Dvl2 and Dvl3, we observed that all three Dvls are expressed in MaxP dual reporter cells (Figure 2Ai-iii). Like previous reports, we noted that Dvl1, Dvl2, and Dvl3 each appeared as a characteristic doublet of bands that, upon addition of rWnt5a or rWnt3a after treatment with Wnt-C59, resulted in an upward mobility shift indicative of phosphorylation (Figure 2A) [5, 37, 42-46].

Although multiple groups have previously established that Dvls are required for Wnt/β-catenin signaling [47-49], whether Dvls are required for Wnt5a-Ror signaling has never been tested. To answer this question, we used CRISPR/Cas9 to generate Dvl triple knockout (TKO) MaxP dual reporter cells (hereafter referred to as Dvl TKO cells, KO validations shown in Figure 2Bi-iii and Supplemental Figure 2A) and evaluated the ability of these cells to undergo Wnt5a-Ror signaling. Importantly, we observed total loss of Wnt5a-Ror signaling in Dvl TKO cells (Figure 2Ci), indicating that Dvls are functionally required for Wnt5a-Ror signaling. Consistent with previous reports, we also noted a corresponding loss of Wnt/β-catenin signaling as well (Figure 2Cii). Thus, we demonstrated conclusively that Dvls are required for both Wnt5a-Ror and Wnt/β-catenin signaling.

Next, we focused on systematically evaluating the contribution of each individual Dvl homolog to Wnt5a-Ror and Wnt/β-catenin signaling. While many studies have focused on Dvl2 activation and function, fewer studies have examined the roles of Dvl1 and Dvl3 in Wnt signaling pathways, in part due to lingering uncertainty surrounding whether Dvl homologs are truly redundant or not [5, 50]. With our experimental paradigm, we could now assess the extent of

functional redundancy among Dvl homologs for both Wnt5a-Ror and Wnt/β-catenin signaling. We again utilized CRISPR/Cas9 to generate single Dvl knockout (KO) MaxP dual reporter cells (Figure 2Bi-iii and Supplemental Figures 2B-D). Here, we observed that genetic deletion of each individual Dvl resulted in a distinct signaling deficit in each pathway. Within the Wnt5a-Ror signaling pathway, genetic deletion of Dvl1 had no statistically significant effect on Wnt5a-Ror signaling activity (Figure 2Ci), indicating that Dvl1 is either not required for this signaling pathway and/or that its function can be fully compensated by other family members. In contrast, genetic deletion of Dvl2 and Dvl3 each resulted in a partial and significant reduction in Wnt5a-Ror signaling activity (Figure 2Ci), with loss of Dvl3 causing a greater effect than loss of Dvl2. Overall, these findings indicate that, in our MaxP dual reporter system, each Dvl has a unique requirement in Wnt5a-Ror signaling and that Dvl3 has the greatest contribution to this signaling event.

To assess the requirement of individual Dvls in Wnt/β-catenin signaling, we examined the induction of the miRFP670 reporter in Dvl1, Dvl2, and Dvl3 KO MaxP dual reporter cells. Here, we observed striking differences in the utilization of individual Dvl homologs in Wnt5a-Ror versus Wnt/β-catenin signaling. Whereas genetic deletion of each individual Dvl impacted Wnt5a-Ror signaling to different degrees, we noticed that loss of any of the three Dvls minimally impacted Wnt/β-catenin signaling (Figure 2Cii). Taken all together, these results suggest that Dvl homologs are non-redundant in Wnt5a-Ror signaling but redundant in Wnt/β-catenin signaling in MaxP cells.

To further validate our discovery that Dvls are differentially utilized and required in Wnt5a-Ror and Wnt/β-catenin signaling, we utilized a rescue strategy conducted in our Dvl TKO cells in which we re-expressed N-terminally myc-tagged mouse Dvl1, Dvl2, or Dvl3 to near-endogenous (i.e., parental reporter) levels (Figure 2Di-iii). Similar to our findings observed in Dvl KO MaxP dual reporter cells, we observed differential utilization of individual Dvls in Wnt5a-Ror

versus Wnt/β-catenin signal pathways with re-expression of each Dvl homolog. As compared to no rescue (Dvl TKO) or an empty vector rescue, re-expression of Dvl1-3 rescued Wnt5a-Ror signaling to varying degrees (Figure 2Ei). Both re-expression of Dvl1 and Dvl2 rescued Wnt5a-Ror signaling to similar extents, mirroring the Wnt5a-Ror signaling changes observed in the Dvl1 and Dvl2 KO MaxP dual reporter cells (compare 2Ci and 2Ei). Further, we noticed that re-expression of Dvl3 was able to restore the most Wnt5a-Ror signaling activity (Figure 2Ei), mirroring the significant decrease observed in Dvl3 KO MaxP dual reporter cells. However, examination of Wnt/β-catenin signaling similarly paralleled our observations from Figure 2Cii, which showed that re-expression of any of the three Dvls can fully rescue signaling activity and that Dvls are redundant in this pathway (Figure 2Eii). All together these results indicate that Dvls are indeed required for Wnt5a-Ror signaling, a long-standing hypothesis that until this study remained untested. Further, our evidence indicates that Dvls are differently required and utilized in Wnt5a-Ror versus Wnt/β-catenin signaling.

Dvl domains are differentially used to facilitate Wnt5a-Ror and Wnt/β-catenin signaling

We next questioned which domains of Dvl are required for Wnt5a-Ror versus Wnt/β-catenin signaling. Dvl scaffolding proteins all possesses three highly conserved and modular domains: DIX, known for its interactions with Axin, a component of the destruction complex utilized in Wnt/β-catenin signaling; PDZ, known to mediate many protein-protein interactions in multiple Wnt signaling pathways; and DEP, involved in Dvl interactions with Frizzled receptors at the cell membrane (Figure 3A) [5]. Earlier reports that relied on overexpression of Dvl domain truncation mutants suggested that the more N-terminal domains, DIX and PDZ, are required for Wnt/β-catenin signaling, whereas the more C-terminal domains, PDZ and DEP, are involved in

non-canonical Wnt pathways [11, 12, 19, 21, 51-54]. However, more recent studies that have taken approaches similar to the one used in this study, where Dvls are re-expressed at near endogenous levels in Dvl triple knockout cells, have refined this paradigm and demonstrated that the DIX as well as the DEP domains are highly critical to Wnt/β-catenin signaling [45, 49, 55]. However, corresponding studies examining Dvl domain truncations and their effects in non-canonical Wnt pathways, particularly Wnt5a-Ror signaling, have yet to be conducted under such conditions. Therefore, our understanding of the domains required for Dvl function in different Wnt signaling pathways is likely incomplete. In addition to these modular domains, Dvls possess an unstructured C-terminus (Figure 3A). While this region of Dvls can be highly variable between individual homologs, the final ~30 amino acids are highly conserved across organisms and between isoforms and culminates in a PDZ domain binding motif (Figure 3A). This region has a few reported functions, including one wherein the C-terminus acts as an autoregulatory feature that modulates conformational changes [56, 57]. However, the importance of this region to Wnt5a-Ror signaling has remained largely unexamined.

To systematically compare which domains are required for the Wnt5a-Ror pathway versus the Wnt/β-catenin signaling pathway, we analyzed the ability of Dvl3 domain truncation mutants rescue signaling in Dvl TKO cells (Supplemental Figure 3A). We selected mouse Dvl3 to generate the truncation mutants based on its strong ability to rescue signaling in both Wnt5a-Ror and Wnt/β-catenin signaling (see Figure 2Ei and 2Eii). Using this approach, we tested mDvl3 mutants lacking the DIX, PDZ, or DEP domains or the C-terminus (Figure 3A). Here, we observed that different domains were required for Wnt5a-Ror versus Wnt/β-catenin signaling. Contrary to traditional thinking where non-canonical Wnt pathways rely solely on the PDZ and DEP domains to facilitate signal transduction, we noted that each domain is strongly required for Wnt5a-Ror signaling, including the DIX domain (Figure 3Bi). In contrast, deletion of the C-terminus had no impact on signaling and was indistinguishable from the wild-type Dvl3 rescue

(Figure 3Bi). Collectively, these findings suggest that the modular DIX, PDZ, and DEP domains are critical to Dvl function in Wnt5a-Ror signaling activity while the Dvl C-terminus is dispensable.

When we examined the effects of Dvl3 domain truncation mutants on Wnt/β-catenin signaling (Figure 3Bii), our findings agreed with those previously reported by others. The most devastating effects on Dvl3-mediated Wnt/β-catenin signal transduction were caused by loss of the DEP and DIX domains, both of which are critical for establishing multimeric signalosomes that facilitate Wnt/β-catenin signaling [45, 49, 55]. In contrast, the PDZ domain is dispensable for Wnt/β-catenin signal transduction, which has been shown previously [5] (Figure 3Bii). Additionally, we noted that deletion of the C-terminus had no impact on Wnt/β-catenin signaling and was indistinguishable from the wild-type Dvl3 rescue. Overall, these findings indicate that different domains are required to facilitate Wnt5a-Ror versus Wnt/β-catenin signaling and that the Dvl C-terminus is not required for signal transduction of either pathway.

We noted that deletion of the DEP domain significantly limits both Wnt5a-Ror and Wnt/β-catenin signaling. The DEP domain possesses a critical lysine that, when mutated, causes a strong planar cell polarity (PCP) phenotype in *Drosophila* [63], which is a non-canonical Wnt signaling pathway. Subsequent analysis showed that this mutant protein can still support canonical Wnt/β-catenin signaling in *Drosophila* [52]. Because this lysine is highly conserved across multiple organisms and in mouse and human Dvl1-3 (Figure 3C), we wondered if mutating the analogous mouse Dvl3 lysine (K435M) would impact Wnt5a-Ror signaling and/or Wnt/β-catenin signaling. To test this, we introduced Dvl3^{K435M} into Dvl TKO cells and assayed both Wnt5a-Ror and Wnt/β-catenin signaling (Figure 3D). Interestingly, we observed that, like the mDvl3ΔDEP domain truncation mutant, Dvl3^{K435M} was completely incapable of rescuing Wnt5a-Ror signaling (compare 3Bi with 3Di). In contrast, Dvl3^{K435M} strongly reduces, but does not completely abolish, Wnt/β-catenin signaling (Figure 3Dii), indicating that K435 also plays a

major role in signaling. While these differences are perhaps not as stark as those reported in *Drosophila* (i.e., an absolute loss of signaling in the non-canonical Wnt pathway but no changes in signaling in the canonical Wnt pathway), previous publications examining the Dvl DEP domain in vertebrates and *Drosophila* Dsh suggest that there may be sequence differences that account for mechanistic changes that we cannot yet appreciate, particularly in Wnt/β-catenin signaling [45]. Regardless, all together these data demonstrate the importance of the DEP domain to both Wnt5a-Ror and Wnt/β-catenin signaling.

These results further build on the paradigm wherein different domains of Dvl are differentially used in Wnt5a-Ror and Wnt/β-catenin signaling. In this augmented model, the DEP domain is critical to both Wnt5a-Ror and Wnt/β-catenin signaling. Moreover, we find that under our assay conditions, Dvl C-terminus does not impact Dvl function's signaling function in both Wnt5a-Ror and Wnt/β-catenin signaling.

Wnt5a-Ror-induced phosphorylation of the Dvl C-terminus impacts Dvl activity in Wnt5a-Ror but not Wnt/β-catenin signaling

Dvl phosphorylation has long been used as an indicator of signaling activity for both Wnt5a-Ror and Wnt/β-catenin signaling pathways [19, 20, 37, 42, 44-46, 58, 59]. From our previous phospho-proteomic studies, we identified multiple phosphorylation events within Dvl1, Dvl2, and Dvl3 that were driven by Wnt5a-Ror signaling activity [8, 9]. All of the identified phosphorylation sites were located in the Dvl C-terminus and clustered into two groups (Figure 4A). Group 1 sites consisted of a series of alternating serine residues detected in Dvl2 (Figure 4B, green bolded residues; S614, S616, S618, and S620). Although not experimentally detected in Dvl1 or Dvl3 in our phospho-proteomic study, some of these serines are also conserved in

both Dvl1 and Dvl3 (Figure 4B, bolded residues are conserved). Group 2 appeared to encode a Casein Kinase 1 (CK1) motif (S/T-X-X-S/T), a kinase that is known to phosphorylate Dvl in Wnt/β-catenin signaling (Figure 4C, green bolded residues; Dvl1 Group 2 sites are S675 and S678, and Dvl3 Group 2 sites are S696 and S699) [37, 42, 44, 46, 59, 60]. Although only detected in Dvl1 and Dvl3 in our phospho-proteomic analysis, these residues are conserved across all three mouse Dvl homologs (Figure 4C, green and black bolded residues). Interestingly, these residues were previously identified in Dvl3 in another mass spectrometry screen in which CK1ε was overexpressed [44]; however, as far as we are aware, the functionality of these phosphorylation sites have not been examined.

Given that we identified these phosphorylation sites in Wnt5a-Ror-specific proteomic screens, we hypothesized that mutating these C-terminus phosphorylation residues might selectively impact this pathway, which in turn could providing mechanistic insights into pathway-specific regulation of Dvl function. We generated Dvl constructs with each of these phosphorylation sites mutated to alanines in Dvl2 (Group 1 sites S614A, S616A, S618A, S620A) and Dvl1 and Dvl3 (Group 2 sites S675 and S678 in Dvl1 and Group 2 sites S696 and S699 in Dvl3) and re-expressed them in Dvl TKO cells (Supplemental Figure 4Ai-iii). First, we examined the Group 1 phosphorylation sites identified in Dvl2. Interestingly, mutation of the Group 1 sites in Dvl2 ($Dvl2^{S614A, S616A, S618A, S620A}$) did not hinder its ability to rescue signaling in Wnt5a-Ror signaling, and in fact was indistinguishable from its wild-type counterpart (Figure Di). Instead, there was a small but significant reduction in Wnt/β-catenin signaling (Figure Dii). In contrast, we observed that mutation of the Group 2 sites in Dvl1 ($Dvl1^{S675A, S678A}$) as well as in Dvl3 ($Dvl3^{S696A, S699A}$) led to a significant reduction in their capacity to rescue Wnt5a-Ror signaling (Figure 4Ei and Fi). Within the Wnt/β-catenin signaling pathway, $Dvl1^{S675A, S678A}$ only slightly signaling (Figure 4Eii), while $Dvl3^{S696A, S699A}$ had no effect on signaling (Figure 4Fii).

Taken together, this analysis identified key phosphorylation sites that are selectively required for Wnt5a-Ror signal transduction.

Robinow and Robinow-like syndrome DVL mutations alter Wnt5a-Ror and Wnt/β-catenin signaling via distinct mechanisms

With our newfound understanding of how Dvls mediate signal transduction of both Wnt5a-Ror and Wnt/β-catenin signaling pathways, we next questioned how RS mutations might impact DVL activity. RS mutations identified in human *DVL1* and *DVL3*, in addition to bulldog *DVL2* mutation, are all frameshift mutations that that alter their C-termini sequences (Figure 5A), leading to the production of a short novel protein sequence as well as a slight truncation. Based on the locations of RS mutations, the modular DIX, PDZ, and DEP domains are predicted to be unaffected [25, 27, 61].

Given the close connection between RS and Wnt5a-Ror signaling, we and others have hypothesized that RS DVL variants affect Wnt5a-Ror signaling activity. However, we also recognized the possibility that RS DVLs might affect signaling in multiple Wnt pathways, such as Wnt/β-catenin signaling. Further, based on our findings from this study that Dvls are functionally non-redundant in Wnt5a-Ror signaling, we realized that each RS DVL variant could potentially act through a unique mechanism that was influenced by their individual capacities to signal (Figure 2Ei and Eii). In fact, this notion is further supported by several patient studies, which demonstrate that patients with mutations in *DVL1* often present with symptoms unique from those exhibited by patients with mutations in *DVL3* and vice versa [23, 24]. To test these hypotheses and determine how RS DVL variants affect downstream signaling in multiple Wnt pathways, we re-expressed RS-DVL1, RS-DVL3, and RS-DVL2 (bulldog variant) in Dvl TKO

cells (Supplemental Figure 5Ai-iii) and evaluated changes in Wnt5a-Ror and Wnt/β-catenin signaling activity.

As compared to WT-DVL1, re-expression of RS-DVL1 was unable to rescue Wnt5a-Ror signaling; in fact, RS-DVL1 resulted in slightly increased stabilization of GFP-Kif26b-C, as evidenced by the negative percent degradation, suggesting that this frameshift mutation imparts dominant interfering activity on this DVL variant (Figure 5Bi). However, in the Wnt/β-catenin signaling reporter, we observed entirely different behavior from RS-DVL1, wherein it rescued Wnt/β-catenin signaling far beyond both the parental reporter levels as well as the WT-DVL1 rescue (Figure Bii). These findings, namely that the RS-DVL1 variant is overactive in Wnt/β-catenin signaling, align with those previously reported based on overexpression of RS-DVL1 in a heterologous system [61]. In summary, we determined that RS-DVL1 differentially affects Wnt5a-Ror and Wnt/β-catenin signaling pathways.

Interestingly, we discovered that the RS-DVL3 variant exhibits qualitatively different effects on Wnt5a-Ror and Wnt/β-catenin signaling. Here, we observed that, in contrast to RS-DVL1, the rescue activity of RS-DVL3 in Dvl TKO cells resulted in overactivation of both Wnt5a-Ror and Wnt/β-catenin signaling, suggesting it may act as a gain of function mutant (Figure 5Ci and Cii) in both signaling pathways. These findings indicate that a combination of signaling defects in both pathways contribute to the underlying molecular etiology of RS.

Remarkably, we discovered that the bulldog RS-DVL2 variant displays yet another mechanism distinct from both RS-DVL1 and RS-DVL3. When re-expressed in Dvl TKO cells, RS-DVL2 can rescue less than 50% of the Wnt5a-Ror signaling activity that WT-DVL2 rescues (Figure 5Di), suggesting that this is a loss of function variant. Additionally, similar to RS-DVL3 but unlike RS-DVL1, RS-DVL2 also exhibits a reduced ability to rescue Wnt/β-catenin signaling (Figure 5Dii). Taken together, we conclude that despite their strikingly similar genetic signature

(i.e. -1 frame shift affecting the C-terminal domain), each RS and RS-like mutant alters Wnt5a-Ror and Wnt/β-catenin signaling pathways through a unique mechanism.

Discussion

Dvls have long been a point of fascination within Wnt signaling. Their discovery as a scaffolding protein capable of differentially transmitting signals to non-canonical or canonical signaling pathways has garnered decades of intense scrutiny to understand Dvl function. However, the expression of multiple Dvl homologs in vertebrates has long complicated analysis of individual homolog function. Moreover, while the development of molecular tools to track Wnt/β-catenin signaling has facilitated interrogation of Dvl function specific to this pathway, corresponding readouts and molecular tools that can monitor non-canonical Wnt signaling pathways have remained limited until recent years. Instead, changes in non-canonical Wnt pathways driven by Dvls and corresponding mutants have long depended on phenotypic analyses, which is readily influenced by the presence of wild-type Dvl homologs and can complicate data interpretation. Thus, to evaluate Dvl function, specificity, and differential regulation more directly in multiple Wnt signaling pathways in the same cell type, we developed a dual reporter system in which Wnt5a-Ror and Wnt/β-catenin signaling can be assayed in the same cells. In the present study is a proof of concept that demonstrates the utility of this platform and its ability to generate insight into Dvl-mediated signal transduction at the intersection of Wnt5a-Ror and Wnt/β-catenin signaling.

Using this genetically tractable and quantitative system, we determine conclusively for the first time that Dvls are required for Wnt5a-Ror signaling. Additionally, we used this platform to answer questions about Dvl redundancy by interrogating the individual contributions of Dvl1-3 to Wnt5a-Ror and Wnt/β-catenin signaling. We discovered that individual Dvl homologs are differentially utilized in Wnt5a-Ror versus Wnt/β-catenin signaling. Here, we observed that Dvl1, Dvl2, and Dvl3 individually possess differential abilities to rescue Wnt5a-Ror signaling, suggesting that Dvls are functionally non-redundant in MaxP cells. In contrast, we find that Wnt/β-catenin signaling is more tolerant of different Dvl homologs, and any of the three Dvls can

mediate signaling, making them more redundant in this pathway. Taken together, these data indicate one mechanism by which Dvls differentially transmit signals to distinct Wnt signaling pathways.

Through analysis of Dvl domain truncation mutants, we also determined which Dvl domains are required in Wnt5a-Ror and in Wnt/β-catenin signaling. Our work confirms that the DIX and DEP domains are indeed most critical for Wnt/β-catenin signal transduction, whereas loss of the PDZ domain slightly impacts Wnt/β-catenin signaling but not to the same extent as deletion of the DIX or DEP domains. Within Wnt5a-Ror signaling, we noticed that loss of any of the three domains does significantly reduce activity, with deletion of the PDZ and DEP domains impacting downstream signaling the most. Further detailed molecular studies focused on identifying specific domain interactors may provide additional insight in the future.

Perhaps most interesting from our domain truncation analysis is the finding that deletion of the Dvl C-terminus does not impact Dvl function in either Wnt5a-Ror or Wnt/β-catenin signaling, which suggests that this region of Dvl is not required for signal transduction. However, these results appear to contradict our data showing that specific Wnt5a-Ror phosphorylation sites within the Dvl C-terminus regulate signaling activity in this pathway. Here, we observed that mutation of the Group 2 sites identified in Dvl1 (Dvl1$^{S675A, S678A}$) and Dvl3 (Dvl3$^{S696A, S699A}$) significantly reduced their ability to rescue Wnt5a-Ror signaling but minimally impacted Wnt/β-catenin signaling. To reconcile these findings, we propose that the Dvl C-terminus itself functions as a molecular switch to direct signals towards distinct Wnt pathways. When present, phosphorylation of the Group 2 sites within the Dvl C-terminus are needed to propagate signals downstream to the Wnt5a-Ror pathway; ablation of these sites limits Dvl function within this pathway but not in Wnt/β-catenin signaling. In removing the Dvl C-terminus entirely, this molecular switch is lost, and Dvl signals at nearly wild-type rescue levels in both pathways without discriminating one from the other.

This model could also, in part, explain some of the downstream signaling changes driven by RS DVL variants. Our analysis of the human RS-DVL1 and -DVL3 along with the bulldog DVL2 (RS-DVL2) demonstrated that each individual variant disrupted both Wnt5a-Ror and Wnt/β-catenin signaling through a distinct mechanism. With the introduction of RS DVL mutations into the C-terminus, perhaps the ability of DVL to discriminate between Wnt signaling pathways is lost, leading to concurrent changes in multiple Wnt pathways. This concept aligns with our data. There is also the possibility that in addition to disrupting the molecular switch present in the wild-type Dvl C-terminus, RS DVL C-termini sequences themselves bestow DVLs with new functions. While further detailed molecular analysis is necessary to truly pinpoint the underlying signaling changes, the knowledge generated in this study concerning wild-type Dvl function within Wnt5a-Ror and Wnt/β-catenin signaling will serve as an important baseline to understand the molecular etiology of RS DVL variants in future studies.

Figures

Figure 1. Development of MaxP dual reporter cells as a platform to study Dvl at the intersection of Wnt5a-Ror and Wnt/β-catenin signaling. A) Derivation and immortalization of MaxP cells. Shaded circle and arrow indicate maxillary prominence region, just below the eye. **B**) Signaling analysis conducted on immortalized MaxP cells as analyzed via western blotting. Here, Kif26b and Pdzrn3 abundance decrease over time, which correlates with increases in Ror2 and Dvl2 phosphorylation. **C**) MaxP cells undergo robust Wnt/β-catenin signaling based on real-time quantitative PCR (RT-qPCR) analysis of *Axin2* transcripts after treatment with rWnt3a. **D**) Schematic depicting creation of dual reporter and flow cytometry analysis. **E**) GFP-Kif26b/7TR dual reporter (hereafter referred to as MaxP dual reporter cells) characterization: **i**) Representative bar graph showing changes in Wnt5a-Ror signaling activity driven by rWnt5a, **ii**) rWnt5a dose response curve, **iii**) representative bar graph showing changes in Wnt/β-catenin signaling driven by rWnt3a, and **iv**) rWnt3a dose response curve. Error bars represent ± SEM. P-values: *=p<0.05, **=p<0.01, ***=p<0.001, for this and all subsequent figures.

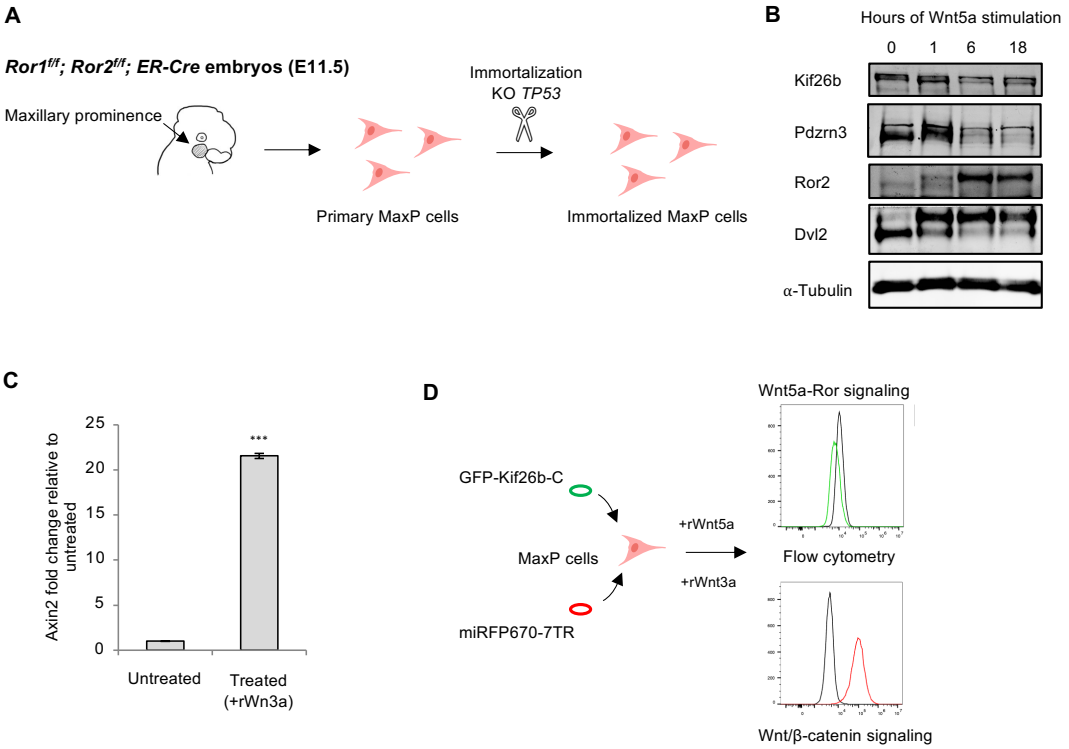
A
Ror1f/f; Ror2f/f; ER-Cre embryos (E11.5)
Maxillary prominence
Immortalization
KO TP53
Primary MaxP cells
Immortalized MaxP cells
B
Hours of Wnt5a stimulation
0 1 6 18
Kif26b
Pdzrn3
Ror2
Dvl2
α-Tubulin
C
Axin2 fold change relative to untreated
25
20
15
10
5
0
***
Untreated
Treated (+rWn3a)
D
Wnt5a-Ror signaling
GFP-Kif26b-C
MaxP cells
miRFP670-7TR
+rWnt5a
+rWnt3a
Flow cytometry
Wnt/β-catenin signaling
E
GFP-Kif26b/7TR dual reporter
i
GFP percent degradation (%)
45
40
35
30
25
20
15
10
5
0
***
Wnt buffer
rWnt5a
ii
Percent degradation (%)
EC50 = 83.6ng/mL
40
20
0
10^1
10^2
10^3
rWnt5a concentration (ng/ml)
iii
7TR fold change
40
35
30
25
20
15
10
5
0
***
Wnt buffer
rWnt3a
iv
Fold change
EC50 = 68ng/mL
40
20
0
10^1
10^2
10^3
rWnt3a concentration (ng/ml)

Figure 2. Dvls are required for Wnt5a-Ror signaling and functionally non-redundant. A) Western blot depicting Dvl1, Dvl2, and Dvl3 expressed in MaxP dual reporter cells. With the addition of rWnt5a or rWnt3a, each Dvl homolog exhibits a mobility shift upward, indicative of phosphorylation. **B**) Western blot validation of Dvl knockout cell lines. **C**) Bar graph depicting changes in **i**) Wnt5a-Ror signaling and **ii**) Wnt/β-catenin signaling in Dvl triple knockout (TKO) and single knockout (Dvl1 KO, Dvl2 KO, and Dvl3 KO) MaxP dual reporter cells. **D**) Representative western blots depicting re-expression of mDvl1-3 in Dvl TKO cells at near-endogenous levels. **E**) Bar graph depicting changes in **i**) Wnt5a-Ror signaling and **ii**) Wnt/β-catenin signaling driven by mDvl1-3 re-expressed in Dvl TKO cells.

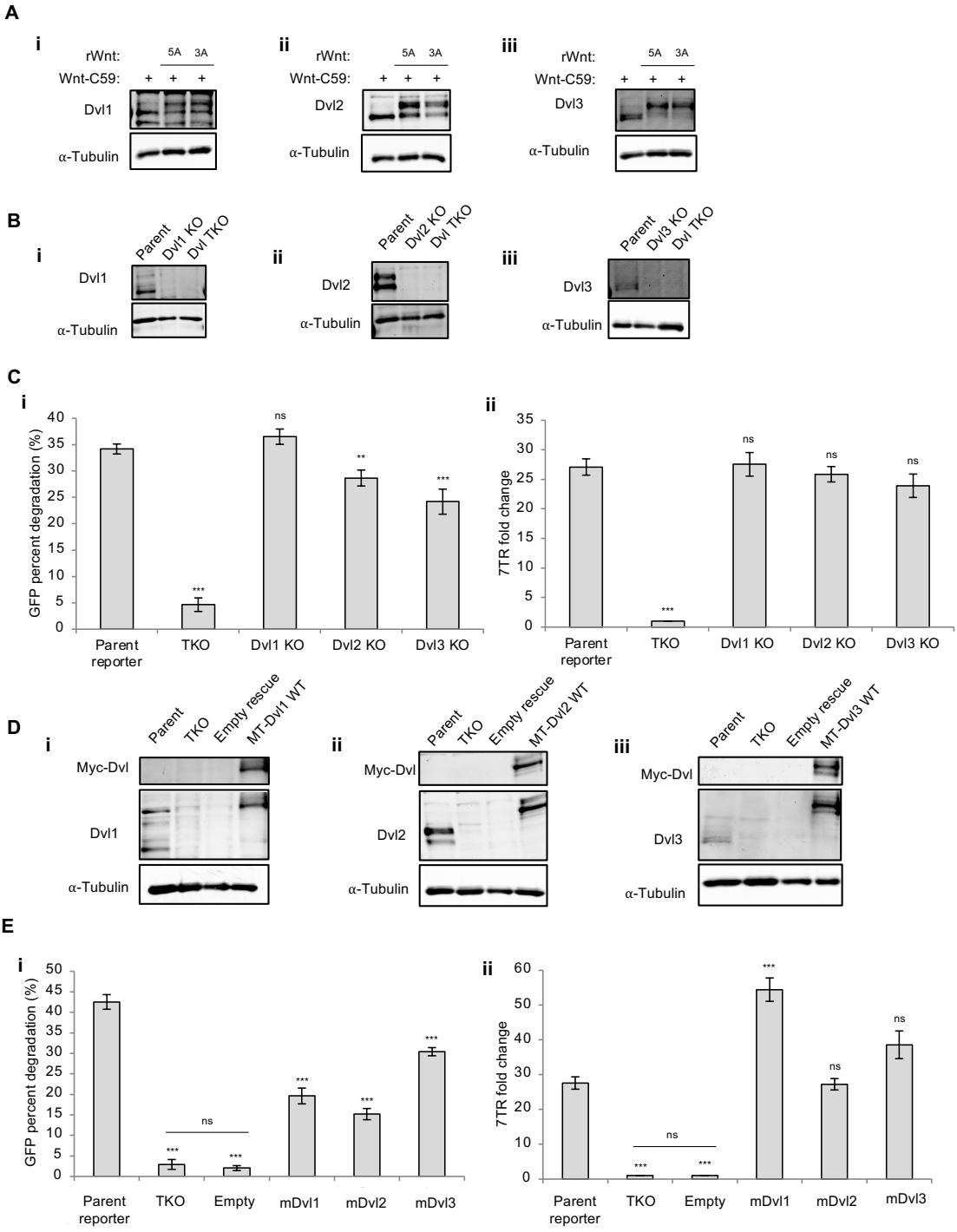
A
i
rWnt:
5A 3A
Wnt-C59:
+ + +
Dvl1
α-Tubulin
ii
rWnt:
5A 3A
Wnt-C59:
+ + +
Dvl2
α-Tubulin
iii
rWnt:
5A 3A
Wnt-C59:
+ + +
Dvl3
α-Tubulin
B
i
Parent
Dvl1 KO
Dvl TKO
Dvl1
α-Tubulin
ii
Parent
Dvl2 KO
Dvl TKO
Dvl2
α-Tubulin
iii
Parent
Dvl3 KO
Dvl TKO
Dvl3
α-Tubulin
C
i
GFP percent degradation (%)
0 5 10 15 20 25 30 35 40
ns
**
***
***
Parent reporter
TKO
Dvl1 KO
Dvl2 KO
Dvl3 KO
ii
7TR fold change
0 5 10 15 20 25 30 35
ns
ns
ns
***
Parent reporter
TKO
Dvl1 KO
Dvl2 KO
Dvl3 KO
D
i
Parent
TKO
Empty rescue
MT-Dvl1 WT
Myc-Dvl
Dvl1
α-Tubulin
ii
Parent
TKO
Empty rescue
MT-Dvl2 WT
Myc-Dvl
Dvl2
α-Tubulin
iii
Parent
TKO
Empty rescue
MT-Dvl3 WT
Myc-Dvl
Dvl3
α-Tubulin
E
i
GFP percent degradation (%)
0 5 10 15 20 25 30 35 40 45 50
ns
***
***
***
***
***
Parent reporter
TKO
Empty
mDvl1
mDvl2
mDvl3
ii
7TR fold change
0 10 20 30 40 50 60
ns
***
***
***
ns
ns
Parent reporter
TKO
Empty
mDvl1
mDvl2
mDvl3

Supplemental Figure 2. CRISPR/Cas9 mediated deletions of Dvl1-3 in MaxP dual reporter cells. References sequences for Dvl TKO (**A**), Dvl1 (**B**), Dvl2 (**C**), and Dvl3 (**D**) aligned to mutated alleles detected through deep sequencing.

A

B

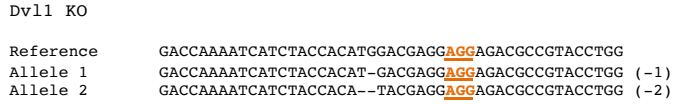

C

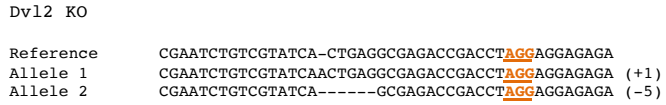

D

Figure 3. Dvl domain truncations identify domains differentially required for Wnt5a-Ror and Wnt/β-catenin while the C-terminus acts as a regulatory domain. A) Schematic representation of Dvl and the domain truncations analyzed in this study. **B**) Bar graph depicting changes in Wnt5a-Ror (**i**) and Wnt/β-catenin signaling (**ii**) driven by Dvl domain truncation mutants. **C**) Alignment of a portion of the *Drosophila*, *Xenopus*, mouse and human Dsh/Dvl DEP domain. The conserved lysine (K) that is mutated to a methionine (M) in the *Drosophila Dsh* mutant is highlighted in red. **D**) Bar graph depicting changes in Wnt5a-Ror (**i**) and Wnt/β-catenin signaling (**ii**) driven by mDvl3 WT or mDvl3^{K435M}.

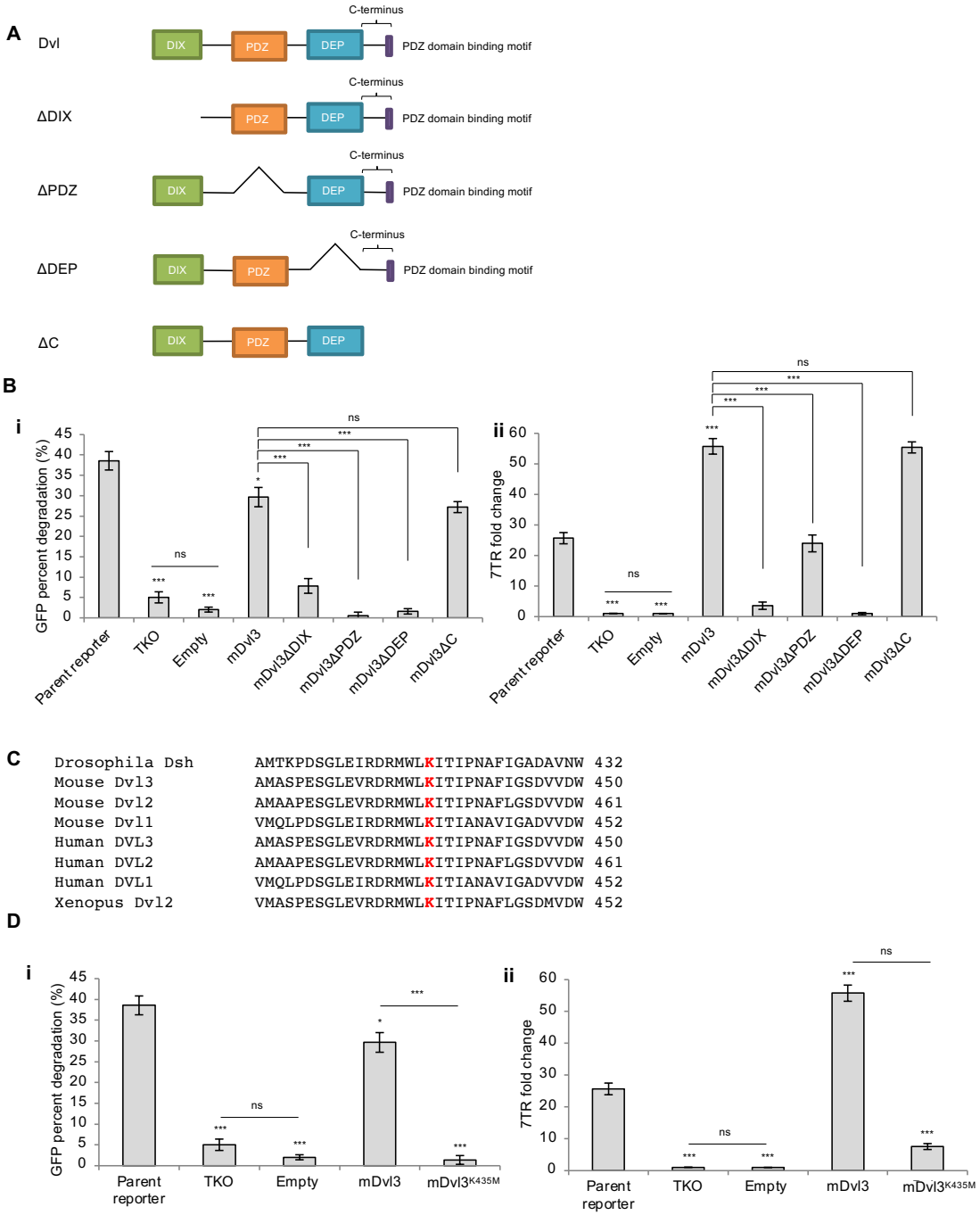
A
Dvl
ΔDIX
ΔPDZ
ΔDEP
ΔC
DIX
PDZ
DEP
C-terminus
PDZ domain binding motif
B
i
GFP percent degradation (%)
ii
7TR fold change
Parent reporter
TKO
Empty
mDvl3
mDvl3ΔDIX
mDvl3ΔPDZ
mDvl3ΔDEP
mDvl3ΔC
ns
C
Drosophila Dsh AMTKPDSGLEIRDRMWLKITIPNAFIGADAVNW 432
Mouse Dvl3 AMASPESGLEVRDRMWLKITIPNAFIGSDVVDW 450
Mouse Dvl2 AMAAPESGLEVRDRMWLKITIPNAFLGSDVVDW 461
Mouse Dvl1 VMQLPDSGLEIRDRMWLKITIANAVIGADVVDW 452
Human DVL3 AMASPESGLEVRDRMWLKITIPNAFIGSDVVDW 450
Human DVL2 AMAAPESGLEVRDRMWLKITIPNAFLGSDVVDW 461
Human DVL1 VMQLPDSGLEIRDRMWLKITIANAVIGADVVDW 452
Xenopus Dvl2 VMASPESGLEVRDRMWLKITIPNAFLGSDMVDW 452
D
i
GFP percent degradation (%)
ii
7TR fold change
Parent reporter
TKO
Empty
mDvl3
mDvl3K435M
ns

Supplemental Figure 3. Representative western blot depicting expression levels of mDvl3 A) domain truncation mutants and B) mDvl3^{K435M} in Dvl TKO cells.

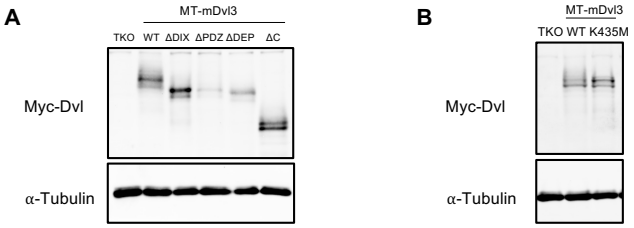

Figure 4. Wnt5a-Ror-induced phosphorylation in the Dvl C-terminus regulates Dvl function. A) Schematic of Dvl indicating the location of Group 1 and Group 2 Wnt5-Ror-induced phosphorylation sites in the C-terminus, represented with two red stars. **B**) Alignment of Group 1 alternating serines identified in Dvl2 in previous Wnt5a-Ror signaling TMT screens. Green and bolded residues represent serines detected in the screen, whereas bolded residues indicate serines that are conserved in either mouse Dvl1 or Dvl3. **C**) Alignment of Group 2 residues identified in mouse Dvl1 and Dvl3 in previous Wnt5a-Ror signaling TMT screens. Green and bolded residues represent serines detected in the screen, whereas bolded residues indicate serines that are conserved in mouse Dvl2. **D**) Bar graph depicting changes in Wnt5a-Ror (**i**) and Wnt/β-catenin signaling (**ii**) caused by either mDvl2 WT or mDvl2 S614A, S616A, S618A, S620A. **E**) Bar graph depicting changes in Wnt5a-Ror (**i**) and Wnt/β-catenin signaling (**ii**) caused by mDvl1 WT or phosphomutant mDvl1 S675A, S678A. **F**) Bar graph depicting changes in Wnt5a-Ror (**i**) and Wnt/β-catenin signaling (**ii**) caused by either mDvl3 WT or phosphomutant.

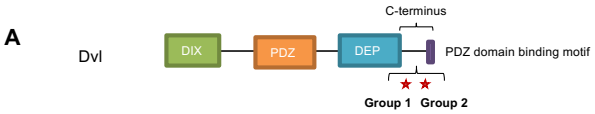

B **Group 1**

```
Mouse Dvl1 --TPGRE-ERRATGAGGSGSESDH----------TVPSGSGSTG 615
Mouse Dvl2 AGRTGRPEERAPESKSGSGSESELSSRGGSLRRGGEPGGTGDGG 644
Mouse Dvl3 -RRKEKDPKAGDSKSGGSGSESDHTTRSSLRG-PRERAPSERSG 626
```

C **Group 2**

```
Mouse Dvl1     GPPVRELAAVPPELTGSRQSFQKAMGNPCEFFVDIM* 695
Mouse Dvl2     APPVRDLGSVPPELTASRQSFHMAMGNPSEFFVDVM* 736
Mouse Dvl3     APPGRDLASVPPELTASRQSFRMAMGNPSEFFVDVM* 716
```

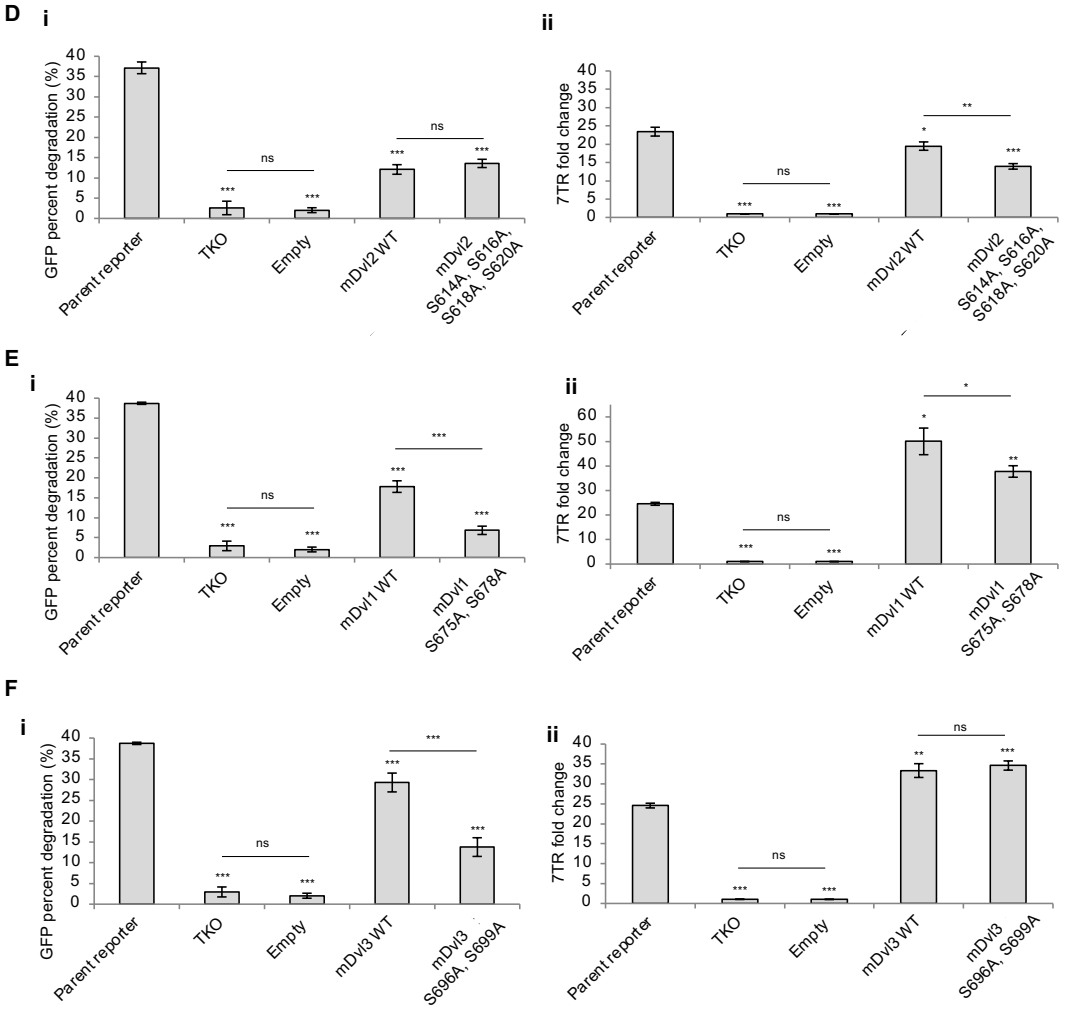

Supplemental Figure 4. Representative western blot depicting expression levels of Ai) wild-type (WT) and phosphomutant Dvl1, Ai) Dvl2, and Aiii) Dvl3 in Dvl TKO cells.

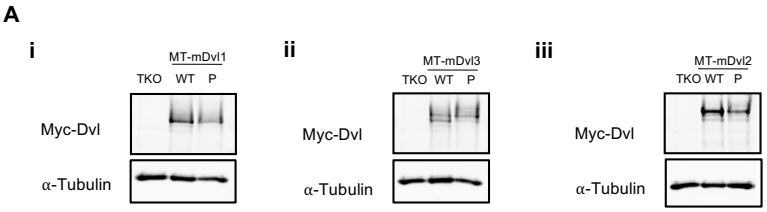

Figure 5. Robinow and Robinow-like mutations in the DVL C-terminus alter Wnt5a-Ror and Wnt/β-catenin signaling via distinct mechanisms. A) Alignment demonstrating the changes in C-terminus sequence in **i**) human DVL1, **ii**) human DVL3, and **iii**) bulldog DVL2, which were used in this study. **B**) Bar graph depicting changes in Wnt5a-Ror (**i**) and Wnt/β-catenin signaling (**ii**) driven by hDVL1 WT or RS variant. **C**) Bar graph depicting changes in Wnt5a-Ror (**i**) and Wnt/β-catenin signaling (**ii**) driven by hDVL3 WT or RS variant. **D**) Bar graph depicting changes in Wnt5a-Ror (**i**) and Wnt/β-catenin signaling (**ii**) driven by dDVL2 WT or RS variant.

A

```
hDVL1 WT PGLPPPHPTTKAYTVVGGPPGGPPVRELAAVPPELTGSRQSFQKAMGNPCEFFVDIM
hDVL1 RS RGSPRPTPRPRPIQWWGGHPGDPLSGSWLPSPRN-----------------------

hDVL3 WT PPGVPPLYGPPMLMMPPPPAAMGPPGAPPGRDLASVPPELTASRQSFRMAMGNPSEFFVDVM
hDVL3 RS LPECPLSTAPPC-----------------------------------------------------

dDVL2 WT PPGMALPYNPMMVVMMPPPPPPVPPAVQPPGAPPVRDLGSVPPELTASRQSFHMAMGNPSEFFVDVM
dDVL2 RS PPGMALPYNPMMVVMMPPLHPLSHQQCSPQGPLLSETWALCPQN-----------------------
```

B

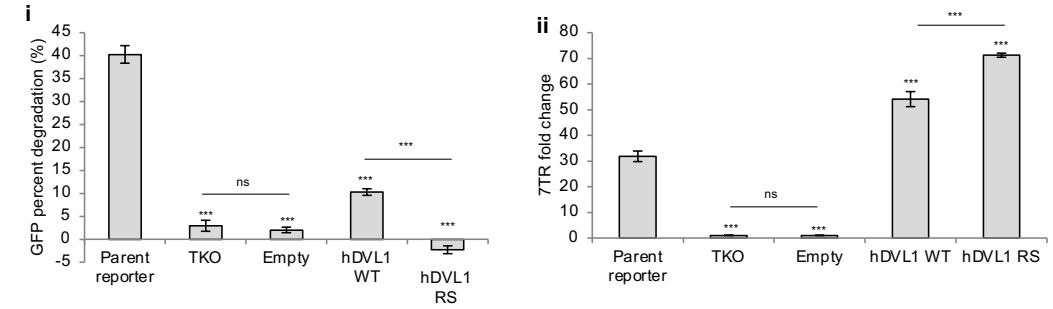

C

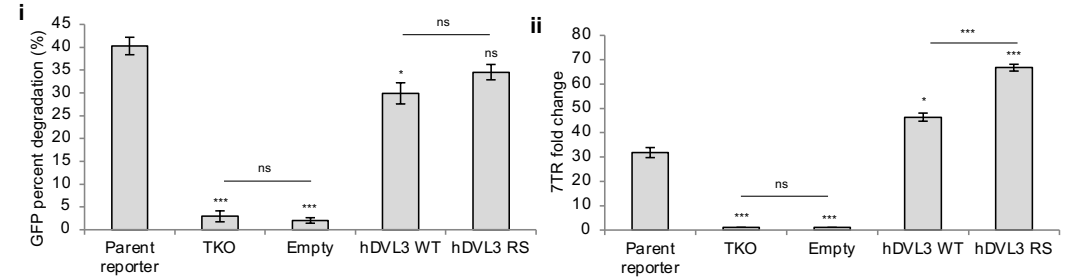

D

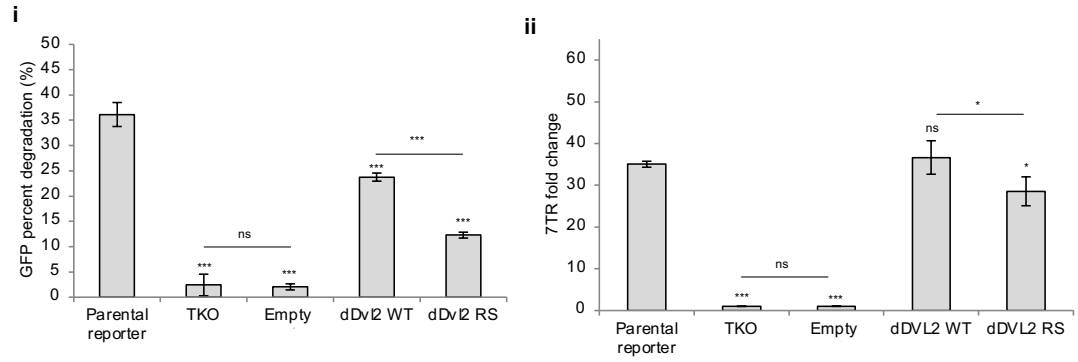

Supplemental Figure 5. Representative western blot depicting expression levels of Ai) WT and RS hDVL1, Ai) WT and RS hDVL3, and Aiii) WT and RS (bulldog) dDVL2 in Dvl TKO cells.

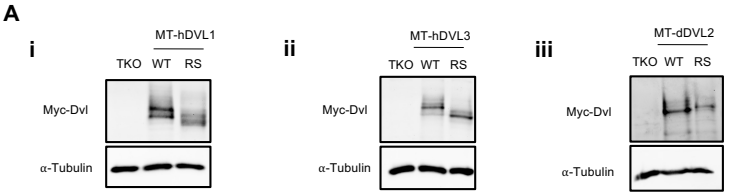

References

1. Zhong, Z., et al., *Wnts and the hallmarks of cancer.* Cancer Metastasis Rev, 2020. **39**(3): p. 625-645.
2. Steinhart, Z. and S. Angers, *Wnt signaling in development and tissue homeostasis.* Development, 2018. **145**(11).
3. Zhan, T., N. Rindtorff, and M. Boutros, *Wnt signaling in cancer.* Oncogene, 2017. **36**(11): p. 1461-1473.
4. Nusse, R. and H. Clevers, *Wnt/beta-Catenin Signaling, Disease, and Emerging Therapeutic Modalities.* Cell, 2017. **169**(6): p. 985-999.
5. Sharma, M., et al., *Dishevelled: A masterful conductor of complex Wnt signals.* Cell Signal, 2018. **47**: p. 52-64.
6. Ho, H.Y., et al., *Wnt5a-Ror-Dishevelled signaling constitutes a core developmental pathway that controls tissue morphogenesis.* Proc Natl Acad Sci U S A, 2012. **109**(11): p. 4044-51.
7. Yamaguchi, T.P., et al., *A Wnt5a pathway underlies outgrowth of multiple structures in the vertebrate embryo.* Development, 1999. **126**(6): p. 1211-23.
8. Konopelski Snavely, S.E., et al., *Proteomic analysis identifies the E3 ubiquitin ligase Pdzrn3 as a regulatory target of Wnt5a-Ror signaling.* Proc Natl Acad Sci U S A, 2021. **118**(25).
9. Susman, M.W., et al., *Kinesin superfamily protein Kif26b links Wnt5a-Ror signaling to the control of cell and tissue behaviors in vertebrates.* Elife, 2017. **6**.
10. Sokol, S.Y., *Analysis of Dishevelled signalling pathways during Xenopus development.* Curr Biol, 1996. **6**(11): p. 1456-67.

11. Axelrod, J.D., et al., *Differential recruitment of Dishevelled provides signaling specificity in the planar cell polarity and Wingless signaling pathways.* Genes Dev, 1998. **12**(16): p. 2610-22.

12. Boutros, M., et al., *Dishevelled activates JNK and discriminates between JNK pathways in planar polarity and wingless signaling.* Cell, 1998. **94**(1): p. 109-18.

13. Gentzel, M. and A. Schambony, *Dishevelled Paralogs in Vertebrate Development: Redundant or Distinct?* Front Cell Dev Biol, 2017. **5**: p. 59.

14. Gao, C. and Y.G. Chen, *Dishevelled: The hub of Wnt signaling.* Cell Signal, 2010. **22**(5): p. 717-27.

15. Lijam, N., et al., *Social interaction and sensorimotor gating abnormalities in mice lacking Dvl1.* Cell, 1997. **90**(5): p. 895-905.

16. Hamblet, N.S., et al., *Dishevelled 2 is essential for cardiac outflow tract development, somite segmentation and neural tube closure.* Development, 2002. **129**(24): p. 5827-38.

17. Etheridge, S.L., et al., *Murine dishevelled 3 functions in redundant pathways with dishevelled 1 and 2 in normal cardiac outflow tract, cochlea, and neural tube development.* PLoS Genet, 2008. **4**(11): p. e1000259.

18. Wynshaw-Boris, A., *Dishevelled: in vivo roles of a multifunctional gene family during development.* Curr Top Dev Biol, 2012. **101**: p. 213-35.

19. Rothbacher, U., et al., *Dishevelled phosphorylation, subcellular localization and multimerization regulate its role in early embryogenesis.* EMBO J, 2000. **19**(5): p. 1010-22.

20. Gonzalez-Sancho, J.M., et al., *Wnt proteins induce dishevelled phosphorylation via an LRP5/6- independent mechanism, irrespective of their ability to stabilize beta-catenin.* Mol Cell Biol, 2004. **24**(11): p. 4757-68.

21. Wallingford, J.B. and R. Habas, *The developmental biology of Dishevelled: an enigmatic protein governing cell fate and cell polarity.* Development, 2005. **132**(20): p. 4421-36.

22. Lee, Y.N., Y. Gao, and H.Y. Wang, *Differential mediation of the Wnt canonical pathway by mammalian Dishevelleds-1, -2, and -3.* Cell Signal, 2008. **20**(2): p. 443-52.

23. Zhang, C., et al., *Novel pathogenic variants and quantitative phenotypic analyses of Robinow syndrome: WNT signaling perturbation and phenotypic variability.* HGG Adv, 2022. **3**(1): p. 100074.

24. Zhang, C., et al., *Novel pathogenic genomic variants leading to autosomal dominant and recessive Robinow syndrome.* Am J Med Genet A, 2021. **185**(12): p. 3593-3600.

25. White, J., et al., *DVL1 frameshift mutations clustering in the penultimate exon cause autosomal-dominant Robinow syndrome.* Am J Hum Genet, 2015. **96**(4): p. 612-22.

26. White, J.J., et al., *WNT Signaling Perturbations Underlie the Genetic Heterogeneity of Robinow Syndrome.* Am J Hum Genet, 2018. **102**(1): p. 27-43.

27. White, J.J., et al., *DVL3 Alleles Resulting in a -1 Frameshift of the Last Exon Mediate Autosomal-Dominant Robinow Syndrome.* Am J Hum Genet, 2016. **98**(3): p. 553-561.

28. Mansour, T.A., et al., *Whole genome variant association across 100 dogs identifies a frame shift mutation in DISHEVELLED 2 which contributes to Robinow-like syndrome in Bulldogs and related screw tail dog breeds.* PLoS Genet, 2018. **14**(12): p. e1007850.

29. Dirac, A.M. and R. Bernards, *Reversal of senescence in mouse fibroblasts through lentiviral suppression of p53.* J Biol Chem, 2003. **278**(14): p. 11731-4.

30. Karuna, E.P., et al., *Identification of a WNT5A-Responsive Degradation Domain in the Kinesin Superfamily Protein KIF26B.* Genes (Basel), 2018. **9**(4).

31. Hooper, J.E., et al., *Systems biology of facial development: contributions of ectoderm and mesenchyme.* Dev Biol, 2017. **426**(1): p. 97-114.

32. Summerhurst, K., et al., *3D representation of Wnt and Frizzled gene expression patterns in the mouse embryo at embryonic day 11.5 (Ts19).* Gene Expr Patterns, 2008. **8**(5): p. 331-48.

33. Lustig, B., et al., *Negative feedback loop of Wnt signaling through upregulation of conductin/axin2 in colorectal and liver tumors.* Mol Cell Biol, 2002. **22**(4): p. 1184-93.

34. Jho, E.H., et al., *Wnt/beta-catenin/Tcf signaling induces the transcription of Axin2, a negative regulator of the signaling pathway.* Mol Cell Biol, 2002. **22**(4): p. 1172-83.

35. Leung, J.Y., et al., *Activation of AXIN2 expression by beta-catenin-T cell factor. A feedback repressor pathway regulating Wnt signaling.* J Biol Chem, 2002. **277**(24): p. 21657-65.

36. Fuerer, C. and R. Nusse, *Lentiviral vectors to probe and manipulate the Wnt signaling pathway.* PLoS One, 2010. **5**(2): p. e9370.

37. Bryja, V., et al., *Wnt-5a induces Dishevelled phosphorylation and dopaminergic differentiation via a CK1-dependent mechanism.* J Cell Sci, 2007. **120**(Pt 4): p. 586-95.

38. Witze, E.S., et al., *Wnt5a control of cell polarity and directional movement by polarized redistribution of adhesion receptors.* Science, 2008. **320**(5874): p. 365-9.

39. Witze, E.S., et al., *Wnt5a directs polarized calcium gradients by recruiting cortical endoplasmic reticulum to the cell trailing edge.* Dev Cell, 2013. **26**(6): p. 645-57.

40. Park, H.W., et al., *Alternative Wnt Signaling Activates YAP/TAZ.* Cell, 2015. **162**(4): p. 780-94.

41. Connacher, M.K., J.W. Tay, and N.G. Ahn, *Rear-polarized Wnt5a-receptor-actin-myosin-polarity (WRAMP) structures promote the speed and persistence of directional cell migration.* Mol Biol Cell, 2017. **28**(14): p. 1924-1936.

42. Hanakova, K., et al., *Comparative phosphorylation map of Dishevelled 3 links phospho-signatures to biological outputs.* Cell Commun Signal, 2019. **17**(1): p. 170.

43. Gonzalez-Sancho, J.M., et al., *Functional consequences of Wnt-induced dishevelled 2 phosphorylation in canonical and noncanonical Wnt signaling.* J Biol Chem, 2013. **288**(13): p. 9428-37.

44. Bernatik, O., et al., *Functional analysis of dishevelled-3 phosphorylation identifies distinct mechanisms driven by casein kinase 1 and frizzled5.* J Biol Chem, 2014. **289**(34): p. 23520-33.

45. Beitia, G.J., et al., *Regulation of Dishevelled DEP domain swapping by conserved phosphorylation sites.* Proc Natl Acad Sci U S A, 2021. **118**(26).

46. Bryja, V., G. Schulte, and E. Arenas, *Wnt-3a utilizes a novel low dose and rapid pathway that does not require casein kinase 1-mediated phosphorylation of Dvl to activate beta-catenin.* Cell Signal, 2007. **19**(3): p. 610-6.

47. Jiang, X., et al., *Dishevelled promotes Wnt receptor degradation through recruitment of ZNRF3/RNF43 E3 ubiquitin ligases.* Mol Cell, 2015. **58**(3): p. 522-33.

48. Paclikova, P., et al., *The N-Terminal Part of the Dishevelled DEP Domain Is Required for Wnt/beta-Catenin Signaling in Mammalian Cells.* Mol Cell Biol, 2017. **37**(18).

49. Gammons, M.V., et al., *Essential role of the Dishevelled DEP domain in a Wnt-dependent human-cell-based complementation assay.* J Cell Sci, 2016. **129**(20): p. 3892-3902.

50. Paclikova, P., et al., *Roles of individual human Dishevelled paralogs in the Wnt signalling pathways.* Cell Signal, 2021. **85**: p. 110058.

51. Moriguchi, T., et al., *Distinct domains of mouse dishevelled are responsible for the c-Jun N-terminal kinase/stress-activated protein kinase activation and the axis formation in vertebrates.* J Biol Chem, 1999. **274**(43): p. 30957-62.

52. Penton, A., A. Wodarz, and R. Nusse, *A mutational analysis of dishevelled in Drosophila defines novel domains in the dishevelled protein as well as novel suppressing alleles of axin.* Genetics, 2002. **161**(2): p. 747-62.

53. Wallingford, J.B., et al., *Dishevelled controls cell polarity during Xenopus gastrulation.* Nature, 2000. **405**(6782): p. 81-5.

54. Tada, M. and J.C. Smith, *Xwnt11 is a target of Xenopus Brachyury: regulation of gastrulation movements via Dishevelled, but not through the canonical Wnt pathway.* Development, 2000. **127**(10): p. 2227-38.

55. Gammons, M.V., et al., *Wnt Signalosome Assembly by DEP Domain Swapping of Dishevelled.* Mol Cell, 2016. **64**(1): p. 92-104.

56. Qi, J., et al., *Autoinhibition of Dishevelled protein regulated by its extreme C terminus plays a distinct role in Wnt/beta-catenin and Wnt/planar cell polarity (PCP) signaling pathways.* J Biol Chem, 2017. **292**(14): p. 5898-5908.

57. Lee, H.J., D.L. Shi, and J.J. Zheng, *Conformational change of Dishevelled plays a key regulatory role in the Wnt signaling pathways.* Elife, 2015. **4**: p. e08142.

58. Bernatik, O., et al., *Sequential activation and inactivation of Dishevelled in the Wnt/beta-catenin pathway by casein kinases.* J Biol Chem, 2011. **286**(12): p. 10396-410.

59. Strakova, K., et al., *Dishevelled enables casein kinase 1-mediated phosphorylation of Frizzled 6 required for cell membrane localization.* J Biol Chem, 2018. **293**(48): p. 18477-18493.

60. Harnos, J., et al., *Dishevelled-3 conformation dynamics analyzed by FRET-based biosensors reveals a key role of casein kinase 1.* Nat Commun, 2019. **10**(1): p. 1804.

61. Bunn, K.J., et al., *Mutations in DVL1 cause an osteosclerotic form of Robinow syndrome.* Am J Hum Genet, 2015. **96**(4): p. 623-30.

62. Griffiths, S.C., et al., *Structure and function of the ROR2 cysteine-rich domain in vertebrate noncanonical WNT5A signaling.* bioRxiv.

63. Fahmy O. G., Fahmy M., 1959. New mutants report. *Dros. Inf. Serv.* 33: 82–94.

Concluding remarks

While our understanding of the mechanisms driving certain Wnt pathways has advanced over the years, there is still much to learn about non-canonical Wnt pathways. In particular, Wnt5a-Ror signaling has long been associated with distinct tissue morphogenesis defects but has remained understudied at the molecular and cellular levels. In this dissertation, I expand upon our knowledge of Wnt5a-Ror signaling mechanisms by further defining the molecular events and cellular outcomes that occur during physiological signaling and provide insight into how these normal processes are disrupted by RS-causing mutations. Here, I demonstrate critical roles for both Pdzrn3, as a regulatory effector of the Wnt5a-Ror signaling pathway, as well as Dvls, as mediators of signal transduction for Wnt5a-Ror and Wnt/β-catenin signaling.

In Chapter 2, I discussed the identification and characterization of the E3 ubiquitin ligase Pdzrn3 as a downstream regulatory target of Wnt5a-Ror signaling. In a broader context, there are several features shared by Pdzrn3 and the other major effector of Wnt5a-Ror signaling, Kif26b. Both effectors are highly expressed in mouse embryonic fibroblasts (MEFs), a tissue type that undergoes robust Wnt5a-Ror signaling, and Wnt5a-Ror signaling regulates Kif26b and Pdzrn3 abundance through the ubiquitin proteasome system (UPS), which indicates that regulated proteolysis is a major mechanism by which Wnt5a-Ror signaling regulates downstream effectors. Additionally, Wnt5a-Ror signaling relies on Kif26b and Pdzrn3 to affect cell migration in similar ways. Independent of Wnt5a, both Kif26b and Pdzrn3 act as promigratory factors [1-4]; however, when Wnt5a is present, cell migration is reduced, suggesting that Wnt5a-Ror signaling tunes the levels of Kif26b and Pdzrn3 to modulate cell migration. Finally, neither *Kif26b* nor *Pdzrn3* knockout mice phenocopy Wnt5a-Ror signaling. *Kif26b* knockout embryos have been shown to be perinatal lethal and display kidney defects, whereas Pdzrn3 knockout embryos are embryonic lethal around E11.5 exhibit vascular defects

in the placenta. The tissue specific defects observed in *Kif26b* and *Pdzrn3* knockout embryos suggest the potential existence of multiple tissue specific effectors that collectively carry out the many biological functions of the pathway and/or potential compensatory effects driven by closely related homologs, which may also be regulated by Wnt5a-Ror signaling.

Beyond their promigratory roles, the molecular functions of Pdzrn3 and Kif26b remain elusive. While the signaling cascade regulating their degradation is reasonably similar, the substrates on which Pdzrn3 and Kif26b act as well as any adapter proteins they may work in tandem with are unknown. The answers to these questions will help further define wild-type signaling mechanisms of Wnt5a-Ror signaling.

In Chapter 3, I developed a new platform in which Dvl function and activity as a mediator of multiple Wnt signaling pathways can be analyzed in detail. Perhaps the longest standing question surrounding Dvl function has been how Dvls direct signals to one Wnt pathway or another. With this platform, I begin to answer this question, by establishing the domains and key phosphorylation sites that are common to Dvl activity in both pathways (such as the C-terminus, which regulates Dvl activity itself) as well as unique to one or another (such as the C-terminal CK1 phosphorylation sites specific to Wnt5a-Ror signaling but not Wnt/β-catenin signaling). This fundamental knowledge will help interpret the changes in function driven by RS mutations.

My initial assessment of the effects of RS DVL variant impacts on downstream signaling pathways strongly indicate that both decreases in signaling (as observed with RS-hDVL1 and RS-dDVL2) as well as increases (as observed with RS-hDVL3) can result in the similar phenotypic outcomes. In many ways, this harkens back to the quintessential Wnt5a KO phenotype, which can arise from both loss of function and overexpression of Wnt5a in mice [5-7]. Collectively, these findings suggests that Wnt signaling pathways operate within an optimal range to properly orchestrate developmental processes.

While these studies focused on analyzing Dvl as the major intersection between Wnt5a-Ror and Wnt/β-catenin signaling, my MaxP dual reporter system could be used to interrogate additional molecular players involved in multiple Wnt signaling pathways. More specifically, Frizzled receptors are another signaling component utilized in Wnt5a-Ror and Wnt/β-catenin signaling pathways that have growing connections to RS. Thus, this MaxP dual reporter cell platform will enable further molecular dissection of the pathway and augment our understanding of the mechanistic features common to multiple Wnt pathways. Overall, this dissertation establishes fundamental knowledge regarding Wnt5a-Ror signaling mechanisms in both normal physiological and pathological contexts, paving the way for even more detailed interrogation and potential development of therapeutics in the future.

References

1. Guillabert-Gourgues, A., et al., *Kif26b controls endothelial cell polarity through the Dishevelled/Daam1-dependent planar cell polarity-signaling pathway.* Mol Biol Cell, 2016. **27**(6): p. 941-53.
2. Sewduth, R.N., et al., *The ubiquitin ligase PDZRN3 is required for vascular morphogenesis through Wnt/planar cell polarity signalling.* Nat Commun, 2014. **5**: p. 4832.
3. Konopelski Snavely, S.E., et al., *Proteomic analysis identifies the E3 ubiquitin ligase Pdzrn3 as a regulatory target of Wnt5a-Ror signaling.* Proc Natl Acad Sci U S A, 2021. **118**(25).
4. Susman, M.W., et al., *Kinesin superfamily protein Kif26b links Wnt5a-Ror signaling to the control of cell and tissue behaviors in vertebrates.* Elife, 2017. **6**.
5. Moon, R.T., et al., *Xwnt-5A: a maternal Wnt that affects morphogenetic movements after overexpression in embryos of Xenopus laevis.* Development, 1993. **119**(1): p. 97-111.
6. van Amerongen, R., et al., *Wnt5a can both activate and repress Wnt/beta-catenin signaling during mouse embryonic development.* Dev Biol, 2012. **369**(1): p. 101-14.
7. Yamaguchi, T.P., et al., *A Wnt5a pathway underlies outgrowth of multiple structures in the vertebrate embryo.* Development, 1999. **126**(6): p. 1211-23.

Appendix

Whole genome variant association across 100 dogs identifies a frame shift mutation in *DISHEVELLED 2* which contributes to Robinow-like syndrome in Bulldogs and related screw tail dog breeds

Abstract

Domestic dog breeds exhibit remarkable morphological variations that result from centuries of artificial selection and breeding. Identifying the genetic changes that contribute to these variations could provide critical insights into the molecular basis of tissue and organismal morphogenesis. Bulldogs, French Bulldogs and Boston Terriers share many morphological and disease-predisposition traits, including brachycephalic skull morphology, widely set eyes and short stature. Unlike other brachycephalic dogs, these breeds also exhibit vertebral malformations that result in a truncated, kinked tail (screw tail). Whole genome sequencing of 100 dogs from 21 breeds identified 12.4 million bi-allelic variants that met inclusion criteria. Whole Genome Association of these variants with the breed defining phenotype of screw tail was performed using 10 cases and 84 controls and identified a frameshift mutation in the WNT pathway gene *DISHEVELLED 2* (*DVL2)* (Chr5: 32195043_32 195044del, $p = 4.37 \text{ X } 10^{-37}$) as the most strongly associated variant in the canine genome. This *DVL2* variant was fixed in Bulldogs and French Bulldogs and had a high allele frequency (0.94) in Boston Terriers. The *DVL2* variant segregated with thoracic and caudal vertebral column malformations in a recessive manner with incomplete and variable penetrance for thoracic vertebral malformations between different breeds. Importantly, analogous frameshift mutations in the human *DVL1* and *DVL3* genes cause Robinow syndrome, a congenital disorder characterized by similar craniofacial, limb and vertebral malformations. Analysis of the canine DVL2 variant protein showed that its ability to undergo WNT- induced phosphorylation is reduced, suggesting that altered WNT signaling may contribute to the Robinow-like syndrome in the screwtail breeds.

Author summary

Some dog breeds are characterized by extreme morphological differences from their ancestor, the wolf. One group of three breeds (Bulldog, French Bulldog, and Boston Terrier) is characterized by a wide head, short muzzle, widely spaced eyes, small size and abnormalities of the vertebral bones of the back and tail. These breeds are referred to as the screw tail breeds since the characteristic that is unique and easy to see in these breeds is their shortened and kinked tails. These breed have become increasingly popular as pet dogs, although they have health issues associated with their morphology. We analyzed the genome sequences of 100 dogs, including 10 screw tail dogs, and identified all the genetic differences between those dogs. We then compared these differences to identify changes in the DNA sequences associated with screw tail. The mutation and the affected gene identified are very similar to the types of mutations that have been shown to be responsible for a rare human disorder with similar clinical abnormalities, called Robinow syndrome. We demonstrate that the dog mutation makes an altered protein that affects an important cell-cell communication system crucial for tissue development.

Introduction

Morphological differences have been one of the primary drivers of dog breed formation since wolf domestication and subsequent selection to create dog breeds [1]. In many cases, the morphological traits are also genetically linked to disease-predisposition traits [2–6]. Therefore, it is of great interest to determine the breed specific genetic variations, as this knowledge could provide insights into not only the evolution of dog breeds, but also the mechanisms of tissue morphogenesis and disease pathogenesis.

Some subsets of dog breeds share distinctive morphologies. A shortened and kinked tail— which is referred to as a “screw tail”—is one of the distinctive morphological traits that characterizes Bulldogs, French Bulldogs and Boston Terriers, which were historically developed from the Bulldog breed and, thus, closely related [7]. These breeds also share a craniofacial morphological phenotype referred to as brachycephaly, which includes both profound shortening of the muzzle and widening of the skull. Possibly due to the width of their heads, these three breeds have the highest rate of cesarean section among dog breeds [8]. The three breeds are also all relatively short in stature being less than 17 inches tall at the shoulder. In addition to morphological features, certain diseases are found at a high prevalence across all 3 breeds such as vertebral malformations [9–13], cleft lip and cleft palate [14–16], congenital heart disease [17, 18, 19], and glioma [5, 20, 21].

Molecular characterization of the cause of short tails in dogs demonstrated that a synonymous mutation in the T box transcription factor gene confers a short tail (bob tail) phenotype in the Pembroke Welsh Corgi breed [22]. Although this mutation is common across a wide range of dog breeds, it is not responsible for the short tail seen in Bulldogs and Boston Terriers [23]. Screw tail is distinguishable from the short tail phenotypes in other breeds due to presence of vertebral malformations and fusion of the caudal vertebrae in addition to absence of

caudal vertebrae. Additional conformational sequelae of vertebral malformation in screw tail breeds includes kyphosis, lordosis or scoliosis most commonly affecting the thoracic vertebral column, and typically resulting from wedge, hemi-vertebrae and butterfly vertebrae [24, 25]. Although vertebral malformations affecting thoracic vertebrae in screw tail breeds are common, they are rarely directly associated with clinical signs [9]. However, it may increase their risk of developing other diseases such as intervertebral disc disease, to which the French Bulldog and Boston Terrier are predisposed [6, 26].

Brachycephalic skull morphology has been previously investigated in dogs and has a complex etiology. Multiple different chromosomal regions are associated and may differ between breeds. In a Genome Wide Association (GWAS) for skull shape across dog breeds, significant associations were identified on CFA (*Canis familiaris*) 1, CFA5, CFA24, CFA30 and CFA32 for brachycephaly. A missense mutation (p.F452L) in the bone morphogenetic protein 3 (*BMP3*) gene was identified as the skull modifying locus on CFA 32. This allele is fixed in Bulldogs and French Bulldogs and has an allele frequency of 0.99 in Boston Terriers [27]. The mutations underlying the associations on CFA5, CFA24 and CFA30 have not been reported. A second group mapped proportional snout length in a GWAS across dog breeds using size as a covariate and identified both the CFA1 and CFA5 loci; however underlying causative mutations were not defined [28]. Recently, a LINE-1 insertion in the SPARC-related modular calcium binding 2 (*SMOC2)* gene was identified as the causative mutation underlying the significant associations to brachycephalic head morphology on CFA 1 [29].

In humans, a rare genetic disorder called Robinow syndrome shares phenotypic similarities with the screw tail breeds. Robinow syndrome is characterized by mesomelic-limbed dwarfism and abnormalities of the head, face, genitalia, and vertebral column [30]. Patients with Robinow syndrome have hypertelorism with a broad nasal root and broad forehead and fusion of thoracic vertebrae with frequent hemivertebrae [31]. Mutations in genes from WNT pathways,

including *ROR2*, *FZD2*, *WNT5A*, *DVL1*, and *DVL3*, have all been found to cause Robinow syndrome in humans [30, 32–34]. WNT pathways control embryonic morphogenesis by regulating crucial developmental processes including cell-fate determination, proliferation, and morphogenetic cell/tissue movement [35–40].

Since the development of SNP genotyping arrays for dogs, the standard approach to mutation identification has been GWAS followed by Sanger or whole genome sequencing to identify causative variants [41]. Compared to other species, long linkage disequilibrium (LD) within the domestic dog allows successful associations with few samples and few SNPs [42]. However the long LD within dogs also presents challenges for mutation identification. In this paper, we bpass the use of SNP genotyping arrays and utilize variant calls from whole genome paired end sequences from 100 canine samples of 21 breeds to perform whole genome variant association in the screw tail breeds. We report the identification of a frameshift mutation in the *DISHEVELLED 2 (DVL2)* gene that segregates with the breed defining phenotype of screw tail and vertebral malformations. The frameshift mutation preserves the majority of the DVL2 protein but replaces the last 49 amino acids in the C-terminus with a novel 26-amino acid sequence. Through biochemical analysis of the bulldog DVL2 variant protein in cultured cells, we further demonstrate that the mutant protein has a reduced capacity to undergo WNT-dependent phosphorylation, suggesting that aspects of WNT signaling might be compromised. Our data suggest that the bulldog-related breeds share similar genetic, morphological and pathological origins with human Robinow syndrome.

Materials and methods

Ethics statement

The following application was reviewed and approved by the UC Davis IACUC on January 19, 2018. Title: Canine DNA collection from privately owned animals. Principal Investigator: Danika L. Bannasch (Protocol # 20356) Institution: University of California, Davis. Active protocols are reviewed annually. This institution is accredited by the Association for Assessment and Accreditation of Laboratory Animal Care, International (AAALAC). This institution has an Animal Welfare Assurance on file with the Office of Laboratory Animal Welfare (OLAW). The Assurance Number is A3433-01. The IACUC is constituted in accordance with U.S. Public Health Service (PHS) Animal Welfare Policy and includes a member of the public and a non-scientist.

Canine samples

Buccal swabs or blood samples were collected from privately owned dogs through the William R. Pritchard Veterinary Medical Teaching Hospital at UC Davis. Owners specified the breed of each dog. Samples used for whole genome sequencing included 96 dogs from 21 pure breeds and 4 dogs from mixed breeds (S2 Table).

Phenotype

Images of screw tail breeds were obtained during the course of necessary veterinary procedures and 3D computed tomography reconstructions were perfomed on selected images. The American Kennel Club breed standards were used as a guide to describe typical dogs of each breed. Vertebral column phenotypes defined as a) thoracic vertebral malformation and b) caudal malformation (“screw tail”) were based on assessment of imaging (radiographs, computed tomography or magnetic resonance imaging) by a board certified veterinary

radiologist and a board certified veterinary neurologist. Cases were considered affected if there was evidence of thoracic vertebral malformations characterized by the presence of wedged vertebrae, hemi-vertebrae or butterfly vertebrae, or the presence of similar malformations as well as shortening and vertebral fusions affecting the caudal vertebrae. Inclusion required the availability of imaging for all thoracic vertebrae in lateral and dorso-ventral /ventro-dorsal planes for thoracic vertebrae, and imaging of a minimum of 6 caudal vertebrae. Phenotyping of 4 cases for the presence of caudal malformation ("screw tail") was based on visual and physical examination by a veterinarian.

DNA extraction and whole genome sequencing

Genomic DNA was extracted using the Qiagen kit (QIAGEN, Valencia, CA). 96 biological samples (including 6 trios) were subjected to next generation sequencing using Illumina paired end cycles. The whole genome sequencing of 4 Pug samples was publically available by Tgen company (https://www.tgen.org/). The metadata table contains details about the sequencing libraries and coverage (S2 Table).

Variant calling

Adaptors and low quality sequences were removed using the Trimmomatic software (V 0.36) [71]. Adaptor trimming was done using recommended parameters of simple matching (threshold of 10) and palindromic matching (threshold of 30 and minimum adapter length of 1). High quality reads were aligned to the dog reference genome CanFam3 [72] using the BWA-MEM algorithm of the BWA software package (v0.7.7) [73]. Duplicate reads were excluded using the Picard tool MarkDuplicates (v2.2.4) (http://broadinstitute.github.io/ picard). Variant calling was performed with the GATK HaplotypeCaller (v3.5) [74] using joint genotyping across all sequenced samples. Known variants from the Ensembl variation database (release 82) [75] and canine annotation of

Broad institute (https://www.broadinstitute.org/ftp/pub/vgb/dog/trackHub/canFam3/variation/final.Broad.SNPs.vcf.gz) were used for variant annotation. Candidate variants were filtered using the following thresholds: QualByDepth (QD) < 2.0, FisherStrand (FS) > 60.0, StrandOddsRatio (SOR) > 4.0, ReadPosRankSum < -8.0, and depth of coverage (DP) > 3105 for both SNPs and indels, RMSMappingQuality (MQ) < 40.0, MQRankSum < -12.5 for SNPs, and InbreedingCoeff < -0.8 for indels. After quality filtration and exclusion of variants of uncharacterized chromosomes, 13,591,986 SNPs and 7,126,341 indels passed our filters.

Including indels in the PLINK analysis

The PLINK software for GWAS is designed to deal with SNPs for association studies[76]. To allow PLINK to deal with indels as well, we developed a script which changed the bi-allelic indels into SNPs. Here, we excluded multi-allelic variants then replaced multi-character alleles by a single character (A or T) chosen to maintain allelic variation between reference and alternatives (https://github.com/dib-lab/dogSeq).

Identity by state (IBS) distance

An IBS matrix was calculated to document the breed-based population stratification and examine the similarities between the breeds used. A subset of autosomal and X chromosome variants genotyped in >95% of samples with MAF > 5% was selected and then subjected to linkage disequilibrium based pruning using a threshold of variance inflation factor (VIF) equals 2. Pruning recursively removed SNPs within a sliding window of 50 SNPs, with a window step size of 5 SNPs producing 645,697 variants for IBS calculation. The distance matrix was constructed using the '—distance 1-ibs' function of PLINK 1.9 and plotted as a dendrogram using the 'ape' package in R. The "—mendel" option in PLINK 1.9 was used to calculate the rate

of Mendelian errors per meiosis in the sequenced trios using the pruned subset of variants. The average rate of Mendel errors was used as an index for the genotyping accuracy.

Genome wide association using variants identified by whole genome sequence

Among the 100 dogs sequenced, there were 6 trios whose offspring were excluded from further analysis. All variants were subjected to mild filtration to exclude those failing to genotype in more than 10% of all sequenced samples as well as those with MAF of less than 1%. Following this, we used PLINKv1.9 to perform a case/control association analysis (S3 Table). Statistical probabilities were adjusted for genomic inflation using the Genomic Control (GC) approach GC correction is based on the assumption that most of variants are not associated with the trait of interest and thus the chi-square values of statistical tests should have a mean of one. Genomic inflation increases this mean and to correct for this, all test statistics values are divided by the mean of the test statistics to restore the expected distribution [77]. Bonferroni correction for multiple testing was performed using pruned variants as an index for independently tested haplotypes to obtain a list of candidate loci [78]. Pruning was done as described above for IBS calculations but after excluding the offspring of the 6 trios. All variants belonging to the same haplotype are dependent and should have similar association probabilities. Correction of multiple testing should be applied to the “independent” statistical trials. In our experiment, correcting for all tested variants did not prevent the detection of the causative variant (p = 4.37 X 10^{-37} uncorrected) even with a threshold of 0.01 after Bonferroni correction. Fixed variants in affected breeds that were approaching absence from unaffected breeds were selected as those with more than 90% allelic differences between cases and controls.

Variant effect annotation

The Variant Effect Predictor (VEPv85) tool from Ensembl [79] was used to annotate possible effects of all detected variants. Variant annotation was done using the NCBI dog genome annotation (last modified on 9/18/15)[80].

Genotyping

Primers were designed using Primer3 [81]. Primers to amplify the *DVL2* mutation produced a 297 base pair product (Forward Primer: CGGCTAGCTGTCAGTTCTGG; Reverse Primer: CAGTGAGTCTGAGCCCTCCA). PCR products were sequenced using the Big Dye termination kit on an ABI 3100 Genetic Analyzer (Applied Biosystems, Foster City, CA). Segregation analysis was evaluated by Fisher's exact test. Sequences were evaluated using Chromas (Technelysium, South Brisbane, QLD, Australia). The sequences were aligned to the Boxer dog reference sequence (CanFam 3.1) using BLAT (UCSC Genome Browser). Primers described by Marchant et al. [29] were used to evaluate the SMOC2 mutation status for 152 dogs. PCR products sizes were visualized via gel electrophoresis.

RNA extraction and cDNA Sequencing

All primers were designed using Primer 3 (Forward Primer: CCACGAGCTGTCATCCTACA; Reverse Primer: CAACTGACAGGGCAGACAGA) [81]. RNA was isolated from skeletal muscle and spleen using Qiagen QIAamp Blood Mini Kit tissue protocols (QIAGEN, Valencia, CA). RNA was reverse transcribed into cDNA using Qiagen QuantiTect Reverse Transcription Kit. *DVL2* and *RPS5* [82] cDNA was PCR amplified from skeletal muscle tissue from one Bulldog and one Labrador Retriever. *RPS5* was amplified in skeletal muscle to ensure equivalent amounts of cDNA were produced. The PCR products were sequenced on an ABI 3500 Genetic Analyzer and analyzed using Chromas (Technelysium, South Brisbane, QLD, Australia). The sequences were aligned to the reference Boxer dog genome (Can Fam 3.1), using BLAT (UCSC Genome

Browser), to confirm sequences matched *DVL2*. Semiquantitative RT PCR was performed by PCR amplification (Forward Primer: CGAGCTGTCATCCTACACCT, Reverse primer: TGACGAGCCTCTGGAAGG) of cDNA from Spleen from two different dogs of each genotype (homozygous mutant and wildtype for *DVL2*c.2044delC). Reduced PCR cycle number (to 28) were used to estimate the transcript differences. PCR products were visualized on agarose gels.

DVL2 gene cloning

Due to extremely high GC-content, attempts to clone the canine *DVL2* open reading frame (ORF) were unsuccessful. We therefore commercially synthesized the wild type and the bulldog variant of *DVL2* and subcloned them into a modified pENTR-2B vector containing an N-terminal Myc tag (MT) using the FseI and AscI restriction sites. The ORFs were verified by Sanger sequencing. To generate lentiviral transfer vectors, the pENTR-2B-MT constructs were recombined with the pLEX_307 vector (a gift from David Root; Addgene plasmid #41392) using LR clonase (Thermo Fisher Scientific, Hanover Park, IL). Transgene expression from pLEX_307 is driven by the *EF1* promoter.

Generation of stable NIH/3T3 cell lines

Lentiviruses were generated in HEK293T cells via co-transfection of lentiviral vectors with the following third generation packaging plasmids: pMD2.G (Addgene plasmid # 12259), pRSV-rev (Addgene plasmid #: 12253) and pMDLg/pRRE (Addgene plasmid #: 12251) [83]. 0.75mL of viral supernatant was used to infect NIH/3T3 cells plated at 20% confluency in 24-well plates. Puromycin selection (0.002mg/mL) was carried out for 4 days.

Western blotting

To block synthesis and production of endogenous Wnt proteins, the porcupine inhibitor Wnt-C59 (100nM final concentration) was added to cells 24 hours prior to lysis. For WNT stimulation, cells were incubated for 6 hours with Wnt5a (R&D, catalog #645WN010, 200ng/mL final concentration) or Wnt3a (R&D, catalog #1324-WN-002 100ng/mL final concentration). For casein kinase 1 inhibitor treatment, cells were pre-treated with D4476 (APEXBIO catalog #A3342, 100nM final concentration) for 1h prior to WNT5A or WNT3A treatment. D4476 was maintained in the culture during the 6-hr WNT stimulation period. Cells were washed in 1X cold PBS and lysed in 200µL RIPA buffer supplemented with HaltTM Protease Inhibitor Cocktail (100X) (Prod # 186127, Thermo Fisher Scientific). BCA analyses were conducted to determine the absolute concentrations of protein in lysate samples. For phosphatase treatment, 17.3µg of protein from cell lysates were treated with 7 U of CIP (NEB, catalog #M0290S; final concentration of 350U/mL) at 37C for 30 minutes. Lysates subjected to mock treatment were incubated at the same temperature and duration without enzyme. Protein concentrations were normalized and lysates were mixed with 1/3 the volume of 4X LDS sample buffer (NP0008, Thermo Fisher Scientific) supplemented with 2-mercaptoethanol (4.25% final concentration). Lysates were heated at 95℃ for 5 minutes before SDS-PAGE and western blots were generated.

For detecting exogenous DVL2, a commercially purchased monoclonal anti-c-Myc anti- body (clone 9E10, Thermo Fisher Scientific, catalog #9801) was used as the primary antibody at a dilution ratio of 1/1000, and a goat anti-rabbit IgG polyclonal antibody (conjugated to IRDye 800CW; catalog # 926–32211, Li-cor Biosciences, Lincoln, NE) was used as the secondary antibody at a dilution ratio of 1/30,000. For detecting α-tubulin, the DM1A mouse monoclonal antibody (catalog # SC-32292, Santa Cruz Biotechnology, Dallas, TX) was used as the primary antibody at a dilution ratio of 1/1000, and a goat anti-mouse IgG polyclonal antibody (conjugated to the IRDye 800CW; catalog # 926–32210, Li-cor Biosciences) was used at a dilution ratio of

1/30,000). Imaging of the western blots was performed using the Odyssey infrared imaging system (Li-cor Biosciences) according to the manufacturer's instructions. Non-saturated protein bands were quantified using Odyssey software, with a gamma level of 1.

Results

Phenotype

Bulldogs, French Bulldogs and Boston Terriers are the only American Kennel Club recognized dog breeds characterized by a screw tail (Fig 1A). The 'screw tail' is caused by a variety of malformed and fused vertebrae and lack of approximately 8 to 15 caudal vertebrae, which normally form the canine tail (Fig 1B 4). In addition to deformities of the caudal vertebrae, these breeds may also have variable morphological deformities of vertebrae along the vertebral column including hemivertebrae, wedge vertebrae, butterfly vertebrae and fused vertebrae (Fig 1B 1–3). Based on breed standards, the three breeds share physical characteristics including short stature, head shape and include eyes to be as wide apart as possible (hypertelorism) and for them to have a broad muzzle (Fig 1A and S1 Table). These breeds are considered brachycephalic meaning that they have a short muzzle length. The degree of brachycephaly in the three screw tail breeds is more prominent than in some other brachycephalic breeds due to an even shorter and broadened maxilla, broadened frontal bone, and an increased curvature to the zygomatic bone creating a wider and more extreme orbit as compared to, for example, the Boxer breed (Fig 1C). Due to the similarity in phenotype and historical relationships between these breeds, we hypothesized that they would share a mutation responsible for their morphology.

Variant calling and calculation of identity by state distance

To identify variants responsible for the screw tail phenotype, we used paired end whole genome sequence data generated from 100 dogs from 21 breeds followed by association analysis of all biallelic variants identified. There were 6 trios included in the dataset. The twenty-one breeds included 5 Bulldogs, 3 French Bulldogs and two Boston Terriers. The remainder of

the dogs did not have screw tails; however, two of the breeds were brachycephalic (Boxer and Pug). A complete list of breeds is available in S2 Table.

The variant calling pipeline identified 15,353,085 SNPs and 8,514,447 indels within the 100 canine genomes. After quality filtration and exclusion of variants of uncharacterized chromosomes, 13,591,986 SNPs and 7,126,341 indels passed our filters. The average rates of Mendelian errors per meiosis were calculated to be 4.1% in the six dog trios. A dendrogram was constructed to examine the historical relatedness of the breeds. Clustering of dogs by their breed and the relatedness in the case of the trios confirms the sensitivity of the technique to detect genetic relatedness (S1 Fig). The dendrogram highlights a common origin of all screw tail breeds (Bulldogs, French Bulldogs and Boston Terriers) and shows the bifurcation from Boxer dogs and Pugs, the other two brachycephalic breeds (Fig 2A and S1 Fig).

Whole genome variant association

A whole genome association analysis was performed using the 10 dogs of the screw tail breeds compared to 84 dogs belonging to 21 pure and 4 mixed breeds (related dogs were removed). The association analysis started with 20,342,844 biallelic variants identified through the whole genome sequence (excluding 375,483 multi-allelic loci) with a total genotyping rate of ~93.6%. 3,023,667 variants were removed due to missing genotype data and 4,852,941 variants were removed for low minor allele frequency. Association testing was performed using the remaining 12,461,460 variants. Genomic inflation was high (estimated lambda = 3.2761) due to the expected population stratification. To minimize false positive associations caused by genomic inflation, a simple genomic control approach was used instead of other modeling approaches that correct for relatedness to avoid the exclusion of variants that were identical by descent.

Since there is relatively long linkage disequilibrium in dogs, statistical thresholds were further corrected for multiple testing of 587,159 variants representing common haplotypes in the tested population. After adjustment, a $P_{Bonferroni}$ of 0.05 is equivalent to a $p = 3.99 \times 10^{-22}$ and $P_{Bonferroni}$ of 0.01 is equivalent to a $p = 1.96 \times 10^{-24}$ (Fig 2B, Fig 2C). A list of all the significantly associated variants is shown in S3 Table. The most associated variant was CFA5: 32195043_32195044del, $p = 4.37 \times 10^{-37}$ (uncorrected); however there were many associated regions (Fig 2C). This variant remained significantly associated at a $P_{Bonferroni}$ of 0.01 corrected for all 12,461,460 variants as well ($p = 1.5 \times 10^{-28}$).

In addition to being highly associated, we predicted that variants responsible for breed defining characteristics would have a high allele frequency in affected breeds and an extremely low allele frequency in unaffected breeds. We therefore selected variants with more than 90% allelic difference between cases and controls. Long regions of fixed candidate variants were then selected for further analysis and included CFA5, CFA26 and CFA 32 (Fig 2D). There were two additional significant loci on CFA 25 and 29 that were not evaluated further since they were less significant and did not show long regions of homozygosity to support Identical by descent inheritance [43]. The two peaks on CFA 26 (6772912–10171935) and CFA 32 (4533724–6620950) were previously reported to be associated in these breeds with canine glioma and brachycephaly respectively [5, 27]. The highest association was to the region on CFA 5, which also had a long region of homozygosity (5:29243555–34607475). The single most significantly associated variant found was a frame shift mutation in the *Dishevelled 2* (*DVL2)* gene (g.32195043_32195044del). The mutation was homozygous in all cases and absent from controls except a single Labrador retriever that was called as heterozygous in the absence of supporting read coverage (S3 Table). This dog was later confirmed by Sanger sequencing to be wild-type at this location.

DVL2 mutation

The single base deletion found on CFA 5(g.32195043_32195044del) that was homozygous in the three screw tail breeds (5 Bulldogs, 3 French Bulldogs and 2 Boston Terriers) was located within the 15th and penultimate exon of the canine *DVL2* gene. *DVL2* cDNA was sequenced from the skeletal muscle of a dog with a normal tail and a screw tail Bulldog (Fig 3A) to confirm the presence of the mutation in the mRNA in the Bulldog sample (*DVL2*c.2044delC). In orde to determine if there was a difference in transcript level between animals with the *DVL2*c.2044delC mutation and without semiquantitative RT PCR was performed. Mutant transcript levels were comparable to wildtype (S2 Fig). This deletion is predicted to lead to a frameshift mutation, causing a premature stop codon that truncates the translated protein by 23 amino acids (p.Pro684LeufsX26). In addition, 26 altered amino acids are predicted to be present in the highly conserved C-terminus of the mutant protein (Fig 3B, Fig 3C). The location of the truncation of the protein is remarkably similar to the effect of mutations within the other Dishevelled family members, *DVL1* and *DVL3*, that lead to Robinow syndrome in people. Alteration of the amino acid sequence in the highly conserved C-terminal region as well as truncation of 21 to 50 amino acids also occurs in the human Robinow *DVL* mutations (Fig 3D and S4 Table).

To confirm the association of the *DVL2*c.2044delC mutation with the screw tail phenotype, 667 dogs, from 49 breeds, were genotyped for the *DVL2* mutation (Table 1). 177 dogs were from the screw tail breeds including 33 Bulldogs, 79 French Bulldogs and 65 Boston Terriers. All were homozygous for the mutant allele except 6 of the Boston Terriers (4 heterozygous, 2 wildtype). In addition, we identified dogs from several other breeds, including Pit bulls, Staffordshire Bull Terrier, Shih Tzu and mixed breeds, that are heterozygous or homozygous for the *DLV2* mutation. The Pug breed has sometimes been classified with the

screw tail breeds due to its *curled tail; however, the tail is full length and does not have caudal vertebral malformations (S3 Fig). 29 Pugs tested were wild-type for the DVL2 mutation. Likewise, the Pug dogs do not share the high MAF with the screw tail breeds around the DVL2 mutation (S4 Fig). Three hundred and eighty five dogs from 43 other breeds were also tested and were all wild- type (S5 Table).*

Segregation and penetrance

In order to determine the penetrance of vertebral malformations, dogs homozygous for the DVL2 variant from the screw tail breeds were evaluated for thoracic and caudal vertebral malformations (Table 2). The penetrance of the thoracic malformations varied between the three breeds from 45–100%, while the caudal vertebral malformations were 100% penetrant. Since the DVL2 variant is virtually homozygous in these breeds, it was important to evaluate segregation of the variant with phenotype. In order to confirm the association of the DVL2 mutation with the vertebral column malformations, additional dogs were identified that had radiographs or imaging available and segregated the DVL2 mutation. Segregation of the caudal vertebral column malformations and genotype at DVL2 was consistent with a fully penetrant recessive mode of inheritance in Boston Terriers, Shih Tzus, Pit Bulls and mixed breeds (Table 3). Segregation of the thoracic vertebral malformations was consistent with a recessive mode of inheritance with variable penetrance between breeds. In order to evaluate the molecular contribution to brachycephalic skull shape, the DVL2 mutant breeds were genotyped for the previously identified brachycephaly associated Line insertion affecting SMOC 2 splicing. Bulldogs and French Bulldogs were homozygous for the variant and the Boston Terriers had an allele frequency of 90.3% (S6 Table). Similar allele frequency for the BMP3 missense mutation was also reported for these three breeds indicating that they are homozygous or have a high allele frequency for three mutations that affect head shape [27].

WNT-dependent phosphorylation of the DVL2 mutant protein is reduced

Based on the significant changes to the DVL2 C-terminus caused by the frameshift mutation, we hypothesized that the expression and/or biochemical properties of the mutant variant DVL2 might be altered. To test this hypothesis, we synthesized full-length cDNA of both the wild-type and mutant variant dog *DVL2* gene, N-terminally tagged them with the MYC epitope, and expressed them via lentiviral vectors in NIH/3T3 cells. We chose to use NIH/3T3 cells because they have been used previously to study WNT pathways and DVL regulation [44, 45]. Western analysis of lysates from cell lines expressing a wild-type or mutant variant of DVL2 showed that both proteins were expressed at similar levels (Fig 4A), suggesting that the mutant protein is properly synthesized and its novel C-terminus does not affect the stability of the DVL2 protein.

It has been previously established that Wnt stimulation results in the phosphorylation of DVL2, which can be observed on western blots as gel motility shifts and is often used as an indicator of pathway activity [46–49]. To compare the capacity of wild-type and mutant variant DVL2 to respond to WNT signals, we stimulated cells expressing these proteins with purified, recombinant WNT5A or WNT3A and analyzed the extent of DVL2 gel mobility shifts on western blots. We observed prominent DVL2 gel motility shifts in cells expressing the wild-type DVL2 protein after WNT5A or WNT3A treatment (Fig 4A). However, DVL2 gel motility shifts were reduced in cells expressing the mutant protein, suggesting that phosphorylation of the mutant variant DVL2 may be impaired. To demonstrate that the gel motility shifts observed were indeed due to phosphorylation, we treated cell lysates with calf intestinal phosphatase (CIP) to remove any potential phosphate groups. CIP treatment resulted in loss of the slower migrating DVL2 bands and an increased amount of unphosphorylated DVL2 in all conditions (Fig 4B). These results indicate that Wnt-dependent phosphorylation of the mutant variant DVL2 protein is reduced compared to wild-type DVL2.

Additional studies conducted in human and mouse cells have demonstrated that WNT-dependent phosphorylation of DVL2 is dependent on casein kinase 1 (CK1) [50, 51]. To assess if this mechanism also drives phosphorylation of the canine DVL2 protein, we pretreated cells with D4476, a small molecule inhibitor of CK1, and then stimulated with either WNT5A or WNT3A. D4476 treatment resulted in the loss DVL2 phosphorylation in all conditions, thereby demonstrating that CK1 also mediates Wnt-dependent phosphorylation of the canine DVL2 protein (Fig 4C). Collectively, these results demonstrate that the canine mutant variant DVL2 protein exhibits reduced WNT- and CK1-dependent phosphorylation and further suggest that reduced WNT signaling may contribute to the Robinow-like phenotype of bulldogs and associated screw tail breeds.

Discussion

Whole genome sequence data from 100 dogs was utilized to interrogate the molecular cause of the breed defining trait screw tail. Using over 12 million bi-allelelic variants and comparing 10 cases to 84 controls, a frame shift mutation in the *DVL2* gene was found to be the most strongly associated of all variants. The mutation leads to a 23 amino acid truncation of the protein in the last exon within the highly conserved C-terminal domain. Analogous truncations in the same regions of human DVL1 and DVL3 proteins result in Robinow syndrome in humans. This shared genetic signature, taken together with the similar anatomical changes, strongly suggests that the bulldog-related breeds share common pathological origins with human Robinow syndrome. DVL2 is part of an evolutionarily conserved cytoplasmic scaffolding protein family that also includes DVL1 and DVL3 in vertebrates [52, 53]. The three mammalian DVL homologs display significant sequence identity to each other [54, 55] as well as across species [56, 57]. Our results suggest that the mutant variant DVL2 protein likely has reduced capabilities to mediate WNT signaling. Although DVL proteins are key players in a variety of WNT pathways, the Robinow-like phenotypes of bulldogs and human patients coupled with mouse developmental expression patterns lead us to believe that the frameshift mutations in DVL2 in screw tail dog breeds primarily affect a noncanonical branch of WNT signaling, the WNT5A-ROR pathway. In addition to the bulldog DVL2 frameshift mutation, human mutations causing Robinow syndrome have been identified in *WNT5A*, *ROR2*, *FZD2*, *DVL1*, and *DVL3*, which are all major components of the WNT5A-ROR pathway [32, 33, 58–61]. Further, WNT5A and ROR2 are highly expressed in the facial primordia, limb buds, and vertebrae of mice, all areas of the body that are affected in Robinow syndrome patients and bulldogs; additionally, *Wnt5a* and *Ror2* knockout mice exhibit Robinow-like features, including truncated limbs and broad, flat faces [44, 46]. Collectively, this suggests that screw tail dog breeds and Robinow syndrome patients at least partly share similar underlying pathophysiology.

In both bulldogs and human patients, frameshift mutations in the penultimate or ultimate exon of DVL proteins result in the substitution of the highly conserved C-terminus region of the proteins with a new stretch of amino acids. Given that the frameshift mutation leaves most of the protein intact, it remains plausible that the more N-terminal modular domains of DVL2 can still function in other Wnt pathways, such as canonical WNT/beta-catenin signaling, which primarily uses the DIX domain, and planar cell polarity, which primarily uses the DEP domain [53]. Beyond these modular domains, however, few roles have been assigned to the DVL2 C-terminus; work by Bernatik et al has shown that human DVL3 C-terminus contains some CK1 phosphorylation sites that are conserved in DVL2 and would be lost by the frameshift mutation [62]. This correlates with our observations that the mutant DVL2 variant exhibits reduced CK1-dependent phosphorylation in response to WNT stimulation and is consistent with a recessive mode of inheritance. Given the importance of DVL2 in WNT5A-ROR signaling and the potential roles that these pathways play in defining the unique phenotypical and pathological characteristics of the screw tail bulldog breeds, additional follow up studies are required to define the molecular mechanism(s) by which the DVL2 variant protein affects downstream WNT signaling activity during development.

In addition to the *Dvl2* frameshift mutation, the three Bulldog related breeds harbor other mutations in developmentally important genes that could affect their craniofacial morphology. For example, these breeds also carry a missense mutation in *BMP3* and a Line 1 insertion that affects splicing of the *SMOC2* gene [27, 29]. The absence of homozygosity for these mutant alleles in breeds fixed for the brachycephalic head phenotype indicates that this is a complex trait influenced by multiple loci. Screw tail breeds are distinguished from some of the other brachycephalic dogs by additional shortening and broadening of the muzzle, broadening of the skull, and hypertelorism suggesting the presence of more variants affecting their skull morphology (Fig 1A, S1 Table and [27, 63]). We did not undertake the evaluation of head

morphology in this work since recruiting pet dogs for head CT that is not medically warranted is ethically challenging since it requires general anesthesia and carries a risk to dogs with brachycephalic head conformation. However, previous across breed genome wide associations for head morphology identified this locus on CFA 5 [27, 28]. Boyko et al used breed-based averages for a large number of linear measurements followed by QTL mapping [28]. Schoenebeck et al performed principal component analysis of geometric morphometry of museum specimen skulls from breeds followed by GWAS using DNA samples from the same breeds [27]. Both groups identified the same highly associated SNP (CFA5:32359028) within 160 Kb of the *DVL2* mutation as having a significant contribution to skull shape in dogs. A third study on canine skull morphology that was based on individual measurements taken from skull CTs did not identify the CFA 5 locus; however, the screw tail breeds only made up ~2% of the sample sets used in this across breed study to identify QTLs that affect head morphology [29]. Since the study was designed to capture common loci across many breeds it is not surprising that the *DVL2* locus would not be identified. Based on our allele frequency measures, the mutation is rare across breeds and virtually homozygous in affected breeds.

Additional, as yet undiscovered, deleterious variants could be present in these breeds that affect their skull shape considering the extremely strong selection based on head phenotype applied to these breeds by dog breeders. Normal development of the skull requires coordinated development of cranial sutures, skull base synchondroses and brain, and it is likely that genetic abnormalities may affect both suture and synchondrosis development directly, or indirectly due to secondary effects [64, 65]. WNT signaling has been shown to regulate cranial base development and growth, and abnormalities in WNT signaling have been implicated in cranial synostosis in humans, most commonly with brachycephaly-associated coronal synostosis [66– 68]. Given the apparent polygenic pathogenesis of brachycephaly in dog breeds, and the essentially fixed nature of the *DVL2* mutant allele in the Bulldog and Boston

breeds, assigning specific skull morphometric sequelae to the *DVL2* mutation is challenging. The cranial dysmorphology seen in Robinow patients and the more extreme nature of the brachycephaly in the *DVL* mutant dog breeds is, however, highly suggestive of *DVL2*'s involvement in the brachycephalic phenotype. A more detailed study of skull morphology, particularly in animals segregating the various associated genes isnecessary to define specific gene contributions to the brachycephalic phenotype in dogs.

Although caudal vertebral malformations appear to be a consistent finding within *DVL2* mutant dog breeds, thoracic vertebral malformations are more variable in their presence and severity. Similar findings are observed in mouse models and human patients with WNT pathway abnormalities where penetrance of vertebral anomalies is variable. Even in highly inbred *Dvl2* knockout mice, only 90% were reported to have vertebral anomalies [69], and hemivertebrae and associated scoliosis/kyphosis are seen variably in >75% and <25% of cases with recessive and dominant forms of Robinow syndrome respectively [70]. In addition to vertebral abnormalities, Dvl2 knockout mice exhibit 50% perinatal lethality due to cardiac defects, 25% have tail kinks and 4% have tail truncations [69]. Based on the presence of protein product found in MYC tagged experiments, we propose that the canine DVL2 mutation is not a null mutation but rather a hypomorphic mutation with respect to vertebral malformations. This is also consistent with the more severe phenotype seen in *DVL2* knockout mice. The possibility exists that there are different effects in different developmental pathways or tissues, and possibly, polygenic effects due to the presence of many segregating mutations that are already known to affect size and skull shape in domestic dogs.

The ability to perform whole genome association in dogs allowed the elimination of the fine structure mapping step in causative variant identification. This whole genome variant association approach successfully replicated two previously identified loci that were known to be fixed within the screw tails breeds namely the *BMP3* missense mutation (CFA32) associated

with head morphology and the glioma susceptibility locus (CFA26) [5, 27]. This approach is particularly tractable in the dog where deleterious variants are shared within and across breeds and only a single causative variant is expected. However, it should be noted that only SNPs and small insertion deletions were identified in this analysis, and there are many examples of disease causing variants that would not have been identified using this approach [6, 29]. As whole genome sequencing costs continue to decrease and our abilities to call variants improves, whole genome variant association provides an efficient method to define disease causing variants.

Figures

Fig 1. Phenotype of screw tail breeds. (A) Photographs of typical representatives of breeds: 1. Boxer (brachycephalic and normal but docked tail), 2. Bulldog (brachycephalic and screw tail), 3. French Bulldog (brachycephalic and screw tail), and 4. Boston Terrier (brachycephalic and screw tail) (photographs courtesy of Nestle Purina PetCare).(B) 3D computed tomography reconstructions of 1) Boxer thoracic vertebrae, ventrodorsal view, 2) French Bulldog thoraco-lumbar vertebrae, ventrodorsal 3) French Bulldog thoraco-lumbar vertebrae lateral view. Pronounced kyphosis of the French Bulldog vertebral column is associated with multiple vertebral abnormalities including shortened vertebrae, hemivertebrae and butterfly vertebrae. 4) Lateral vertebral column radiograph of a Bulldog demonstrating the breed typical "screw tail" associated with multiple caudal vertebral malformations and truncation. (C) Computed tomography images of canine skulls showing the variation of skull morphologies: 1) German Shepherd (dolichocephalic), 2) Boxer 3) Bulldog 4) French Bulldog 5) Boston Terrier 6) Pug. White scale bar is 2 cm for each orientation.

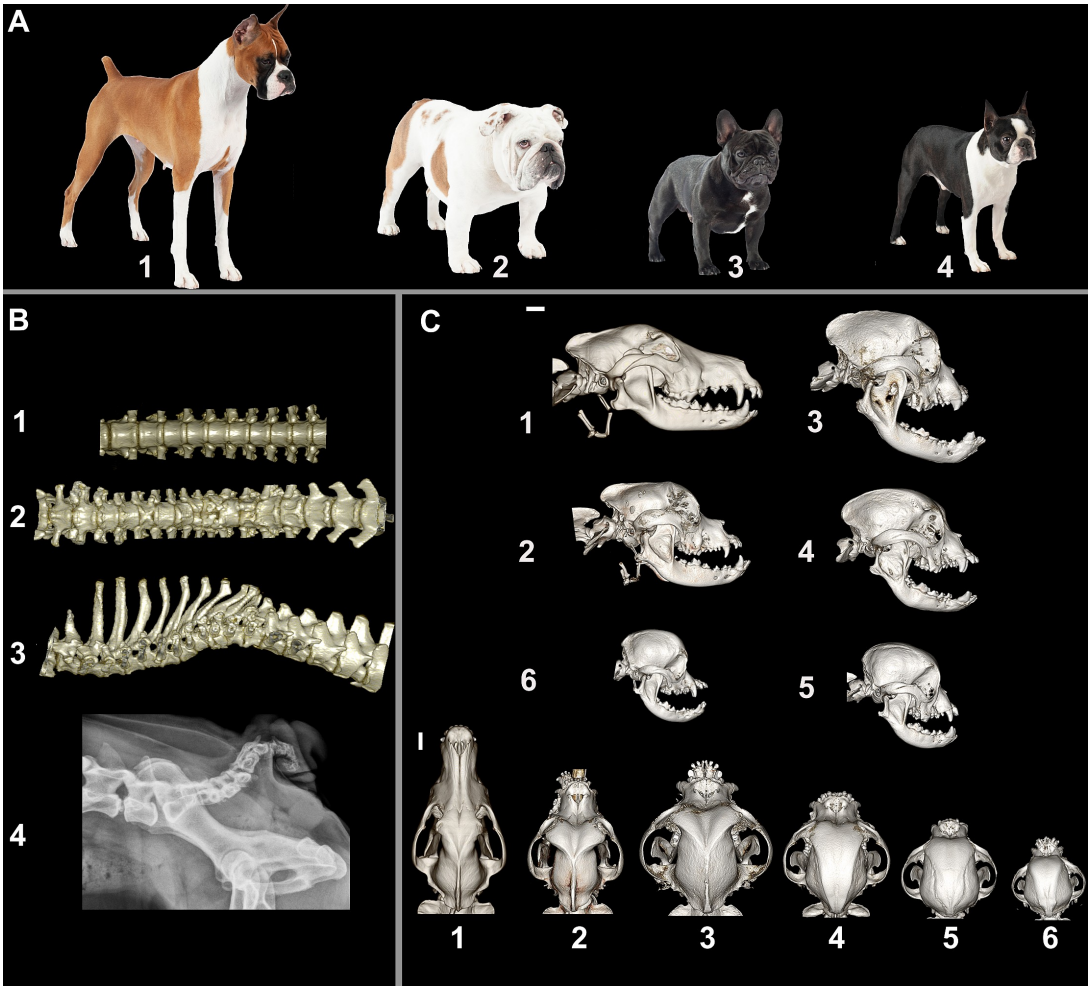
A
1
2
3
4
B
1
2
3
4
C
1
2
3
4
5
6
I
1
2
3
4
5
6

Fig 2. Across breed genome-wide association for screw tail. (A) Hierarchical clustering of Identity by state distance of screw tail breeds. (B) QQ plot of–log 10 of p values before (Unadj) and after genomic (GC) and statistical correction (BONF). (C) and (D) Manhattan plots with–log 10 of p values on y axis and chromosome on the x axis with horizontal blue and red lines indicating p values of 0.05 and 0.01 after correction showing all tested genotypes (C) or 90% allelic difference (D).

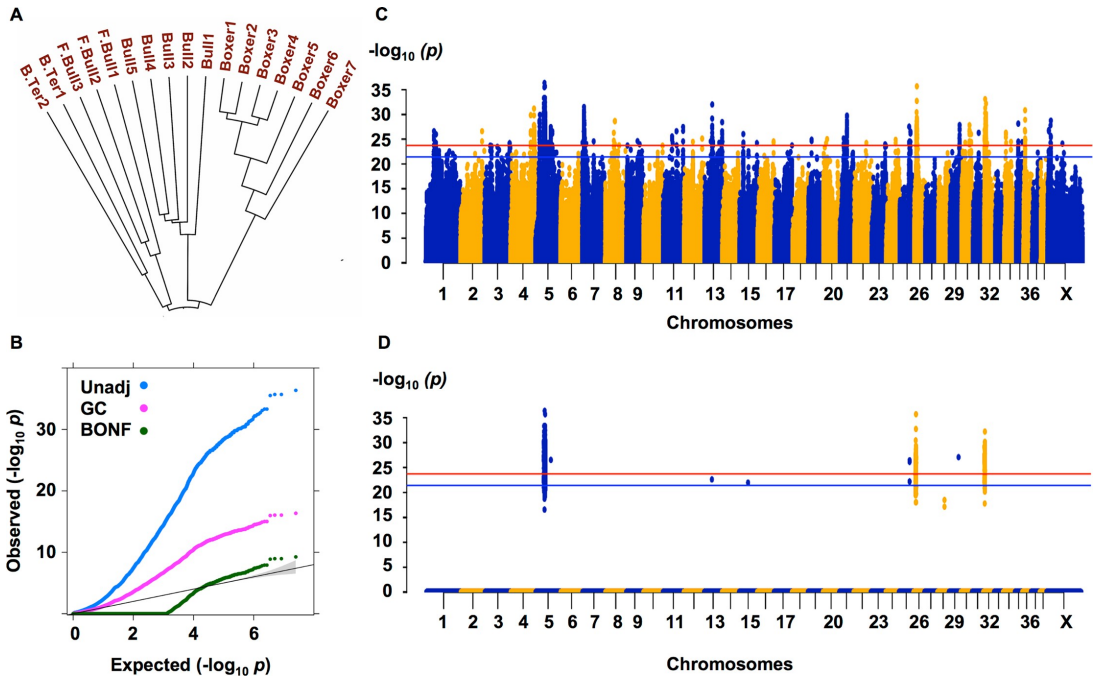

Fig 3. *Dishevelled 2* mutation, location within the protein and amino acid alignment with comparison to Robinow Syndrome. (A) Electropherograms of the single base pair deletion within the cDNA of *DVL2*. (B) Schematic representation of Dishevelled protein domains. Approximate locations of known mutations are marked by vertical grey bars within their respective *Dishevelled* gene (h–human; c–canine). The number of reported clinical mutations in that region, in their respective gene, is in parentheses. (C) Human wild type DVL1, DVL2, and DVL3 C-terminus protein sequences (192, 221, and 216 amino acids respectively) aligned with canine wild type DVL2 (221 amino acids). Colors of amino acids indicate their respective physiochemical property: red–small, hydrophobic; blue–acidic; magenta–basic; green– hydroxyl, sulfhydryl, amine. The location of the Dishevelled frameshift mutations (specific amino acid) are boxed in black. The highly conserved C-terminus is boxed in blue. (D) Altered amino acid sequence of human Robinow syndrome mutations in DVL1 and DVL3 and the canine DVL2 mutation identified in this work. Truncated amino acids marked by black dashes. Highly conserved region is indicated in the wild type sequence by a blue box.

A

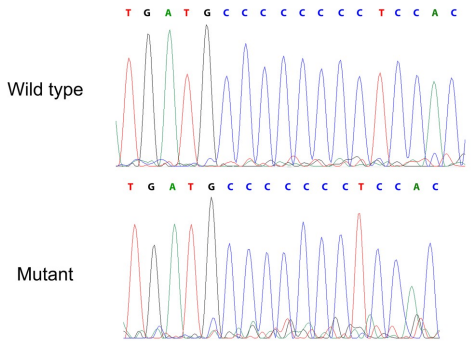

B

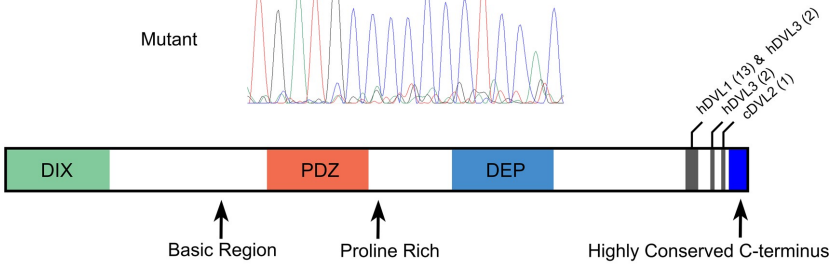

C

```
H_DVL1_wt   ...--LATLNLNSGSSGTSDQDTLAPLPHP-AAPMELGQGYPYQYPGPPCP----PPAYQDPGFSYGSCSTGSQQSE
H_DVL3_wt   ...MANLSLHDHDGSSGASDQDTLAPLPHPGAAPWPMA--FPYQYPPPPHPYNPHP--GFPELGYSYGGGSASSQHSE
H_DVL2_wt   ...LVNLSLNDNDGSSGASDQDTLAPLP--GATPWPLLPTFSYQYPA-PHPYSPQPPPYHELSSYTYGGGSASSQHSE
C_DVL2_wt   ...LVNLSLNDNDGSSGASDQDTLAPLP--GATPWPLLPTFSYQYPT-PHPYSPQPPPYHELSSYTYGGGSASSQHSE

H_DVL1_wt   GSKSSGSTRSSRRAPG--REKER-RAAGAGGSGSESDHTAPSGVGSSWRERPAGQLSRGSSP----------------
H_DVL3_wt   GSRSSGSNRSGSDRRKEKDPK--AGDSKSGGSGSESDHTTRS-SLRGPRERAP--SERSGPAASEHSHRSHHSLASSL
H_DVL2_wt   GSRSSGSTRSDGGAGRTGRPEERAPESK-SGSGSESEPSSRGGSLRRGGEASG--TSDGGPPPSRGS----TGGAPNL
C_DVL2_wt   GSRSSGSTRSDGGAGRTGRPEERAPESK-SGSGSESEPSSRGGSLRRGGEPGG--AGDGGPPPSRGS----SGGVPNL

H_DVL1_wt   RSQ----ASATAPGLPPPH---------PTTKAYTVVGGPPGGPPVRELAAVPPELTGSRQSFQKAMGNPCEFFVDIM
H_DVL3_wt   RSHHTHPSYG-PPGVPPLYGPPMLMMPPP-----PAAMGPPGAPPGRDLASVPPELTASRQSFRMAMGNPSEFFVDVM
H_DVL2_wt   RAHPGLHPYGPPPGMALPYNPMMVVMMPPPPPPVPPAVQPPGAPPVRDLGSVPPELTASRQSFHMAMGNPSEFFVDVM
C_DVL2_wt   RAHPGLHPYGPPPGMALPYNPMMVVMMPPPPPVPPAVQPPGAPPVRDLGSVPPELTASRQSFHMAMGNPSEFFVDVM
```

D

```
H_DVL1_wt             ...PGLPPPHPTTKAYTVVGGPPGGPPVRELAAVPPELTGSRQSFQKAMGNPCEFFVDIM
H_DVL1_p.S539Rfs*112  ...RPRGSPRPTPRPRPIQWWGGHPGDPLSGSWLPSPRN---------------------- 21
H_DVL1_p.G510Vfs*139  ...RGSPRPTPRPRPIQWWGGHPGDPLSGSWLPSPRN---------------------- 23
H_DVL1_p.W507Gfs*140  ...RGSPRPTPRPRPIQWWGGHPGDPLSGSWLPSPRN---------------------- 23
H_DVL1_p.P508Lfs*139  ...RGSPRPTPRPRPIQWWGGHPGDPLSGSWLPSPRN---------------------- 23
H_DVL1_p.S539Afs*108  ...RGSPRPTPRPRPIQWWGGHPGDPLSGSWLPSPRN---------------------- 23
H_DVL1_p.S542Vfs*105  ...RGSPRPTPRPRPIQWWGGHPGDPLSGSWLPSPRN---------------------- 23
H_DVL1_p.P521Hfs*126  ...RGSPRPTPRPRPIQWWGGHPGDPLSGSWLPSPRN---------------------- 23
H_DVL1_p.F524Sfs*123  ...RGSPRPTPRPRPIQWWGGHPGDPLSGSWLPSPRN---------------------- 23
H_DVL1_p.P526Afs*119  ...RPRPTPRPRPIRWWGGHPGDPLSGSWLPSPRN---------------------- 25
H_DVL1_p.P499Rfs*144  ...RPTPRPRPIQWWGGHPGDPLSGSWLPSPRN---------------------- 27
H_DVL1_p.P503Rfs*144  ...RGSPRPTPRPRPIQHPGDPLSGSWLPSPRN---------------------- 27
H_DVL1_p.H502Pfs*141  ...RPTPRPRPIQWWGGHPGDPLSGSWLPSPRN---------------------- 27
H_DVL1_p.S537Vfs*105  ...PTPRPRPIQWWGGHPGDPLSGSWLPSPRN---------------------- 28

H_DVL3_wt             ...PPGVPPLYGPPMLMMPPPPAAMGPPGAPPGRDLASVPPELTASRQSFRMAMGNPSEFFVDVM
H_DVL3_p.Q539Hfs*127  ...LPECPLSTAPPC---------------------------------------------- 50
H_DVL3_p.A529Pfs*137  ...LPECPLSTAPPC---------------------------------------------- 50
H_DVL3_p.S573Vfs*93   ...LPECPLSTAPPC---------------------------------------------- 50
H_DVL3_p.S583Rfs*83   ...LPECPLSTAPPC---------------------------------------------- 50

C_DVL2_wt             ...PPGMALPYNPMMVVMMPPPPPPVPPAVQPPGAPPVRDLGSVPPELTASRQSFHMAMGNPSEFFVDVM
C_DVL2_p.P684Lfs*26   ...PPGMALPYNPMMVVMMPPLHPLSHQQCSPQGPLLSETWALCPQN---------------------- 23
```

Fig 4. WNT-dependent phosphorylation of the DVL2 mutant protein is reduced. (A) Lysates from NIH/3T3 stable cell lines expressing the dog, Myc-tagged wild-type (Wt) or mutant variant (Mut) DVL2, which is 23 aa shorter than wild-type exogenous DVL2, were analyzed by western blotting using an anti-c-Myc antibody. To assess the ability of the wild-type and mutant proteins to respond to WNT stimulation, cells were treated with WNT5A or WNT3A for 6 hours. Both treatments resulted in increased gel mobility shifts of the wild-type DVL2 protein, indicative of increased phosphorylation; this effect was reduced on the mutant DVL2 protein. (B) To confirm that the DVL2 gel mobility shifts observed in (A) were due to phosphorylation, cell lysates were subjected to mock treatment (30 min incubation at 37 C), or calf intestinal phosphatase (CIP) treatment (30 min incubation at 37 C in the presence of CIP) before separation by SDS-PAGE. The DVL2 gel mobility shifts above wild-type and mutant proteins were lost after CIP treatment, confirming that they are caused by phosphorylation. (C) To test whether the DVL2 gel mobility shifts observed in (A) were driven by casein kinase 1 (CK1), cells were treated with D4476, a CK1 inhibitor, for 1 hour prior to and concurrently during the Wnt stimulation for 6 hours. The DVL2 gel mobility shifts were lost after D4476 treatment, further indicating that they are caused by CK1-dependent phosphorylation. α-tubulin was used for loading controls. Cell lysates were normalized by BCA assays for total protein.

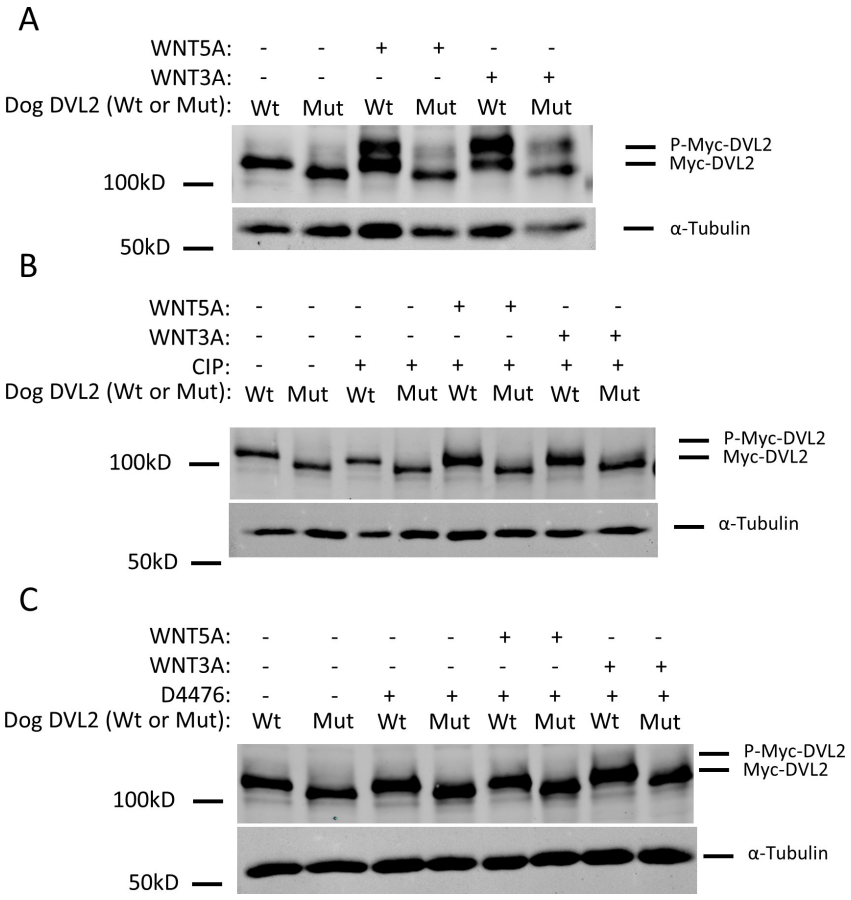
A
WNT5A: - - + + - -
WNT3A: - - - - + +
Dog DVL2 (Wt or Mut): Wt Mut Wt Mut Wt Mut
100kD
50kD
P-Myc-DVL2
Myc-DVL2
α-Tubulin
B
WNT5A: - - - - + + - -
WNT3A: - - - - - - + +
CIP: - - + + + + + +
Dog DVL2 (Wt or Mut): Wt Mut Wt Mut Wt Mut Wt Mut
100kD
50kD
P-Myc-DVL2
Myc-DVL2
α-Tubulin
C
WNT5A: - - - - + + - -
WNT3A: - - - - - - + +
D4476: - - + + + + + +
Dog DVL2 (Wt or Mut): Wt Mut Wt Mut Wt Mut Wt Mut
100kD
50kD
P-Myc-DVL2
Myc-DVL2
α-Tubulin

Table 1. Genotypes of *DVL2 (DVL2*c.2044delC) variant across breeds.

Breed	+/+	+/*dvl2*	*dvl2/dvl2*
Boston Terrier	2	4	59
French Bulldog	0	0	79
Bulldog	0	0	33
Pit Bull	18	9	6
Mixed Breed	11	2	0
Shih Tzu	27	1	0
Staffordshire Bull Terrier	0	1	0
Pug	29	0	0
43 other Breeds	385	0	0

Table 2. Penetrance of Vertebral Malformations within dogs homozygous for DVL2c.2044delC.

	Thoracic Vertebral Malformation			Caudal Vertebral Malformation		
Breed	**Present**	**Absent**	**Penetrance**	**Present**	**Absent**	**Penetrance**
Boston Terrier	20	24	45.5	12	0	100
French Bulldog	47	4	92.1	42	0	100
Bulldog	7	0	100	3	0	100

Table 3. Segregation Analysis of the *DVL2* (*DVL2*c.2044delC) Variant with Vertebral Phenotype.

		Thoracic Vertebral Malformation		Caudal Vertebral Malformation	
Breed	**Genotype**	**Yes**	**No**	**Yes**	**No**
Boston Terrier	+/+	0	2	0	1
	dvl2/+	0	2	0	2
	dvl2/ *dvl2*	20	24	12	0
Shih Tzu	+/+	0	17	0	8
	dvl2/+	0	1	0	1
Pit Bull and Mixes	+/+	0	14	0	7
	dvl2/+	0	5	0	3
	dvl2/ *dvl2*	0	2	4	0
Fisher's exact test		$p = 1.5 \text{ X } 10^{-5}$		$p = 4.5 \text{ X } 10^{-11}$	

References

1. Parker HG. Genomic analyses of modern dog breeds. Mamm Genome. 2012; 23(1-2):19-27. https://doi.org/10.1007s00335-011-9387-6 PMID: 22231497; PubMed Central PNCID: PMCPMC3559126.
2. Salmon Hillbertz NH, Isaksson M, Karlsson EK, Hellmen E, Pielberg GR, Savolainen P, et al. Duplica- tion of FGF3, FGF4, FGF19 and ORAOV1 causes hair ridge and predisposition to dermoid sinus in Ridgeback dogs. Nat Genet. 2007; 39(11):1318–20. https://doi.org/10.1038/ng.2007.4 PMID: 17906623.
3. Bannasch D, Safra N, Young A, Karmi N, Schaible RS, Ling GV. Mutations in the SLC2A9 gene cause hyperuricosuria and hyperuricemia in the dog. PLoS Genet. 2008; 4(11):e1000246. https://doi.org/10. 1371/journal.pgen.1000246 PMID: 18989453; PubMed Central PMCID: PMCPMC2573870.
4. Olsson M, Meadows JR, Truve K, Rosengren Pielberg G, Puppo F, Mauceli E, et al. A novel unstable duplication upstream of HAS2 predisposes to a breed-defining skin phenotype and a periodic fever syn- drome in Chinese Shar-Pei dogs. PLoS Genet. 2011; 7(3):e1001332. https://doi.org/10.1371/journal. pgen.1001332 PMID: 21437276; PubMed Central PMCID: PMCPMC3060080 test.
5. Truve K, Dickinson P, Xiong A, York D, Jayashankar K, Pielberg G, et al. Utilizing the Dog Genome in the Search for Novel Candidate Genes Involved in Glioma Development-Genome Wide Association Mapping followed by Targeted Massive Parallel Sequencing Identifies a Strongly Associated Locus. PLoS Genet. 2016; 12(5):e1006000. Epub 2016/05/14. https://doi.org/10.1371/journal.pgen.1006000 PMID: 27171399; PubMed Central PMCID: PMC4865040.
6. Brown EA, Dickinson PJ, Mansour T, Sturges BK, Aguilar M, Young AE, et al. FGF4 retrogene on CFA12 is responsible for chondrodystrophy and intervertebral disc disease

in dogs. Proc Natl Acad Sci U S A. 2017; 114(43):11476–81. Epub 2017/10/27. https://doi.org/10.1073/pnas.1709082114 PMID: 29073074; PubMed Central PMCID: PMCPMC5664524.

7. Morris D. Dogs: a dictionary of dog breeds: Trafalgar Square Pub.; 2002.
8. Evans KM, Adams VJ. Proportion of litters of purebred dogs born by caesarean section. J Small Anim

   Pract. 2010; 51(2):113–8. https://doi.org/10.1111/j.1748-5827.2009.00902.x PMID: 20136998.

9. Ryan R, Gutierrez-Quintana R, Ter Haar G, De Decker S. Prevalence of thoracic vertebral malforma- tions in French bulldogs, Pugs and English bulldogs with and without associated neurological deficits. Vet J. 2017; 221:25–9. Epub 2017/03/12. https://doi.org/10.1016/j.tvjl.2017.01.018 PMID: 28283076.
10. Moissonnier P, Gossot P, Scotti S. Thoracic kyphosis associated with hemivertebra. Vet Surg. 2011; 40 (8):1029–32. Epub 2011/11/19. https://doi.org/10.1111/j.1532-950X.2011.00876.x PMID: 22091966.
11. Bailey CS, Morgan JP. Congenital Spinal Malformations. Veterinary Clinics of North America: Small Animal Practice. 1992; 22(4):985–1015. https://doi.org/10.1016/s0195-5616(92)50089-4 PMID: 1641930
12. Asher L, Diesel G, Summers JF, McGreevy PD, Collins LM. Inherited defects in pedigree dogs. Part 1: disorders related to breed standards. Vet J. 2009; 182(3):402–11. https://doi.org/10.1016/j.tvjl.2009.08. 033 PMID: 19836981.
13. Schlensker E, Distl O. Prevalence, grading and genetics of hemivertebrae in dogs. European Journal of Companion Animal Practice. 2013; 23:119–23.
14. Fox MW. Developmental Abnormalities of the Canine Skull. Canadian Journal of Comparative Medicine and Veterinary Science. 1963; 27:219–22. PMID: 17649461

15. Mulvihill JJ, Mulvihill CG, Priester WA. Cleft palate in domestic animals: epidemiologic features. Teratol- ogy. 1980; 21(1):109–12. https://doi.org/10.1002/tera.1420210115 PMID: 7385051.

16. Moura E, Pimpão CT. Cleft Lip and Palate in the Dog: Medical and Genetic Aspects. 2017. https://doi. org/10.5772/67049

17. Matic SE. Congenital heart disease in the dog. Journal of Small Animal Practice. 1988; 29:743–59.

18. Darke PGG. Congenital Heart Defects In Small Animals. British Veterinary Journal. 1986; 142:203–9.

https://doi.org/10.1016/0007-1935(86)90061-8 PMID: 3297234

19. Patterson DF. Epidemiologic and Genetic Studies of Congenital Heart Disease in the Dog. Journal Of

The American Heart Association. 1968; 23:171–202.
https://doi.org/10.1161/01.RES.23.2.171

20. Dickinson PJ, York D, Higgins RJ, LeCouteur RA, Joshi N, Bannasch D. Chromosomal Aberrations in Canine Gliomas Define Candidate Genes and Common Pathways in Dogs and Humans. J Neuropathol Exp Neurol. 2016; 75(7):700–10. Epub 2016/06/03. https://doi.org/10.1093/jnen/nlw042 PMID: 27251041; PubMed Central PMCID: PMC4913437.

21. Song RB, Vite CH, Bradley CW, Cross JR. Postmortem Evaluation of 435 Cases of Intracranial Neopla- sia in Dogs and Relationship of Neoplasm with Breed, Age, and Body Weight. Journal of Veterinary Internal Medicine. 2013; 27:1143–52. https://doi.org/10.1111/jvim.12136 PMID: 23865437

22. Haworth K, Putt W, Cattanach B, Breen M, Binns M, Lingaas F, et al. Canine homolog of the T-
box transcription factor T; failure of the protein to bind to its DNA target leads to a short-tail phenotype. Mamm Genome. 2001; 12(3):212–8. https://doi.org/10.1007/s003350010253 PMID: 11252170.
23. Hytonen MK, Grall A, Hedan B, Dreano S, Seguin SJ, Delattre D, et al. Ancestral T-box mutation is pres- ent in many, but not all, short-tailed dog breeds. J Hered. 2009; 100(2):236–40. https://doi.org/10.1093/ jhered/esn085 PMID: 18854372.
24. Gutierrez-Quintana R, Guevar J, Stalin C, Faller K, Yeamans C, Penderis J. A proposed radiographic classification scheme for congenital thoracic vertebral malformations in brachycephalic "screw-tailed" dog breeds. Vet Radiol Ultrasound. 2014; 55(6):585–91. Epub 2014/05/17. https://doi.org/10.1111/vru. 12172 PMID: 24833506.
25. Guevar J, Penderis J, Faller K, Yeamans C, Stalin C, Gutierrez-Quintana R. Computer-assisted radio- graphic calculation of spinal curvature in brachycephalic "screw-tailed" dog breeds with congenital tho- racic vertebral malformations: reliability and clinical evaluation. PLoS One. 2014; 9(9):e106957. Epub 2014/09/10. https://doi.org/10.1371/journal.pone.0106957 PMID: 25198374; PubMed Central PMCID: PMCPMC4157857.
26. Inglez de Souza M, Ryan R, Ter Haar G, Packer RMA, Volk HA, De Decker S. Evaluation of the influ- ence of kyphosis and scoliosis on intervertebral disc extrusion in French bulldogs. BMC Vet Res. 2018; 14(1):5. https://doi.org/10.1186/s12917-017-1316-9 PMID: 29304802; PubMed Central PMCID: PMCPMC5756331.
27. Schoenebeck JJ, Hutchinson SA, Byers A, Beale HC, Carrington B, Faden DL, et al. Variation of BMP3 contributes to dog breed skull diversity. PLoS Genet. 2012; 8(8):e1002849. https://doi.org/10.1371/ journal.pgen.1002849 PMID: 22876193; PubMed Central PMCID: PMCPMC3410846.

28. Boyko AR, Quignon P, Li L, Schoenebeck JJ, Degenhardt JD, Lohmueller KE, et al. A simple genetic architecture underlies morphological variation in dogs. PLoS Biol. 2010; 8(8):e1000451. https://doi.org/ 10.1371/journal.pbio.1000451 PMID: 20711490; PubMed Central PMCID: PMCPMC2919785.
29. Marchant TW, Johnson EJ, McTeir L, Johnson CI, Gow A, Liuti T, et al. Canine Brachycephaly Is Asso- ciated with a Retrotransposon-Mediated Missplicing of SMOC2. Curr Biol. 2017; 27(11):1573–84 e6. https://doi.org/10.1016/j.cub.2017.04.057 PMID: 28552356; PubMed Central PMCID: PMCPMC5462623.
30. Soman C, Lingappa A. Robinow Syndrome: A Rare Case Report and Review of Literature. International Journal of Clinical Pediatric Dentistry. 2015; 8(2):149–52. https://doi.org/10.5005/jp-journals-10005- 1303 PMID: 26379386
31. Patton MA, Afzal AR. Robinow syndrome. J Med Genet. 2002; 39(5):305–10. https://doi.org/10.1136/ jmg.39.5.305 PMID: 12011143; PubMed Central PMCID: PMCPMC1735132.
32. White JJ, Mazzeu JF, Hoischen A, Bayram Y, Withers M, Gezdirici A, et al. DVL3 Alleles Resulting in a -1 Frameshift of the Last Exon Mediate Autosomal-Dominant Robinow Syndrome. Am J Hum Genet. 2016; 98(3):553–61. https://doi.org/10.1016/j.ajhg.2016.01.005 PMID: 26924530; PubMed Central PMCID: PMCPMC4800044.
33. White J, Mazzeu JF, Hoischen A, Jhangiani SN, Gambin T, Alcino MC, et al. DVL1 frameshift mutations clustering in the penultimate exon cause autosomal-dominant Robinow syndrome. Am J Hum Genet. 2015; 96(4):612–22. https://doi.org/10.1016/j.ajhg.2015.02.015 PMID: 25817016; PubMed Central PMCID: PMCPMC4385180.
34. Person AD, Beiraghi S, Sieben CM, Hermanson S, Neumann AN, Robu ME, et al. WNT5A mutations in patients with autosomal dominant Robinow syndrome. Dev Dyn.

2010; 239(1):327–37. https://doi.org/ 10.1002/dvdy.22156 PMID: 19918918; PubMed Central PMCID: PMCPMC4059519.

35. Katoh M, Katoh M. WNT signaling pathway and stem cell signaling network. Clin Cancer Res. 2007; 13 (14):4042–5. https://doi.org/10.1158/1078-0432.CCR-06-2316 PMID: 17634527.
36. Yamaguchi TP, Bradley A, McMahon AP, Jones S. A Wnt5a pathway underlies outgrowth of multiple structures in the vertebrate embryo. Development. 1999; 125:1211–23.
37. Komiya Y, Habas R. Wnt Signal Transduction Pathways. Organogenesis. 2008; 4(2):68–75. PMID: 19279717
38. Flaherty MP, Kamerzell TJ, Dawn B. Wnt signaling and cardiac differentiation. Prog Mol Biol Transl Sci. 2012; 111:153–74. https://doi.org/10.1016/B978-0-12-398459-3.00007-1 PMID: 22917230.
39. Shi YN, Zhu N, Liu C, Wu HT, Gui Y, Liao DF, et al. Wnt5a and its signaling pathway in angiogenesis. Clin Chim Acta. 2017; 471:263–9. https://doi.org/10.1016/j.cca.2017.06.017 PMID: 28641961.
40. Zelzer E, Olsen BR. The genetic basis for skeletal disease. Nature. 2003; 423:343–8. https://doi.org/10. 1038/nature01659 PMID: 12748653
41. Karlsson EK, Baranowska I, Wade CM, Salmon Hillbertz NH, Zody MC, Anderson N, et al. Efficient mapping of mendelian traits in dogs through genome-wide association. Nat Genet. 2007; 39(11):1321– 8. https://doi.org/10.1038/ng.2007.10 PMID: 17906626.
42. Lindblad-Toh K, Wade CM, Mikkelsen TS, Karlsson EK, Jaffe DB, Kamal M, et al. Genome sequence, comparative analysis and haplotype structure of the domestic dog. Nature. 2005; 438(7069):803–19. https://doi.org/10.1038/nature04338 PMID: 16341006.
43. Hartl DL, Clark AG. Principles of Population Genetics. 3rd ed: Sinauer Associates Inc; 1997.

44. Yamamoto H, Yoo SK, Nishita M, Kikuchi A, Minami Y. Wnt5a modulates glycogen synthase kinase 3 to induce phosphorylation of receptor tyrosine kinase Ror2. Genes Cells. 2007; 12(11):1215–23. https://doi.org/10.1111/j.1365-2443.2007.01128.x PMID: 17986005.

45. Susman MW, Karuna EP, Kunz RC, Gujral TS, Cantu AV, Choi SS, et al. Kinesin superfamily protein Kif26b links Wnt5a-Ror signaling to the control of cell and tissue behaviors in vertebrates. Elife. 2017; 6. https://doi.org/10.7554/eLife.26509 PMID: 28885975; PubMed Central PMCID: PMCPMC5590807.

46. Ho HY, Susman MW, Bikoff JB, Ryu YK, Jonas AM, Hu L, et al. Wnt5a-Ror-Dishevelled signaling con- stitutes a core developmental pathway that controls tissue morphogenesis. Proc Natl Acad Sci U S A. 2012; 109(11):4044–51. https://doi.org/10.1073/pnas.1200421109 PMID: 22343533; PubMed Central PMCID: PMCPMC3306699.

47. Nishita M IS, Nomachi A, Endo M, Wang Z, Inaba D, et al. Ror2/Frizzled complex mediates Wnt5a- induced AP-1 activation by regulating Dishevelled polymerization. Mol Cell Biol. 2010; 30:3610–9. PubMed Central PMCID: PMCPubMed Central PMCID: PMC2897551. https://doi.org/10.1128/MCB. 00177-10 PMID: 20457807

48. Rothba¨cher U LM, Deardorff MA, Klein PS, Cho KW, Fraser SE. Dishevelled phosphorylation, subcellu- lar localization and multimerization regulate its role in early embryogenesis. EMBO J 2010; 19:1010– 22. PubMed Central PMCID: PMC PubMed Central PMCID: PMC305640.

49. Gonza´lez-Sancho JM BK, Castelo-Soccio LA, Brown AM. Wnt proteins induce dishevelled phosphory- lation via an LRP5/6- independent mechanism, irrespective of their ability to stabilize beta-catenin. Mol Cell Biol 24:4757–47-68. PubMed Central PMCID: PMCPubMed Central PMCID: PMC416421. https:// doi.org/10.1128/MCB.24.11.4757-4768.2004 PMID: 15143170

50. Bryja V SG, Rawal N, Grahn A, Arenas E. Wnt-5a induces Dishevelled phosphorylation and dopaminer- gic differentiation via a CK1-dependent mechanism. J Cell Sci. 2007; 120:586–95. PubMed Central PMCID: PMC https://doi.org/10.1242/jcs.03368 PMID: 17244647.

51. Bryja V SG, Arenas E. Wnt-3a utilizes a novel low dose and rapid pathway that does not require casein kinase 1-mediated phosphorylation of Dvl to activate beta-catenin. Cell Signal 2007; 19:610–6. PubMed Central PMCID: PMC https://doi.org/10.1016/j.cellsig.2006.08.011 PMID: 17027228.

52. Boutros M, Mlodzik M. Dishevelled: at the crossroads of divergent intracellular signaling pathways. Mech Dev. 1999; 83(1–2):27–37. PMID: 10507837.

53. Wallingford JB, Habas R. The developmental biology of Dishevelled: an enigmatic protein governing cell fate and cell polarity. Development. 2005; 132(20):4421–36. https://doi.org/10.1242/dev.02068 PMID: 16192308.

54. Yang Y, Lijam N, Sussman DJ, Tsang M. Genomic organization of mouse Dishevelled genes. Gene. 1996; 180(1–2):121–3. PMID: 8973355.

55. Semenov MV, Snyder M. Human dishevelled genes constitute a DHR-containing multigene family. Genomics. 1997; 42(2):302–10. https://doi.org/10.1006/geno.1997.4713 PMID: 9192851.

56. Sussman DJ, Klingensmith J, Salinas P, Adams PS, Nusse R, Perrimon N. Isolation and characteriza- tion of a mouse homolog of the Drosophila segment polarity gene dishevelled. Dev Biol. 1994; 166 (1):73–86. https://doi.org/10.1006/dbio.1994.1297 PMID: 7958461.

57. Klingensmith J, Yang Y, Axelrod JD, Beier DR, Perrimon N, Sussman DJ. Conservation of dishevelled structure and function between flies and mice: isolation and characterization of Dvl2. Mech Dev. 1996; 58(1–2):15–26. PMID: 8887313.

58. Bunn KJ, Daniel P, Rosken HS, O'Neill AC, Cameron-Christie SR, Morgan T, et al. Mutations in DVL1 cause an osteosclerotic form of Robinow syndrome. Am J Hum Genet. 2015; 96(4):623–30. https://doi. org/10.1016/j.ajhg.2015.02.010 PMID: 25817014; PubMed Central PMCID: PMCPMC4385193.

59. White JJ, Mazzeu JF, Coban-Akdemir Z, Bayram Y, Bahrambeigi V, Hoischen A, et al. WNT Signaling Perturbations Underlie the Genetic Heterogeneity of Robinow Syndrome. Am J Hum Genet. 2018; 102 (1):27–43. https://doi.org/10.1016/j.ajhg.2017.10.002 PMID: 29276006; PubMed Central PMCID: PMCPMC5777383.

60. Afzal AR, Rajab A, Fenske CD, Oldridge M, Elanko N, Ternes-Pereira E, et al. Recessive Robinow syn- drome, allelic to dominant brachydactyly type B, is caused by mutation of ROR2. Nat Genet. 2000; 25 (4):419–22. Epub 2000/08/10. https://doi.org/10.1038/78107 PMID: 10932186.

61. van Bokhoven H, Celli J, Kayserili H, van Beusekom E, Balci S, Brussel W, et al. Mutation of the gene encoding the ROR2 tyrosine kinase causes autosomal recessive Robinow syndrome. Nat Genet. 2000; 25(4):423–6. Epub 2000/08/10. https://doi.org/10.1038/78113 PMID: 10932187.

62. Bernatik O SK, Schille C, Ganji RS, Červenka I, Trant´ırek L, Schambony A, Zdra´hal Z, Bryja V. https://

doi.org/10.1074/jbc.M114.590638 PMID: 24993822. Functional analysis of dishevelled-3 phosphoryla- tion identifies distinct mechanisms driven by casein kinase 1□ and frizzled5. J Biol Chem. 2014;2014 (289):23520–33.

63. Stockard CR. The Genetic and Endocrinic Basis for Differences in Form and Behavior. Philadelphia, Pennsylvania, USA: The Wistar Institute of Anatomy and Biology; 1941 October, 1941.

64. McGrath J, Gerety PA, Derderian CA, Steinbacher DM, Vossough A, Bartlett SP, et al. Differential clo- sure of the spheno-occipital synchondrosis in syndromic craniosynostosis. Plast Reconstr Surg. 2012; 130(5):681e–9e. Epub 2012/07/11. https://doi.org/10.1097/PRS.0b013e318267d4c0 PMID: 22777037.

65. Rosenberg P, Arlis HR, Haworth RD, Heier L, Hoffman L, LaTrenta G. The role of the cranial base in facial growth: experimental craniofacial synostosis in the rabbit. Plast Reconstr Surg. 1997; 99 (5):1396–407. Epub 1997/04/01. PMID: 9105368.

66. Nagayama M, Iwamoto M, Hargett A, Kamiya N, Tamamura Y, Young B, et al. Wnt/beta-catenin signal- ing regulates cranial base development and growth. J Dent Res. 2008; 87(3):244–9. Epub 2008/02/26. https://doi.org/10.1177/154405910808700309 PMID: 18296608.

67. Twigg SR, Forecki J, Goos JA, Richardson IC, Hoogeboom AJ, van den Ouweland AM, et al. Gain-of- Function Mutations in ZIC1 Are Associated with Coronal Craniosynostosis and Learning Disability. Am J Hum Genet. 2015; 97(3):378–88. https://doi.org/10.1016/j.ajhg.2015.07.007 PMID: 26340333; PubMed Central PMCID: PMCPMC4564895.

68. Twigg SR, Wilkie AO. A Genetic-Pathophysiological Framework for Craniosynostosis. Am J Hum Genet. 2015; 97(3):359–77. https://doi.org/10.1016/j.ajhg.2015.07.006 PMID: 26340332; PubMed Cen- tral PMCID: PMCPMC4564941.

69. Hamblet NS, Lijam N, Ruiz-Lozano P, Wang J, Yang Y, Luo Z, et al. Dishevelled 2 is essential for car- diac outflow tract development, somite segmentation and neural tube closure. Development. 2002; 129 (24):5827–38. PMID: 12421720.

70. Mazzeu JF, Pardono E, Vianna-Morgante AM, Richieri-Costa A, Ae Kim C, Brunoni D, et al. Clinical characterization of autosomal dominant and recessive variants of Robinow syndrome. Am J Med Genet A. 2007; 143(4):320–5. https://doi.org/10.1002/ajmg.a.31592 PMID: 17256787.

71. Bolger AM, Lohse M, Usadel B. Trimmomatic: a flexible trimmer for Illumina sequence data. Bioinfor- matics. 2014; 30(15):2114–20. https://doi.org/10.1093/bioinformatics/btu170 PMID: 24695404; PubMed Central PMCID: PMCPMC4103590.

72. Hoeppner MP, Lundquist A, Pirun M, Meadows JR, Zamani N, Johnson J, et al. An improved canine genome and a comprehensive catalogue of coding genes and non-coding transcripts. PLoS One. 2014; 9(3):e91172. https://doi.org/10.1371/journal.pone.0091172 PMID: 24625832; PubMed Central PMCID: PMC3953330.

73. Li H, Durbin R. Fast and accurate short read alignment with Burrows-Wheeler transform. Bioinformatics. 2009; 25(14):1754–60. https://doi.org/10.1093/bioinformatics/btp324 PMID: 19451168; PubMed Cen- tral PMCID: PMCPMC2705234.

74. McKenna A, Hanna M, Banks E, Sivachenko A, Cibulskis K, Kernytsky A, et al. The Genome Analysis Toolkit: a MapReduce framework for analyzing next-generation DNA sequencing data. Genome Research. 2010; 20(9):1297–303. https://doi.org/10.1101/gr.107524.110 PMID: 20644199; PubMed Central PMCID: PMCPMC2928508.

75. Yates A, Akanni W, Amode MR, Barrell D, Billis K, Carvalho-Silva D, et al. Ensembl 2016. Nucleic Acids Res. 2016; 44(D1):D710–6. https://doi.org/10.1093/nar/gkv1157 PMID: 26687719; PubMed Central PMCID: PMCPMC4702834.

76. Purcell S, Neale B, Todd-Brown K, Thomas L, Ferreira MA, Bender D, et al. PLINK: a tool set for whole- genome association and population-based linkage analyses. Am J Hum Genet. 2007; 81(3):559–75. https://doi.org/10.1086/519795 PMID: 17701901; PubMed Central PMCID: PMCPMC1950838.

77. Devlin B, Roeder K. Genomic control for association studies. Biometrics. 1999; 55(4):997–1004. PMID: 11315092.

78. Bush WS, Moore JH. Chapter 11: Genome-wide association studies. PLoS Comput Biol. 2012; 8(12): e1002822. https://doi.org/10.1371/journal.pcbi.1002822 PMID: 23300413; PubMed Central PMCID: PMCPMC3531285.

79. McLaren W, Gil L, Hunt SE, Riat HS, Ritchie GR, Thormann A, et al. The Ensembl Variant Effect Predictor. Genome Biol. 2016; 17(1):122. https://doi.org/10.1186/s13059-016-0974-4 PMID: 27268795; PubMed Central PMCID: PMCPMC4893825.

80. NCBI. NCBI genome annotation of CanFam3 assembly 2015 [9/18/2015]. Available from: ftp://ftp.ncbi. nih.gov/genomes/Canis_lupus_familiaris/GFF/ref_CanFam3.1_top_level.gff3.gz.

81. Rozen S, Skaletsky H. Primer3 on the WWW for general users and for biologist programmers. Methods Mol Biol. 2000; 132:365–86. Epub 1999/11/05. PMID: 10547847.

82. Brinkhof B, Spee B, Rothuizen J, Penning LC. Development and evaluation of canine reference genes for accurate quantification of gene expression. Analytical Biochemistry. 2006; 356(1):36–43. http://dx. doi.org/10.1016/j.ab.2006.06.001. PMID: 16844072

83. Dull T, Zufferey R, Kelly M, Mandel RJ, Nguyen M, Trono D, et al. A third-generation lentivirus vector with a conditional packaging system. J Virol. 1998; 72(11):8463–71. PMID: 9765382; PubMed Central PMCID: PMCPMC110254.